UNIVERSITY OF CALIFORNIA, SAN DIEGO

Correlation-Based Beamforming for Multi-User MIMO Channels

A dissertation submitted in partial satisfaction of the

requirements for the degree

Doctor of Philosophy

in

Electrical and Computer Engineering

by

Adam L. Anderson

Committee in charge:

Professor James R. Zeidler, Chair
Professor Robert R. Bitmead
Professor William S. Hodgkiss
Professor Laurence B. Milstein
Professor Bhaskar Rao

2008

The dissertation of Adam L. Anderson is approved, and it is acceptable in quality and form for publication on microfilm and electronically:

Chair

University of California, San Diego

2008

EPIGRAPH

Every solvable problem
has a solution.
—axiom

TABLE OF CONTENTS

LIST OF FIGURES

LIST OF TABLES

ACKNOWLEDGEMENTS

I would first like to acknowledge my advisor, Dr. Zeidler, and graduate institution, the University of Califronia, San Diego (UCSD), for providing an environment where research and learning can take place. I firmly believe that advanced education (regardless of the focus) is at the core of maximizing the potential of the human individual and they have provided this opportunity for me. I would also like to thank my graduate committee, Drs.: Milstein, Rao, Hodgkiss, and Bitmead for the time they have invested in my progess through the UC graduate system.

My wife, Brita, and children: Max, Chase, Grace, Madi, and Unnamed, are an amazing family for me. My wife has provided support and patience through all these years of advanced study which length of time happens to coincide with all our years of marriage as well. My children are all brilliant in their own way and give me satisfaction in being able to raise the next generation of engineers.

I would also like to thank Dr. Jensen specifically for his interest in my progression since hiring me as an intern when I was an undergraduate student. Thanks to all my fellow doctoral students and their countless discussions on numerous topics with varying degrees of applicability to this dissertation.

The text presented in this dissertation, in part, was originally published in the following papers, of which I was the primary researcher and author: A. L. Anderson, J. R. Zeidler, and M. A. Jensen, "Regularized channel distribution inversion and parameterization in the MIMO broadcast channel," in *Proc. 2008 IEEE 68th Veh. Technol. Conf.*, Calgary, Canada, Sept. 2008;A. L. Anderson, J. R. Zeidler, and M. A. Jensen, "Instantaneous and average rate maximization in MIMO multiple-access channels (MAC) with linear processing," in *42nd Asilomar Conf. Signals, Systems and Computers*, Pacific Grove, CA, Oct. 2008;A. L. Anderson, J. R. Zeidler, and M. A. Jensen, "Linear processing and link scheduling in MIMO mobile ad hoc networks (MANET)," submitted to *28th Conference on Computer Communications (INFOCOM 2008)*;A. L. Anderson, J. R. Zeidler, and M. A. Jensen, "Stable transmission in the time-varying MIMO broadcast channel," *EURASIP Journal on Advances in Signal Processing*, 2008, Article ID 617020, 14

pages, 2008. doi:10.1155/2008/617020;A. L. Anderson, J. R. Zeidler, and M. A. Jensen, "Reduced-feedback linear precoding with stable performance for the time-varying MIMO broadcast channel," *IEEE Journal on Selected Areas of Communications, (Special Issue on Limited Feedback)*. Vol. 26, No. 8, 11 pages, October, 2008.

VITA

2002	BSc in Electrical Engineering, Brigham Young University (BYU)
2002-2003	Intern, Wavetronix LLC
2004	MSc in Electrical Engineering, Brigham Young University
2000-2005	Software Engineer, AJ Design Group, Inc
2004-2008	Graduate Student Researcher, University of California, San Diego (UCSD)
2008	Teaching Assistant, University of California, San Diego
2008	PhD in Electrical Engineering, University of California, San Diego

PUBLICATIONS

A. L. Anderson, J. R. Zeidler, and M. A. Jensen, "Performance of transmit precoding in time-varying point-to-point and multi-user MIMO channels," in *Conference Record of the IEEE Asilomar Conference on Circuits, Systems and Computers*, Nov. 2006.

A. L. Anderson, J. R. Zeidler, and M. A. Jensen, "Parameterized channel feedback using correlation-based channel models for multi-user MIMO systems," in *Proceedings of the 2008 USNC/URSI National Radio Science Meeting*, paper # BS11-4, 1 page, Boulder, CO, Jan. 3-6, 2008. **Invited**

A. L. Anderson, J. R. Zeidler, and M. A. Jensen, "Covariance-based signaling and feedback data parameterization for the time-varying MIMO broadcast channel," *Proceedings of the 28th General Assembly of International Union of Radio Science*, Chicago, IL, Aug. 7-16, 2008. **Invited**

A. L. Anderson, J. R. Zeidler, and M. A. Jensen, "Regularized channel distribution inversion and parameterization in the MIMO broadcast channel," in *Proc. 2008 IEEE 68th Veh. Technol. Conf.*, Calgary, Canada, Sept. 2008.

A. L. Anderson, J. R. Zeidler, and M. A. Jensen, "Instantaneous and average rate maximization in MIMO multiple-access channels (MAC) with linear processing," in *42nd Asilomar Conf. Signals, Systems and Computers*, Pacific Grove, CA, Oct. 2008.

A. L. Anderson, J. R. Zeidler, and M. A. Jensen, "Linear processing and link scheduling in MIMO mobile ad hoc networks (MANET)," submitted to *28th Conference on Computer Communications (INFOCOM 2008)*.

A. L. Anderson, J. R. Zeidler, and M. A. Jensen, "Stable transmission in the time-varying MIMO broadcast channel," *EURASIP Journal on Advances in Signal Processing*, 2008, Article ID 617020, 14 pages, 2008. doi:10.1155/2008/617020.

A. L. Anderson, J. R. Zeidler, and M. A. Jensen, "Reduced-feedback linear precoding with stable performance for the time-varying MIMO broadcast channel," *IEEE Journal on Selected Areas of Communications, (Special Issue on Limited Feedback)*. Vol. 26, No. 8, 11 pages, October, 2008.

A. L. Anderson, J. R. Zeidler, and M. A. Jensen, "Regularized Channel Inversion Dirty-Paper Coding (RCI-DPC)," in preparation.

ABSTRACT OF THE DISSERTATION

Correlation-Based Beamforming for Multi-User MIMO Channels

by

Adam L. Anderson

Doctor of Philosophy in Electrical and Computer Engineering

University of California San Diego, 2008

Professor James R. Zeidler, Chair

Transmit precoding strategies in multiple-input multiple-output (MIMO) systems provide a mechanism for increasing the performance of point-to-point links and enable spatial division multiple access in multi-user networks. However, communication node mobility in such systems can lead to rapid channel variation which limits the quality of attainable channel state information (CSI). This work explores the performance loss of point-to-point and multi-user precoding and detection strategies based on CSI which goes out of date and channel distribution (correlation) information which provides a more average channel representation and ultimately stability in achievable performance.

This correlation-based method is a linear beamforming precoding strategy based on channel distribution information in the form of a full spatial correlation matrix for each user. This algorithm is shown to provide highly stable communication, with a throughput that is higher than that for optimal precoders operating on outdated CSI, in a time-variant environment, indicating that this approach can operate with significantly reduced feedback frequency. Furthermore, the dissertation demonstrates the use of the well-known Kronecker and Weichselberger models to parameterize the full correlation matrix to enable further reduction in the amount of feedback data required for implementation of the new beamforming technique.

Channel measurements based on an experimentally obtained MIMO channels in indoor and outdoor environments are used in defining the statistical nature of the wireless channel.

Finally, the examined beamforming algorithms are extended to work for all possible scheduled, half-duplex link topologies using explicit channel state information or distribution information. Each type of derived beamformer, whether utilizing CSI or CDI, can provide additional scheduling tools for the medium access control and other network layers in optimizing the overall network throughput, in a cross-layer fashion, depending on the state of the network and available information at the nodes.

Chapter 1

Introduction

The host of a cocktail party is concerned about the enjoyment of each of her guests. Let us assume that enjoyment in such settings stems entirely from conversations had with fellow guests and will therefore be entirely dictated at the discretion of the host. Each guest is gainfully equipped with a single mouth and single [set of] ears with which communication can take place. The quality (and equivalently the enjoyment) of each conversation is based on a number of factors: the number of concurrent conversations, the number of participants in each conversation, the distance between guests, the intensity of background music, the type of vocalization used (hands cupped over mouths work well for long distances), and so forth. Consider a poorly attended party populated by only two guests. The host can schedule exactly four types of conversations (the host remains aloof of all talking besides to inform who may speak to whom). Keeping in mind that talking to one's self provides no enjoyment in this setting, the possible conversations are: the first guest can speak to the second, the second to the first, both guests can remain silent (rather boring), or they can talk at the same time (not very enjoyable). Now, throw in additional guests at a more popular party and the task of conversation quality assurance becomes incredible. In fact, with only six guests there are over 1 *billion* different ways the guests can communicate with each other.

Now give each guest multiple mouths and multiple [sets of] ears (assuming

enough brain power to process) and try to organize the conversations. Assume, after an exhausting, Herculean effort, the host finds the optimal set of guests and conversations to make the majority of all guests happy (maximizing the success of the party). And then the guests start using their single [set of] legs to mingle... Though a trite example of multi-user, multi-antenna communications, I use the above analogy with friends and family, who afterward enjoy a small sense of the complexity of the problem, but are not well-versed in the engineering discipline, when they ask "So what is your thesis about?" .

And what is this work about? As extra dimensions are added on communication channels between two or more entities the possibility of performance gains is also increased. A node equipped with multiple antennas will certainly do better than those with just a single antenna as long as such freedom is exploited appropriately. Add more users to the channel and receive additional degrees of freedom on which communication can take place. The multi-user, multiple-input multiple-output (MIMO) channel is complex, but the possibilities are the focus of a significant amount of even *tutorial* papers in just the past decade [1–4] which provide a good foundation for those entering this field of study. As an exhaustive analysis of MIMO processing techniques is intractable for any work; this dissertation focuses on the degradation of optimal transmission schemes under certain system conditions, namely error in knowledge of the channel, and then derives suboptimal schemes that circumvent these described system conditions.

Consider for a moment the multi-user, MIMO channel. Assume an ideal, one-shot, genie-aided (impractical) scenario where all nodes are given knowledge of the channel between all other nodes at some initial time. With enough effort, the optimal transmission schemes can be found for almost any desired scenario or quality of service (QoS) requirement. Now let all the nodes move even slightly. These optimal schemes found when the channel knowledge was perfect will have immediate and severe performance loss due to node mobility (and other effects) if the channel is not repeatedly updated at applicable nodes. Suboptimal, yet stable, transmission schemes are the focus of this work and will ultimately be based on the statistical, rather than instantaneous, properties of the channel.

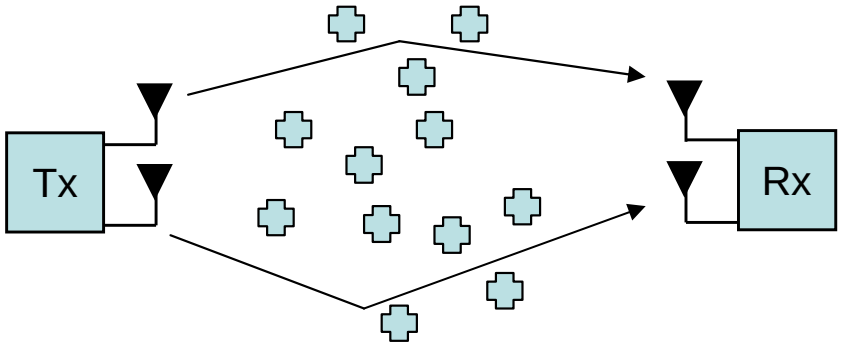

Figure 1.1: A simplified multipath scattering environment where the ith path leaves the transmitter at the angle $\phi_{\mathrm{t},i}$ and arrives at the receiver with angle $\phi_{\mathrm{r},i}$.

This introductory chapter provides a brief overview of the multipath MIMO channel, the multi-user MIMO channel, and a visualization of linear processing or beamforming in multipath channels based off simple line-of-sight (LOS) channels. Afterwards, the bulk of the dissertation is mapped out as we attempt to find a stable transmission scheme using "Correlation-Based Beamforming for Multi-user MIMO Channels".

1.1 Multipath MIMO Channels

The focus of this work is on the spatial structure of the multipath MIMO channel and ways to exploit available knowledge to maximize the system performance in either single- or multi-user channels. Fundamentally, we assist in answering the question, "Are there communicable, stable subspaces in the wireless MIMO channel?". In order to obtain a brief understanding and visualization of this concept, consider a simplified channel model where contributions from all wireless paths departing the transmitter and arriving at the received are accounted for by superposition of each virtual line-of-sight (LOS) component as shown in Fig. 1.1. For this simplified model, the analytic, baseband channel transfer characterization between the N_{t} transmit antennas and N_{r} receive antennas with L distinct paths

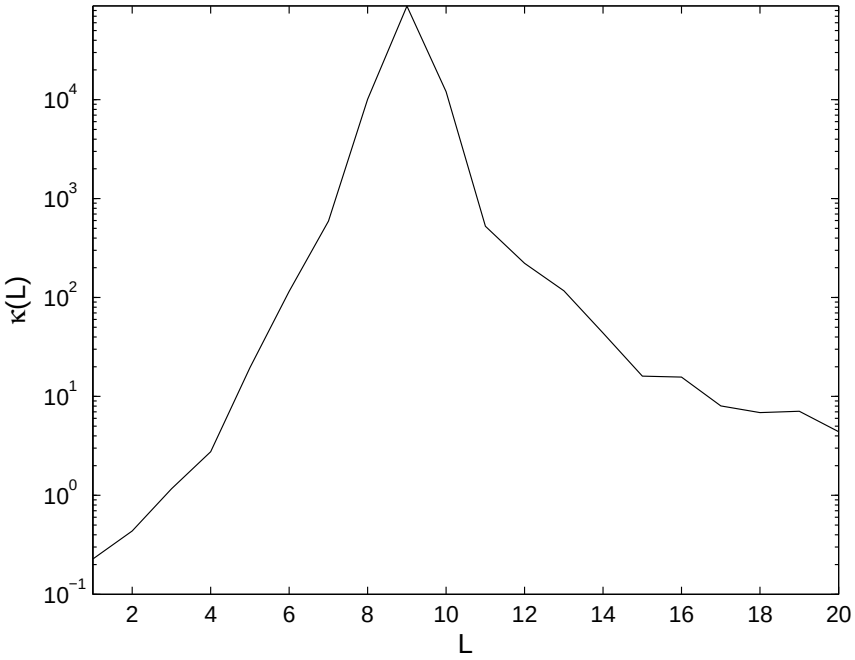

Figure 1.2: Condition number $\kappa(L)$, defined in Section 1.1, as a function of number of multipaths. The number of antennas is fixed at $N_r = N_t = 9$.

can be written as

$$\mathbf{H} = \sum_{l=1}^{L} \beta_l \mathbf{a}\left(\phi_{\mathrm{r},l}\right) \mathbf{a}^H\left(\phi_{\mathrm{t},l}\right) \tag{1.1}$$

where $\mathbf{a}(\phi_{\mathrm{t},l})$ is the $N_\mathrm{t} \times 1$ steering vector for the lth path with angle of departure (AoD) $\phi_{\mathrm{t},l}$, $\mathbf{a}(\phi_{\mathrm{r},l})$ is the $N_\mathrm{r} \times 1$ steering vector for the lth path with angle of arrival (AoA) $\phi_{\mathrm{r},l}$, and β_l represents generic path loss (e.g. loss due to distance traveled or material composition of scatterers). If the transmit and receive nodes are equipped with uniform linear arrays (ULA) with identical (half-wavelength) spacing, and region of interest is constrained to the x-y plane, then the steering vectors are simply functions of the AoD and AoA as written in (1.1).

How good is this channel for communication? There are various methods of defining the "quality" of the channel $\mathbf{H}$ and algorithms that exploit such knowledge in coding schemes. For example, the condition number κ of a matrix can be defined as the ratio of the largest to smallest singular values. With this definition a large

condition number implies a rank deficient matrix while small values of κ suggest a channel with good/numerous spatial subchannels upon which information can be conveyed. For this introductory examination of the multipath MIMO channel, consider defining the channel quality from not only a linear algebra perspective - singular values - but a communication emphasis as well - number of simultaneous data streams - by defining the channel condition number as

$$\kappa(L) = \frac{1}{\sqrt{\sigma\left(\min\left\{L, N_t, N_r\right\}\right)}} \tag{1.2}$$

where the function $\sigma(i)$ returns the ith singular value (given numerical descending order) of the channel matrix. The definition in (1.2) provides further insight into the MIMO channel rather than the standard condition number definition. The denominator expression suggests a situation where communications are pushed to their limits; if a non-zero subspace exists then it will be used to transfer data. A large κ suggests that transmissions are overextending themselves by using subchannels that are non-zero but weak and will certainly result in poor performance for standard beamformers.

Fig. 1.2 shows the average condition number of an 9×9 channel matrix as a function of the number of paths given the described simple LOS model where AoD and AoA are random and the path loss is fixed at $\beta_l = \frac{1}{L}$. Consider the peak shown in Fig. 1.2. With $L = 9$ resolvable paths and $N_r = N_t = 9$ antennas there are theoretically nine subchannels that can be used for information exchange; however, the gain of the weakest path is extremely small and would result in poor quality transmissions. Thus, in a purely LOS, single-path environment the channel can only support a single data stream from transmitter to receiver. Conversely, with rich scattering ($L \gg N_t$) the channel has a nice subspace structure that can be used for spatial multiplexing and maximize the throughput of the link. Section 1.2 helps visualize the combination of channel richness with beamforming that maximizes signal gain.

1.2 Linear Processing (Beamforming)

Linear processing, or beamforming, is a simple method of exploiting knowledge of the channel to maximize the opportunity of desired signal reception. With beamforming, a signal is spread across all transmit antennas with each antenna receiving a separate, complex weight according to some design criterion. Analytically, these separate weights can be written in vector form and are called the transmit beamforming vector or transmit weights. At the receiver, the same method is used to create the receive beamforming vector. The analytical expression for the estimate of the transmitted signal, in the single-user channel, is written as

$$\hat{x} = \mathbf{w}^H \mathbf{H} \mathbf{b} x + \mathbf{w}^H \boldsymbol{\eta} \tag{1.3}$$

where $\mathbf{b}$ and $\mathbf{w}$ are the transmit and receive beamforming vectors, respectively, and $\boldsymbol{\eta}$ is additive white Gaussian noise (AWGN). The goal of beamforming is to maximize some predefined quality given knowledge of the channel at, and cooperation between, the transmitter and receiver.

1.2.1 Beamforming with Channel Transfer Function

Consider (1.3) with the intent of maximizing the signal gain, defined as $\mathbf{w}^H \mathbf{H} \mathbf{b}$, of the received signal. This optimization problem can be written as

$$\begin{aligned} &\max_{\mathbf{w},\mathbf{b}} \ \mathbf{w}^H \mathbf{H} \mathbf{b} \\ &||\mathbf{w}||^2 = 1, \ ||\mathbf{b}||^2 = 1 \end{aligned} \tag{1.4}$$

where the objective function is assumed purely real and the constraints on the beamforming vectors are in place to normalize noise and transmit power. For some non-unity transmit power, P, the power can simply be factored out of the objective function and does not change the analysis. Consider rewriting the channel matrix using the singular-value decomposition (SVD) as $\mathbf{H} = \mathbf{U}\mathbf{S}\mathbf{V}^H$ where the matrix $\mathbf{S}$ is diagonal containing the singular values of the matrix. The optimization problem

can then be rewritten as

$$\max_{\mathbf{w}',\mathbf{b}'} \ \mathbf{w}'^{H}\mathbf{S}\mathbf{b}'$$
$$\mathbf{w}' = \mathbf{U}\mathbf{w}, \ \mathbf{b}' = \mathbf{V}\mathbf{b} \tag{1.5}$$

with the same constraints as previously. It is straightforward to see that the maximum value of the objective function is simply the maximum singular value of $\mathbf{H}$. In fact, the transformed vectors $\mathbf{w}'$ and $\mathbf{b}'$ are simply unit basis vectors that "point" to their corresponding singular vectors for $\mathbf{w}$ and $\mathbf{b}$. Thus, as described in the previous section, the gains available to a multiplexed transmission are related to the singular values of the channel matrix and are achieved by transmissions using the corresponding left- and right-singular vectors.

To gain further insight into this behavior, it is interesting to examine the resulting beam*patterns* that result from this type of optimal beamforming. Consider the simple channel model described by (1.1) with $N_r = N_t = 9$ antennas and constant scaling $\beta_l = \frac{1}{L}$. Assume the AoD are offset by $-70°$ and spaced $35°$ apart. Similarly the AoA are offset by $120°$ and spaced $20°$ apart. Fig. 1.3 shows the resulting patterns as the number of multipath components is increased when beamforming weights are found by (1.5). For this polar plot the transmitter pattern occupies the right hemisphere while the receiver pattern occupies the left hemisphere. Notice that, depending on the path spacing, the transmitter and receiver separately attempt to form specific beams to match the AoD and AoA values or multipaths. However, when the spacing is sufficiently small with enough paths, the patterns are slightly wider as energy is gathered from separate paths in a single beam.

1.2.2 Beamforming with Channel Distribution Function

A difficulty that can arise when just the channel transfer matrix is used to create beamforming vectors, and can cause major performance loss, is a common occurrence - mobility. If the users move such that the beampatterns created are off by just a few degrees, and the channel is not updated accordingly, then the resulting

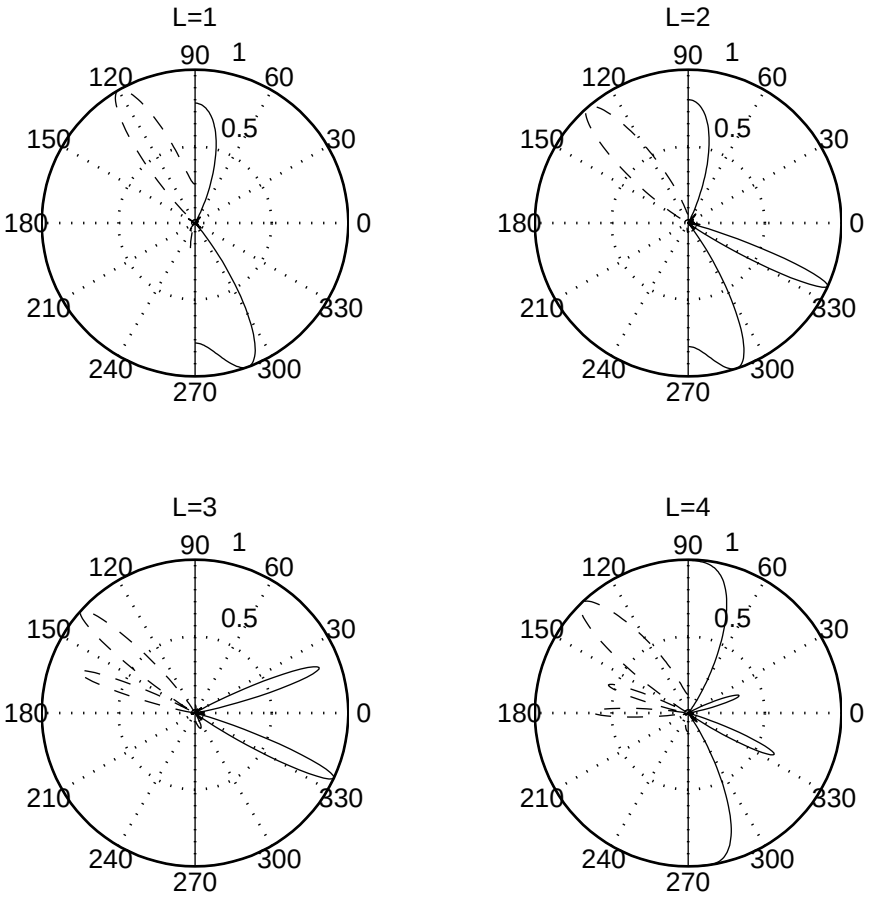

Figure 1.3: Beampatterns when maximizing the single-user, single-stream gain with L propagation paths between transmitter and receiver. The right hemispheres show transmit beampatterns while the left hemispheres are for receive patterns. AoA and AoD values are defined in Section 1.2.1.

performance can be catastrophic. In fact, if a user unknowingly moves into the beampattern nulls while attempting to maximize the signal then a complete outage of communication can occur. This sensitivity to mobility and channel knowledge error helps motivate the topic of this work and is illustrated in a simple example below.

Considering adding mobility to the problem by modifying the simple model under consideration such that the angles of departure and arrival are perturbed around their mean by some random variable. This perturbation could represent movement by the transmitter and/or receiver within some geographical area while keeping the general angular direction the same. With this additional element to the problem the resulting channel matrices can be realized with

$$\begin{aligned} \mathbf{H} &= \sum_{l=1}^{L} \beta_l \mathbf{a}\left(\underline{\phi}_{\mathrm{r},l}\right) \mathbf{a}^H\left(\underline{\phi}_{\mathrm{t},l}\right) \\ \underline{\phi}_{\mathrm{r},l} &= \hat{\phi}_{\mathrm{r},l} + \theta_r \\ \underline{\phi}_{\mathrm{t},l} &= \hat{\phi}_{\mathrm{t},l} + \theta_t \end{aligned}$$

where θ_r and θ_t are uniform random variables defined over some angular extent $\phi_{\max}$ deviation from the mean. Thus, on average, the multipaths will depart and arrive the same as the channel defined in (1.1) though any specific realization of the channel is guaranteed to be off at least slightly and capable of causing significant performance loss depending on the perturbation.

Consider now examining a beamforming vector based on the *average* gain, defined as $E[\mathbf{w}^H\mathbf{H}\mathbf{b}]$, of a single stream of data. In other words, if the maximum singular value of the channel matrix $\mathbf{H}$ is the largest possible gain in any instantiation, what is the maximum possible average gain for a fixed set of beamforming weights? This problem is formulated in a similar manner

$$\begin{aligned} &\max_{\mathbf{w},\mathbf{b}} \; E[\mathbf{w}^H\mathbf{H}\mathbf{b}] \\ &||\mathbf{w}||^2 = 1, \; ||\mathbf{b}||^2 = 1 \end{aligned} \tag{1.6}$$

where $E[\cdot]$ is the expectation operator on a random quantity. Since $\mathbf{w}$ and $\mathbf{b}$ are not random quantities under the assumption of fixed weights then the maximum

average gain will reduce to the maximum singular value of the average channel $E[\mathbf{H}]$ using the same SVD approach as that used for the perfect channel knowledge case.

Fig. 1.4 shows the transformation on the beampatterns when the channel distribution, rather than state, is used for beamforming. For this simulation, the number of paths was fixed at $L = 1$, with average angular values of $\hat{\phi}_{\mathrm{r},l} = 150°$ and $\hat{\phi}_{\mathrm{r},l} = 0°$. The angular deviation $\phi_{\max}$ is swept from 0° to 40°. The number of antennas is set to $N_r = N_t = 9$. Notice that as the angular deviation increases the resulting beampatterns broaden in order to gather energy from all possible angles according to the statistics of the channel matrix. This broadening of the beam in the LOS channel guarantees a good average performance but will certainly result in poorer performance over the channel state beamformer when its knowledge is perfect. This idea of beam broadening will be used as this work delves deeper into the problem of providing stable performance in multi-user, multipath, MIMO channels.

1.3 Multi-user MIMO Channels

The addition of multiple users in the multipath MIMO channel results in extra dimensionality and complexity. Now, in addition to numerous propagating waves impinging on the receiver, *all* receive nodes will experience superimposed multipath interference from all transmitting nodes depending on the transmit precoding used. These additional communicating paths can certainly create detrimental interference rendering the channel useless if exploited improperly, or the multi-user nature of the channel can enhance the system throughput depending on how links are concurrently scheduled.

Consider a multi-user channel where each node is equipped with multiple antennas and each link experiences the multipath phenomenon described in this introduction. Though the possible types of multi-user channels is limitless, Fig. 1.5 shows examples of the possible single- and multi-user links or channels examined

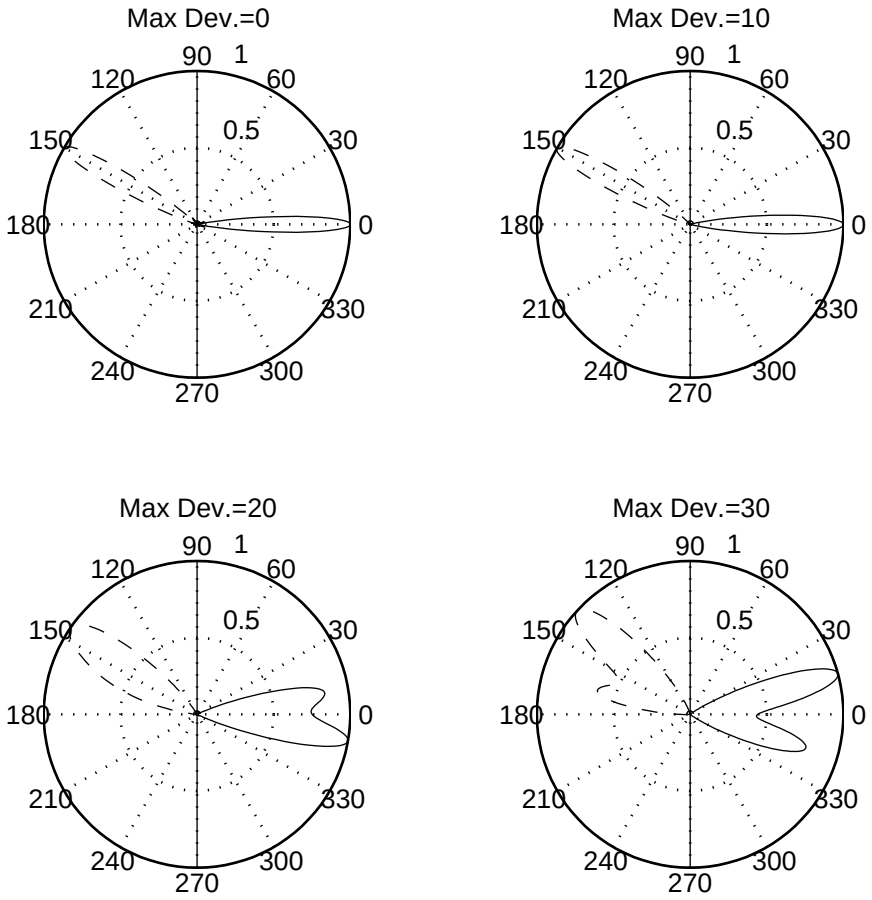

Figure 1.4: Beampatterns when maximizing the single-user, single-stream *average* gain with L propagation paths between transmitter and receiver. The right hemispheres show transmit beampatterns while the left hemispheres are for receive patterns. AoA and AoD values and their deviations are defined in Section 1.2.2.

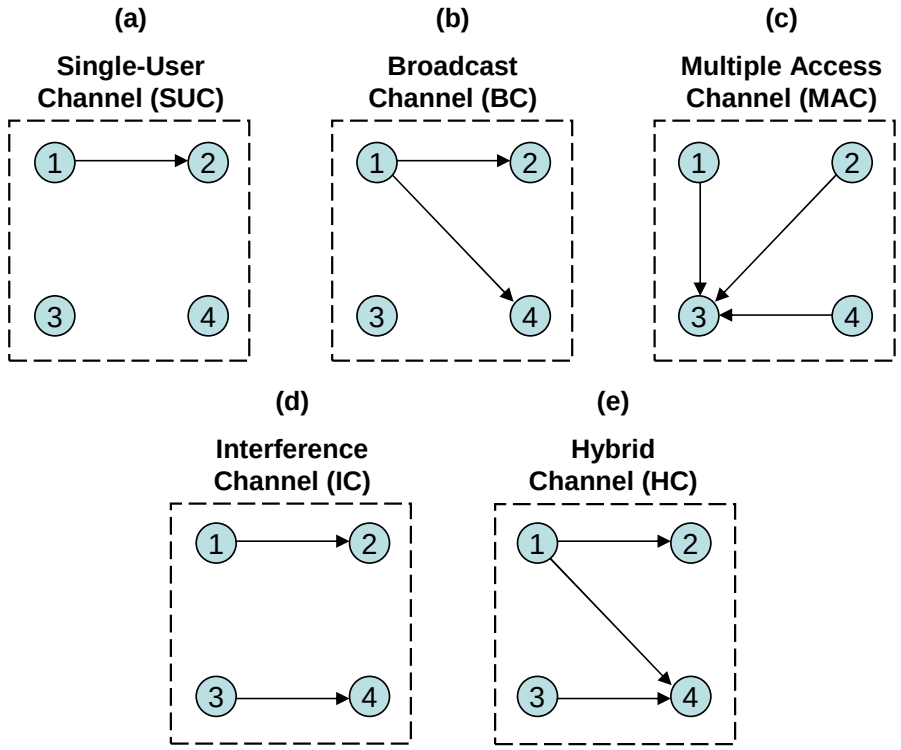

Figure 1.5: Various link topologies in a size $K = 4$ subnetwork which could be contained within a larger MANET or other network. Arrows represent single-stream but simultaneous transmissions between transmitters and receivers.

in this work:

- *single-user channel (SUC)* - Fig. 1.5(a) The standard, interference-free, point-to-point (P2P) transmission between a single transmitter and single receiver.
- *broadcast channel (BC)* - Fig. 1.5(b) A single transmitter sending individual and unique data to multiple receivers.
- *multiple-access channel (MAC)* - Fig. 1.5(c) Multiple transmitters sending simultaneously to a single receiver (not to be confused with the medium access control (MAC) layer).
- *interference channel (IC)* - Fig. 1.5(d) Multiple P2P connections which produce interference with each other if present.
- *hybrid channel (HC)* - Fig. 1.5(e) Multiple interfering and simultaneous BC and MAC links.

Each of the possible links in Fig. 1.5 consists of one or more sublinks representing a single data stream from one transmitting user to one receiving user. If a link contains multiple sublinks then each sublink will cause interference to all receivers attempting to decode. For example, the MAC link shown in Fig. 1.5(c) consists of three sublinks.

1.4 Nonlinear Processing

Though simple to implement and with relatively good performance, beamforming is often suboptimal in multi-user channels especially in the low SNR region when nulls cannot completely remove multiple-access interference (MAI). However, given enough degrees of freedom (i.e. number of antennas) beamforming can use spatial processing to null out interference while maintaining strong signal gain to the desired signal and additionally minimize interference to other users. When this

condition does not hold, beamforming will under-perform other, optimal, processing techniques at the cost of more expensive processing.

1.4.1 Dirty-Paper Coding (DPC)

Consider the simple broadcast channel that was shown in Fig. 1.5(b). In this channel, a single transmitter transmits unique and independent data simultaneously to all the intended receivers. Assume writing the received signal to the ith user generically as

$$\hat{s}_i = s_i + \sum_{j \neq i}^{K} s_j + \eta_i \tag{1.7}$$

where s_i is the desired symbol and all other symbols are treated as interference and specific details on the channel and input covariance matrices are omitted for clarity but will be described in detail further in this work. The idea behind DPC is that if the *transmitter* is aware of this interference it can successively remove interference for future encoded symbols using coding on the symbols themselves. Thus the new received symbol estimates will look like

$$\hat{s}_i = s_i + \sum_{j > i}^{K} s_j + \eta_i. \tag{1.8}$$

where the final encoded user sees no interference. Note that the difference between (1.7) and (1.8) may appear subtle but is vastly important for achieving maximum capacity of the broadcast channel. The first user/symbol that is encoded at the transmitter will be interfered with by all other users/symbols. The last encoding ensures that the only interference is generated by AWGN. The use of DPC certainly incurs additional overhead in processing but is necessary for optimal transmissions especially in the low SNR regimes.

1.4.2 Successive Interference Cancellation (SIC)

The dual to the broadcast channel is the multiple-access channel shown in Fig. 1.5(c). In this scenario multiple users are transmitting to a single receiver

who must be able to separate the incoming signals. Consider again writing the received signal at the receiver as the superposition of all interference and noise

$$y = \sum_{i}^{K} s_i + \eta. \tag{1.9}$$

where the differences between (1.9) (single received signal) and (1.7) (single received signal per user) is defined by the number of receivers. In theory, if the symbol s_i is transmitted at a rate below capacity then it can be detected perfectly assuming a large enough coding block size. Where DPC removes inter-user interference prior to transmission, SIC removes interference after detection. Thus, after detection, this decoded symbol can be subtracted as interference from all symbols that are decoded after it resulting in reduced total interference for each future decoded symbol. This method of detection in the MAC is referred to as successive interference cancellation (SIC) with received estimates written as

$$\hat{s}_i = s_i + \sum_{j>i}^{K} s_j + \eta \tag{1.10}$$

where the duality between MAC/BC and SIC/DPS is readily apparent. Analogous to DPC, this technique will also require additional processing and suffers from nonlinearities just as DPC did. Additionally, SIC is susceptible to error propagation as the criteria for perfect symbol detection is impossible for non-infinite block sizes.

The purpose of introducing these processing techniques now is to give the reader an idea of the general trade-offs that will be examined in this work. The nonlinear techniques such as DPC and SIC are optimal in a throughput sense but require additional processing requirements and assumptions at all nodes. Additionally, these optimal schemes will suffer more from inaccuracies in the channel state information upon which they rely. The linear processors, beamformers, will certainly take a loss in performance over the nonlinear counterparts as they trade-off complexity for optimality. Even with outdated CSI the beamformers can degrade as was visualized by moving into the nulls in the previous section. However, as was also shown, beamforming has the additional capability of trading off throughput gains with stability against mobility in the environment. This stability is the

focus of this work and provides for exciting future possibilities in correlation-based beamforming.

1.5 Dissertation Organization

The remainder of this dissertation delves deeper into the concepts presented in this introduction. In Chapter 2 a brief overview of the channel measurement capabilities used will be examined. This chapter also overviews a few popular channel models and occurrences in the system that can cause CSI to be "bad". Chapter 3 uses the measured channel samples directly to analyze the performance loss seen by linear and nonlinear processing at both the transmitter and receiver when outdated CSI is used. Motivated by this loss, Chapter 4 presents a beamforming technique that provides stable performance in the broadcast channel when receivers have perfect CSIR or imperfect CSIR while Chapter 5 examines the dual multiple-access channel with stable transception. The practicalities of CDI beamforming are addressed in Chapter 6 by parameterizing the distribution and reducing the amount of required feedback. Finally, the beamforming algorithm for any possible half-duplex, multi-user, scheduled, MIMO channel is presented in Chapter 7. Chapter 8 concludes the dissertation.

Chapter 2

The MIMO Channel: Measurements, Models, and Error

In order to simplify the overview on channel measurements[1] we focus on the multi-user broadcast channel; however, the discussion below can easily be adapted to any of the multi-user channels discussed in the introduction. The MIMO broadcast channel communication scenario of interest consists of a single transmitting node equipped with N_{t} antennas and K receiving nodes (users) each with N_{r} antennas. The $N_{\mathrm{r}} \times 1$ received vector for the jth user at time sample n can be expressed as

$$\mathbf{y}_j(n) = \mathbf{H}_j(n)\mathbf{x}_j(n) + \sum_{i \neq j}^{K} \mathbf{H}_j(n)\mathbf{x}_i(n) + \boldsymbol{\eta}_j(n) \tag{2.1}$$

where $\mathbf{H}_j(n)$ is the $N_{\mathrm{r}} \times N_{\mathrm{t}}$ matrix of channel transfer functions for user j, $\mathbf{x}_i(n)$ is the $N_{\mathrm{t}} \times 1$ signal vector destined for the i^{th} user, and $\boldsymbol{\eta}_j(n)$ is additive white Gaussian noise (AWGN). Equation (2.1) presumes no specific transmit precoding and is therefore appropriately modified later in the discussion of specific transmis-

[1]The work presented in this dissertation in its entirety is based on joint collaboration between the University of California, San Diego (UCSD) and Brigham Young University (BYU). However, the measurement data, as explained in this chapter, was taken by BYU prior to commencement of research results presented in this dissertation. The information provided in this chapter, in part, is for the reader's benefit and is not directly integral to work done by the author on the dissertation itself.

sion schemes. Ultimately, channel measurements or models produce instantiations of the channel in time $\mathbf{H}_j(n)$ based on some desired criteria while channel estimation errors produce a discrepancy between what a transmitter uses as input to precoding algorithms and what the state of the channel actually is.

The examination of different precoding and decoding strategies performed in this work considers both modeled channels – which allow a parametric evaluation over a variety of channel conditions but may not accurately represent the physical time-space evolution of the subspace – and measured channels which allow performance quantification over a limited set of realistic environments. This chapter details the models and measurements used to facilitate this study as well as methods of error introduced into estimated channel realizations.

2.1 Wideband Channel Sounding

To assess the loss in rate created by outdated CSIT and CSIR and, perhaps more importantly, to ensure that the beamforming algorithms based on CDIT and CDIR are effective in actual channels and not optimized for specified conditions that are assumed in a generalized channel model, performance analysis in this work will be partially accomplished using channel transfer functions obtained from experimental measurements. The equipment used for these measurements was designed, developed, and tested at Brigham Young University (BYU). The test equipment at BYU allows sampling of a single-user, point-to-point, mobile MIMO link with $N_{\mathrm{r}} = N_{\mathrm{t}} = 8$ antennas. At the the time this work was performed, the measurements could accommodate up to 100 MHz of instantaneous bandwidth at a center frequency between 2 and 8 GHz. Specific details of the measurement equipment are available in [5].

Prior to data collection, calibration measurements were taken with the transmitter "off" to measure background interference. At the chosen carrier frequency of between 2.45 and 2.55 GHz, the external interference was found to be below the noise floor in the environments considered. A second calibration per-

formed with both the transmitter and receiver "on" but stationary revealed that the time variation of the channel caused by ambient changes such as pedestrians, atmospheric conditions, and other natural disturbances was insignificant for the environments examined in this work.

The channel coefficients used in this analysis were measured with a stationary transmitter and a receiver moving at a constant pedestrian velocity ($\approx$ 30 cm/s). Since the channel is highly oversampled, with samples taken every 2.4-3.2 ms, data decimation or interpolation can be used to create any effective node velocity. After channel acquisition, each individual realization of the channel is normalized to have unit average SISO gain [6]. For a given transmitter location, measurements for different receiver locations were taken (using the same receiver velocity), with each location producing the channel matrix for one user in Eq. (2.1) for the simulated multi-user network. Since it was observed that channel time variation results almost exclusively from node movement, the superposition of these asynchronous measurements into a single synchronized multi-user channel seems reasonable. Throughout this work the term "measured channel" refers to channel coefficients acquired in this fashion.

The statistical space-time-frequency structure of the experimental MIMO channels has been well analyzed in the literature [7, 8], with ensemble averages over a variety of locations showing the coefficients to obey a complex Gaussian distribution (Rayleigh channel magnitudes) with spatial and temporal correlation functions that closely resemble those generated using the classic Jakes' model [6]. Because the transmit and receive spatial correlation matrices are used in the development of the transmit precoding strategy introduced in this work as well as the generation of modeled channel matrices, estimation of these matrices from the data is an important consideration. For example, the one-sided transmit correlation matrix estimated using N samples starting at sample n_0 can be written as

$$\mathbf{R}_{\mathrm{t},j}(n_0, N) = \frac{1}{NN_{\mathrm{r}}} \sum_{n=0}^{N-1} \mathbf{H}_j^H(n_0 + n)\mathbf{H}_j(n_0 + n) \tag{2.2}$$

where $\{\cdot\}^H$ is the matrix conjugate transpose. Similarly, the receive one-sided

correlation matrix estimate is

$$\mathbf{R}_{\mathrm{r},j}(n_0, N) = \frac{1}{NN_{\mathrm{t}}} \sum_{n=0}^{N-1} \mathbf{H}_j(n_0 + n)\mathbf{H}_j^H(n_0 + n). \tag{2.3}$$

The fact that the correlation matrices are functions of the starting channel index n_0 and length of the estimate N suggests that the channel is *not* stationary [9]. This nonstationarity is a mathematical manifestation of physical changes in the propagation environment created by changes in the angular characteristics of the propagation environment due to such effects as a node moving around a corner or the introduction of a mobile scatterer. However, drastic nonstationary effects occur on a time scale larger than the channel coherence time, and therefore values of N are chosen to remain within the channel stationarity time. Other statistical properties of the channel - which also must be estimated via the measured channel - will be introduced as needed in future sections.

2.1.1 Indoor

In order to provide results based on different environments this work will run simulations using datasets acquired from BYU from three different measurement campaigns. The first such set of measurements is referred to as "Indoor" and consists of channels measured inside the fourth floor of the Brigham Young University engineering building. The layout of this floor is found in Fig. 2.1. Transmit locations were set in the hallways while receivers were spread through the rooms and hallways of the floor and were moved at pedestrian speeds to measure time variability. Scatterers consist of typical objects found in an office environment: doors, walls, computers, lab equipment, utility fixtures, and so on.

As alluded to in Chapter 1, the distribution of the singular values plays an important role in system performance and multiplexing gains. Fig. 2.2 shows the time variation of the four strongest dominant singular values of the $N_{\mathrm{r}} = N_{\mathrm{t}} = 8$ channel transfer matrix as measured by the BYU equipment in the Indoor environment. Note that the trend in both singular value variation and distribution is consistent with intuition of an indoor environment. These office-like environments

Figure 2.1: Fourth floor schematic of the Brigham Young University engineering building. Measurements taken in this environment are referred to as "Indoor".

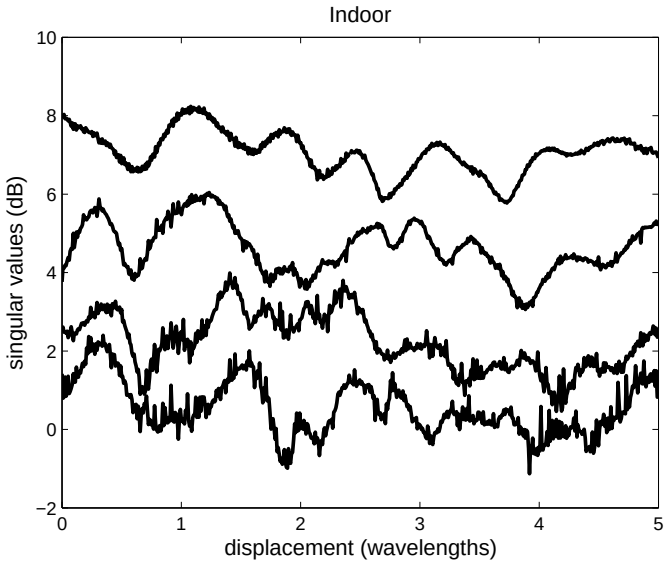

Figure 2.2: Singular value spread and variation in the "Indoor" environment. These measurements were taken with $N_{\mathrm{r}} = N_{\mathrm{t}} = 8$ antennas with the four largest singular values displayed.

will produce higher overall scatter resulting in tighter singular values as well as significant variation for relatively small movement.

2.1.2 Outdoor

A good dual to the rich scattering provided by the Indoor environment is an outdoor location with limited scattering. For these datasets the transmit and receive test equipment was situated upon a large playing field with a single large office building in the corner. An aerial shot of this geographical location is shown in Fig. 2.3 and was produced by the GoogleEarth software. Receiver locations were specifically placed near the large building in an attempt to get a single bounce multipath component to the channel. Otherwise, measurements were taken when the conditions could be considered mostly LOS. This environment will be referred to generically as "Outdoor" for purposes of this work.

Fig. 2.4 shows the same time variation of the four strongest dominant singular values of the $N_{\mathrm{r}} = N_{\mathrm{t}} = 8$ channel transfer matrix as was shown for

Figure 2.3: Overhead view of Deseret Towers field on the campus of Brigham Young University. Measurements taken in this environment are referred to as "Outdoor".

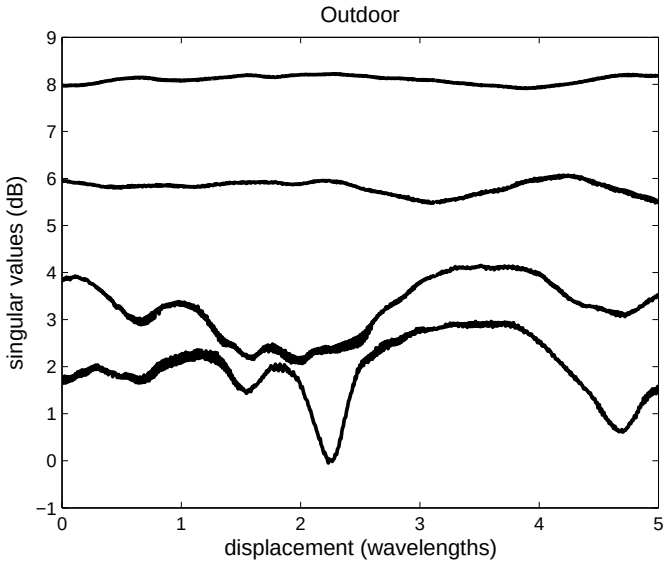

Figure 2.4: Singular value spread and variation in the "Outdoor" environment. These measurements were taken with $N_{\mathrm{r}} = N_{\mathrm{t}} = 8$ antennas with the four largest singular values displayed.

the Indoor channels. The trend in both singular value variation and distribution is significantly different than those shown for the Indoor datasets. The spread between singular values is much larger suggesting that there is a significant LOS component in the channel. Furthermore, the temporal variation of the values is much lower than for Indoor. Though the temporal variation appears stable one cannot immediately assume that stable transmission is possible in this case. For example, the angular deviation of the corresponding singular vectors of the dominant singular value will certainly be highly varying. Though a thorough analysis of the time-varying MIMO channel is beyond the scope of this work, the interested reader may refer to BYU's, and other's, work done on analyzing the measured MIMO channel [7, 10–13].

2.1.3 Urban

Finally, a rough combination of the Indoor and Outdoor channels will also be examined throughout this work a photo of which appears in Fig. 2.5. This

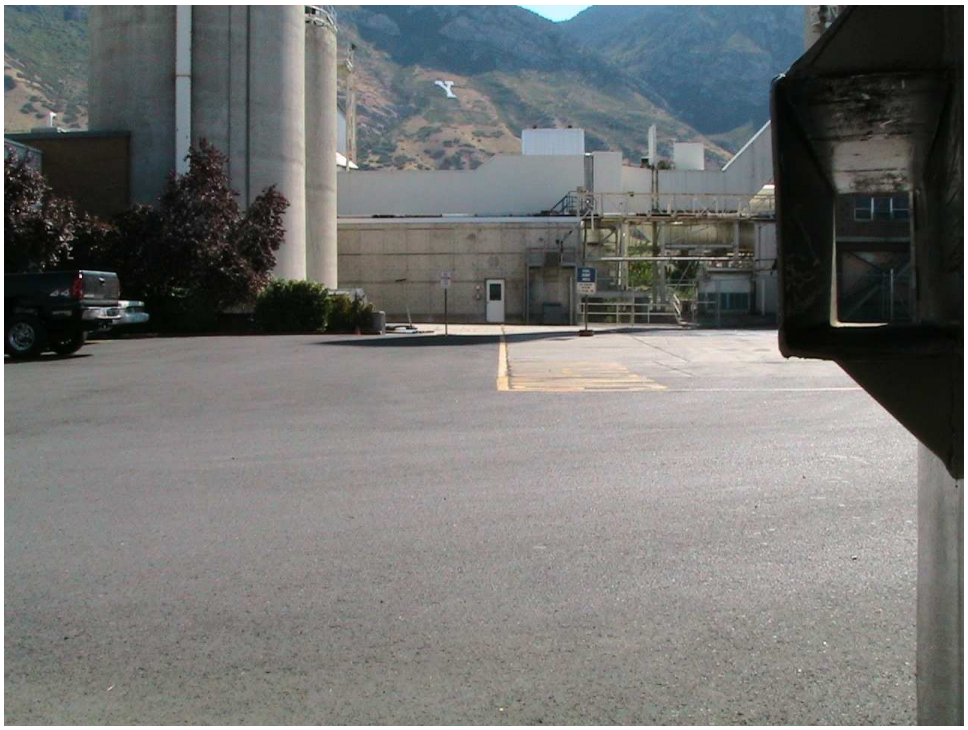

Figure 2.5: Photo of the Brigham Young University coalyard. Measurements taken in this environment are referred to as “Urban”.

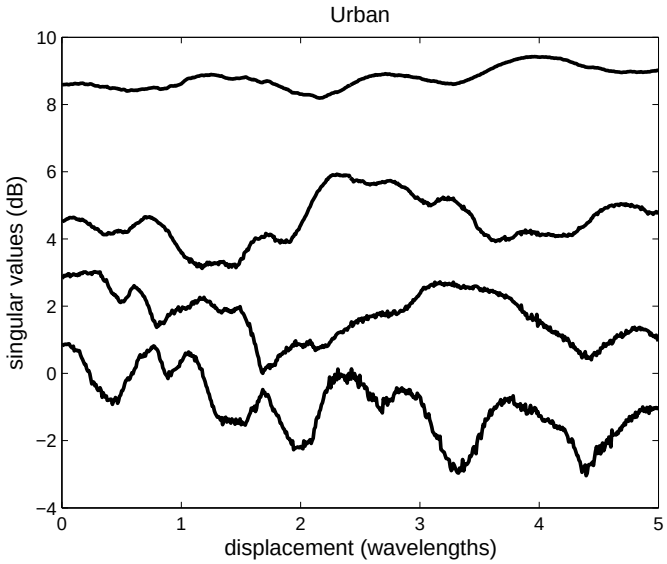

Figure 2.6: Singular value spread and variation in the "Urban" environment. These measurements were taken with $N_{\mathrm{r}} = N_{\mathrm{t}} = 8$ antennas with the four largest singular values displayed.

last environment is located near the coalyard on BYU campus which is tightly surrounded by buildings of varying sizes and shapes and will be referred to as "Urban" when used in further discussions. Additionally, a parking lot dominates the open spaces of the test environment which will further increase the possibility of scattering and multipath. Like the Indoor and Outdoor environments the transmitter is fixed during channel sampling while the receiver is moved at pedestrian velocities. At the time of writing this dissertation the exact configurations for all the environments regarding transmitter/receiver locations and paths travelled can be found at the BYU Wireless Communications Research lab webpage http://ece.byu.edu/wireless/.

Fig. 2.6 is the resulting four strongest singular vectors of the 8×8 time-varying, channel matrix. Note that the behavior demonstrated here has contributions from both the Indoor and Outdoor environments. Like Indoor, the Urban channel has high temporal variation due to abundant local scattering. However, there also exists a strong LOS component to the channel that is shown by the spread in the largest singular value.

In addition to the observations shown thus far for the three types of environments under consideration, these figures provide some foresight into processing with correlation -based beamforming. In an environment where all users experience similarly high scattering, it is most likely that the spatial correlation properties of all users will be similar. Thus the "average" behavior of the channel is the same and we can guess that multiple-access to the channel will be more difficult. With at least some LOS component the user correlation is "different" enough that multiple users accessing the channel simultaneously can be taken care of spatially even in an average sense. The effects of correlation on the multi-user channel will be examined in more detail later.

2.2 Random Matrix Models

Because effective multi-antenna transmit precoding strategies exploit spatial structure, as well as instantaneous knowledge, in the channel, it is important that the channel models used accurately reflect this spatial information. The spatial correlation of the transfer matrix, which is created by the angular properties of the multipath propagation as well as the antenna configuration, is a common mechanism for capturing this spatial structure in the model. Merging the use of channel measurements and models is a straightforward method of easing analysis of complex systems while maintaining realistic properties of the wireless channel. Thus, when a model is used in this work, the spatial correlation defining that model is estimated directly from the measured data resulting in a method that can also provide many more channel realizations than are available when strictly using measurements. Though numerous channel models exist that attempt to accurately describe the channel [4, 14, 15], this work focuses on the three random matrix models described in this section.

2.2.1 Spatial Correlation Model

Accurately modeling spatial and temporal correlation in the multi-user MIMO broadcast channel is facilitated by measurements taken at BYU. Post-processing on the dataset is performed to estimate the full spatial correlation matrix for the jth user (i.e. dataset) over M channel samples

$$\mathbf{R}_j = \frac{1}{M}\sum_{m=1}^{M} \mathrm{vec}\left(\mathbf{H}_j(m)\right) \mathrm{vec}\left(\mathbf{H}_j(m)\right)^H \tag{2.4}$$

where $\mathbf{H}_j(m)$ is integer indexed sample m into the measured data.

Once $\mathbf{R}_j$ has been estimated for each user, new channels can be realized using a temporal correlation model and the full measured correlation matrix

$$\mathbf{H}_j(t) \;=\; \sqrt{\frac{N_\mathrm{r}N_\mathrm{t}}{\mathrm{tr}(\mathbf{R}_j)}}\mathrm{mat}\left\{\sqrt{\mathbf{R}_j}\mathrm{vec}(\mathbf{H}_w(t))\right\} \tag{2.5}$$

where $\mathrm{tr}(\cdot)$ is the matrix trace, and the normalizing constant forces channel realizations to have unit-norm single-input single-output (SISO) gain. $\mathbf{H}_w(t)$ is a spatially white $N_\mathrm{r} \times N_\mathrm{t}$ matrix, where N_t and N_r are the number of transmit and receive antennas per user, respectively, and that satisfy some temporal correlation.

This spatial correlation model is often used as a benchmark to other models as it most accurately generates channel samples with the same distribution as the true underlying channel, assuming Gaussian channel coefficients, and will be referred to as the "full" correlation or just correlation model. In fact, whenever simulations are performed using the "modeled" channel, as referred to in this work, then the full spatial correlation model is used. However, the amount of parameters required for this model is immense which motivates other models that reduce the number of parameters but maintain good representation of the channel itself.

2.2.2 Kronecker Model

The Kronecker model [16] assumes separability between transmit and receive spatial correlation matrices. Using this mechanism, the channel matrix at

time t for the jth user can be generated as

$$\mathbf{H}_j(t) = \sqrt{\mathbf{R}_{\mathrm{r},j}}\mathbf{H}_{\mathrm{w}}(t)\sqrt{\mathbf{R}_{\mathrm{t},j}} \tag{2.6}$$

where $\mathbf{H}_{\mathrm{w}}(t)$ is the same temporally correlated random matrix used for the correlation model, $\mathbf{R}_{\mathrm{r},j}$ and $\mathbf{R}_{\mathrm{t},j}$ are the $N_{\mathrm{r}} \times N_{\mathrm{r}}$ and $N_{\mathrm{t}} \times N_{\mathrm{t}}$ receive and transmit correlation matrices, respectively, for the jth user as estimated from the measured data using (2.2) and (2.3), and the square root operation on some positive semi-definite matrix $\mathbf{Z}$ is defined as $\sqrt{\mathbf{Z}}\sqrt{\mathbf{Z}} = \mathbf{Z}$. There is some debate on the accuracy of the Kronecker model because the model has been verified for a small number of antennas in [17] while deficiencies in the model for a larger number of antennas have been identified in [18]. The application of interest in this work is a mobile ad hoc network (MANET) in which all nodes are equally equipped with a small number of antennas; however, the effects of Kronecker model assumptions will be demonstrated later.

2.2.3 Weichselberger Model

The Weichselberger model [19] was introduced in an effort to overcome some of the deficiencies discovered with the Kronecker model. The Kronecker model deficiencies arise from imposing one-sided correlations on the spatial structure of the channel which result in underestimation of the channel capacity [18]. Under the Weichselberger model, channel matrix realizations are represented as

$$\mathbf{H}_j(t) \;=\; \mathbf{U}_{\mathrm{r}}(\check{\mathbf{\Omega}} \odot \mathbf{H}_w(t))\mathbf{U}_{\mathrm{t}}^T$$

where $\check{\mathbf{A}}$ is the element-wise square root on the matrix $\mathbf{A}$ and the matrices $\mathbf{U}_{\mathrm{r}}$ and $\mathbf{U}_{\mathrm{t}}$ respectively contain the eigenvectors of $\mathbf{R}_{\mathrm{r}}$ and $\mathbf{R}_{\mathrm{t}}$ from the Kronecker model. $\mathbf{H}_w(t)$ is, again, the same spatially-white time-varying matrix used as for the correlation and Kronecker models. Note that the main difference between the Kronecker and Weichselberger models is the coupling matrix $\mathbf{\Omega}$ used to describe power coupling between transmit and receive link ends. This approach allows the Weichselberger model to cover a larger population of possible environments by

mitigating the separability assumption of the Kronecker model resulting in better modeling (the Kronecker model is a subset of the Weichselberger model when the coupling matrix is set to all ones).

2.2.4 Temporal Correlation Model

The channel model used must also ensure that the channel samples possess the proper relationship in time. This can be accomplished by properly representing the temporal correlation between channel samples for sample spacings smaller than the channel coherence time. This work assumes the temporal correlation function model suggested by Jakes [20] which is given by

$$\rho_d(\tau) = J_0(2\pi f_d \tau) \tag{2.7}$$

where $J_0(\cdot)$ is the zeroth-order Bessel function of the first kind and f_d is the normalized Doppler frequency. For simulation purposes a sum of eight weighted sinusoids is used in Jakes' model with the specified normalized Doppler taken into account to produce the temporal correlation in (2.7). There are close similarities between the temporal correlation of Jakes' model and that seen with the measured data.

The channel model realizes both spatially and temporally correlated channel coefficients by exchanging $\mathbf{H}_{\mathrm{w}}(t)$ in (2.5) (2.6) (2.7) with the time-varying coefficients generated from Jakes' model with the Doppler frequency f_d in (2.7) chosen to match that of the measured channel. Throughout this work, the term "modeled channel" refers to a sequence of channel matrices generated using this procedure with the full correlation model. When an analysis is performed not directly related to temporal variation or correlation then the modeled channel replaces $\mathbf{H}_w(t)$ with $\mathbf{H}_w$ a strictly, i.i.d. random, Gaussian matrix.

2.3 Channel Knowledge Error

Though significant gains are guaranteed when CSI is perfectly known, significant loss can also occur when assumed channel estimates are erroneous at the

receiver or additional delay occurs when beamforming weights are fed back to the transmitters. Such errors in the channel can occur when limited training is used for channel estimation or when node mobility happens with infrequent training and feedback. This channel error has the possibility to significantly degrade the performance of the entire system [21] and negate the theoretical rates given for the MIMO multi-user channel as shown in this current work. One method of combating the effects of erroneous CSI is to develop beamforming techniques that use no CSI for processing [22] though it is important to first identify the degradation of CSI-based schemes with channel knowledge errors.

Throughout this analysis assume that multiple user training is orthogonalized such that channel estimation can be performed on the virtual single-user channel. Thus, the user index on the channel matrix will be dropped for channel knowledge error analysis.

2.3.1 Channel Estimation Error

For channel estimation purposes assume that a single transmitter transmits a known training sequence $\mathbf{S}$ of length $N_\mathrm{t} \times L$ resulting in received signal

$$\mathbf{Y} = \mathbf{HS} + \boldsymbol{\eta} \tag{2.8}$$

where $\boldsymbol{\eta}$ is an $N_\mathrm{r} \times L$ additive white Gaussian noise (AWGN) matrix with per-element variance σ_n^2 and time indices are dropped under the assumption that the channel remains constant over the length of the training sequence. Furthermore, the channel is assumed to be estimated under the maximum-likelihood (ML) method with time-division multiple access during training [23], satisfying

$$\hat{\mathbf{H}} = \mathbf{YS}^\dagger \tag{2.9}$$

$$\mathbf{SS}^H = \frac{L}{N_\mathrm{t}}\mathbf{I} \tag{2.10}$$

where $\hat{\mathbf{H}}$ is the channel estimate, $\mathbf{I}$ is the identity matrix, $(\cdot)^\dagger$ is the matrix pseudo-inverse, and power per training time is held to unity. Though exploitation of the spatial correlation is possible to improve channel estimates [24], this work assumes

no such knowledge is available under the CSI-based schemes and the simple ML estimate will be used given the training sequence. For this method of channel estimation the mean square error for $\tau = 0$ (i.e. no delay between the channel estimate and current channel) becomes $\frac{\sigma_{\mathrm{n}}^2 N_{\mathrm{r}} N_{\mathrm{t}}^2}{L}$ and is not a function of the spatial correlation.

2.3.2 Temporal Variation

Additionally, we examine errors in the channel estimate caused by lag between training sequences and data detection at the receiver or data encoding at the transmitter. The quantity in this case is the mean square error (MSE) between the channel at time t and some estimate at time $t - \tau$ when the initial channel estimate is perfect

$$\mathrm{tr}(E\left[\mathbf{E}(t,\tau)\mathbf{E}^H(t,\tau)\right]) = 2(1 - J_0(2\pi f_d \tau))N_{\mathrm{r}}N_{\mathrm{t}} \tag{2.11}$$

where $\mathbf{E}(t,\tau) = \mathbf{H}(t) - \mathbf{H}(t-\tau)$ and the channel random process is assumed wide-sense stationary (WSS). Note that error caused by temporal variation is also not a function of the spatial correlation given the choice of ML channel estimation and temporal model. This lack of dependence on the spatial correlation is easily seen by examining a single cross-term in the MSE expression

$$\begin{aligned} E\left\{\mathrm{vec}\left[\mathbf{H}(t)\right]^H \mathrm{vec}\left[\mathbf{H}(t-\tau)\right]\right\} &= \mathrm{tr}E\left\{\mathrm{vec}\left[\mathbf{H}\left(t\right)\right]\mathrm{vec}\left[\mathbf{H}(t-\tau)\right]^H\right\} \\ &= \mathrm{tr}\left\{\frac{N_{\mathrm{r}}N_{\mathrm{t}}}{\mathrm{tr}(\mathbf{R})}\sqrt{\mathbf{R}}\left(J_0(2\pi f_d\tau)\mathbf{I}\right)\sqrt{\mathbf{R}}\right\} \\ &= N_{\mathrm{r}}N_{\mathrm{t}}J_0(2\pi f_d\tau) \end{aligned} \tag{2.12}$$

where temporally- and spatially-correlated channel samples are defined as in (2.5).

Given these two sources of errors introduced into the channel, the final channel estimation error will be modeled as

$$\hat{\mathbf{H}} = \rho_d(\tau)\mathbf{H} + \sqrt{1-\rho_d^2(\tau)}\mathbf{N}_1 + \sigma_e\mathbf{N}_2 \tag{2.13}$$

where $\sigma_e^2 = \frac{\sigma_{\mathrm{n}}^2 N_{\mathrm{t}}}{L}$, $\mathbf{N}_1$ and $\mathbf{N}_2$ are random matrices with unit-norm complex Gaussian entries representing the worse-case error scenario, and time indices are dropped

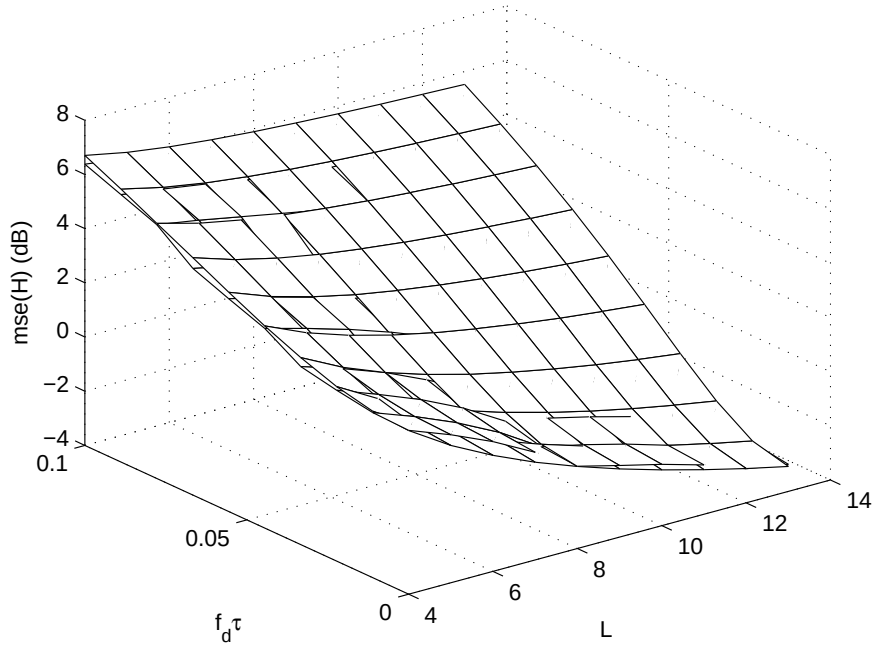

Figure 2.7: Channel estimation mean-square error, mse($\hat{\mathbf{H}}$), as a function of training length L and relative delay $f_d\tau$. The simulation was performed with noise power $\sigma_n^2 = .1$ and $N_\mathrm{t} = N_\mathrm{r} = 4$ antennas.

as the error model is assumed a function of: delay, training length, and noise power. With this model of the error estimate the mean-squared error becomes

$$\mathrm{mse}(\hat{\mathbf{H}}) = 2N_\mathrm{r}N_\mathrm{t}(1 - J_0(2\pi f_d\tau)) + \frac{\sigma_\mathrm{n}^2 N_\mathrm{r}N_\mathrm{t}^2}{L}. \tag{2.14}$$

Figure 2.7 shows a plot of the channel error as a function of both the training length as well as delay between channel estimation and channel use in signal processing. For this plot the noise power is fixed at $\sigma_\mathrm{n}^2 = .1$ and nodes are equipped with $N_\mathrm{t} = N_\mathrm{r} = 4$ antennas. The relative delay is given by the product $f_d\tau$. It is important to note that the independent variables in the figure L and $f_d\tau$ can be considered the training length and training frequency, respectively. Increasing the training length improves channel estimates significantly unless the delay between training is large at which point there will be an error floor regardless of the length of training sequence. Plotted with the analytically derived MSE (2.14) is a simulated MSE validating the channel estimation model.

The work presented in this chapter, in part, was originally published in the following papers, of which the author was also main contributor: A. L. Anderson, J. R. Zeidler, and M. A. Jensen, "Instantaneous and average rate maximization in MIMO multiple-access channels (MAC) with linear processing," in *42nd Asilomar Conf. Signals, Systems and Computers*, Pacific Grove, CA, Oct. 2008; A. L. Anderson, J. R. Zeidler, and M. A. Jensen, "Performance of transmit precoding in time-varying point-to-point and multi-user MIMO channels," in *Conference Record of the IEEE Asilomar Conference on Circuits, Systems and Computers*, Nov. 2006.

Chapter 3

Time-Varying MIMO Channel Analysis

Time variation of the wireless MIMO channel can be a limiting factor in the system throughput, particularly for signaling schemes which require the availability of accurate CSIR and/or CSIT. This time variation can be created by alterations in the scattering environment itself or by mobility of the communicating nodes. Performance loss due to time variation is closely related to the impact of channel estimation error, as studied in [25, 26] and the previous chapter, and is examined in more detail here pertaining to overall system performance degradation.

This chapter summarizes the single-user metrics provided in [12] and utilizes the same analysis to describe performance loss in single- and multi-user channels. Specifically, the achievable rate degradation is studied for the SUC, BC, and MAC when outdated CSI is used to perform optimal or suboptimal processing at the transmitters and/or receivers. Results based on measured data reveal the well-known duality between the MAC and BC [2] when applied to erroneous CSI, namely that while any scheme suffers severe performance loss with outdated CSIR, including the MAC, outdated CSIT in the BC also creates severe and rapid loss in achievable rate. Additionally, the metrics from [12] are used to examine the influence of power availability on capacity with outdated CSI in the SUC which

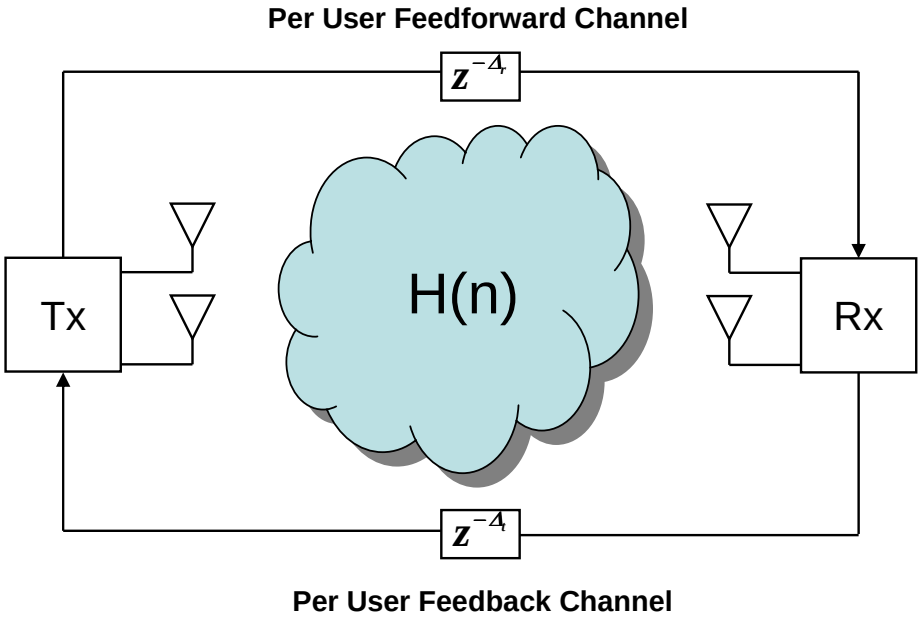

Figure 3.1: A virtual channel knowledge exchange system where the transmitter(s) has channel knowledge of all users delayed by Δ_{t} samples from the current channel and the receiver(s) has individual channel knowledge delayed by Δ_{r} samples from the current channel. All nodes are assumed to have $N_{\mathrm{t}} = N_{\mathrm{r}}$ antennas.

influences multi-user channel behavior. It is shown that increased power benefits a single-user link with outdated CSIT, while, with severely outdated CSIR an increase in power can actually degrade overall system performance. In addition to the optimal schemes analyzed in this chapter, a transmit precoding scheme is addressed which uses no CSI that provides insight into the ultimate goal of finding a precoder that is less susceptible to temporal variations in the channel.

3.1 Single-User Analysis

An integral part of the analysis for time-varying MIMO channels is the delay effect on channel knowledge passing at both transmitters and receivers. Fig. 3.1 shows a diagram of the virtual feedforward and feedback links representing the conveyance of delayed channel information between the transmitters and receivers. For precoding purposes, the transmitter has access to all users' channel matrices

delayed by Δ_{t} samples from the current time. Similarly, during decoding, the receivers possess a channel realization or receive beamforming vector that is delayed Δ_{r} samples from the current channel. We emphasize that the feedforward path simply represents a model for accounting for the delay Δ_{r}, and that the true delay mechanism would be a finite interval between training events combined with network overhead and channel estimation errors. Thus, the feedforward and feedback "channels" as shown in Fig. 3.1 are simply graphical tools in describing the error introduced in the time-varying MIMO channel and do not represent any actual implementation scheme. However, given the additional delay for CSIT that would be incurred for feedback, it is logical to assume that $\Delta_{\mathrm{t}} \geq \Delta_{\mathrm{r}}$ with equality in the ideal, instantaneous feedback case. Other than these delays, the channel estimates and feedback communication are considered error-free; the effects of channel estimation error due to limited training is not examined in this chapter as the focus is on analyzing the measured MIMO channel itself.

Given the virtual system described by Fig. 3.1, consider writing the single-user, narrowband, received signal vector for a P2P link with multiple antennas at the transmitter and receiver as

$$\mathbf{y}^{\mathrm{SUC}} = \widetilde{\mathbf{H}}\mathbf{x} + \mathbf{E}(\Delta_{\mathrm{r}})\mathbf{x} + \boldsymbol{\eta} \tag{3.1}$$

where $\mathbf{x}$ is the Gaussian input vector, $\mathbf{Q}(\Delta_{\mathrm{t}}) = \mathrm{E}\{\mathbf{x}\mathbf{x}^H\}$ is the input covariance matrix with emphasis on its functional dependence of CSIT delayed by Δ_{t} samples, $\mathbf{E}(\Delta_{\mathrm{r}})$ is the self-interference caused by inaccurate CSI due to node mobility. If $\mathbf{H}$ represents the actual channel to the receiver and $\widehat{\mathbf{H}}(\Delta_{\mathrm{n}})$ is outdated CSI used to construct the precoder ($\Delta_{\mathrm{n}} = \Delta_{\mathrm{t}}$) or decoder ($\Delta_{\mathrm{n}} = \Delta_{\mathrm{r}}$), then the error $\mathbf{H} - \widehat{\mathbf{H}}(\Delta_{\mathrm{n}}) = \mathbf{E}_{\mu} + \mathbf{E}(\Delta_{\mathrm{n}})$ where $\mathbf{E}_{\mu}$ is the mean of the error and $\mathbf{E}(\Delta_{\mathrm{n}})$ is a zero-mean random matrix. Finally, $\widetilde{\mathbf{H}} = \widehat{\mathbf{H}}(\Delta_{\mathrm{n}}) + \mathbf{E}_{\mu}$.

With outdated CSIT but no CSIR error or delay (e.g. $\Delta_{\mathrm{t}} > 0, \Delta_{\mathrm{r}} = 0$) the capacity - maximum mutual information - of a single-user MIMO link given the optimal input covariance matrix calculated by the inaccurate CSIT is

$$C_{\mathrm{t}} = \log \left| \mathbf{I} + \mathbf{H}\hat{\mathbf{Q}}\mathbf{H}^H \right| \tag{3.2}$$

where $\mathbf{I}$ is the identity matrix and $\hat{\mathbf{Q}} = \mathbf{Q}(\Delta_{\mathrm{t}})$ is used to emphasize that the input covariance matrix was calculated using CSIT acquired from a previous location $\widehat{\mathbf{H}}(\Delta_{\mathrm{t}})$. If no knowledge of the channel is used at the transmitter then the uninformed transmit capacity can be written as

$$C_{UT} = \log \left| \mathbf{I} + \frac{P}{N_{\mathrm{t}}} \mathbf{H}\mathbf{H}^{H} \right| \tag{3.3}$$

where equal power is split between all sub-channels. As the channel estimate becomes more and more outdated the transmit capacity will tend to approach the uninformed transmit capacity [12].

If erroneous CSIR is included with the received signal (3.1), a lower bound on the mutual information between input and output can be written as (see Appendix A)

$$I^{\mathrm{SUC}}(\mathbf{x}; \mathbf{y}|\widetilde{\mathbf{H}}) \geq \log \left| \mathbf{I} + \widetilde{\mathbf{H}}^{H} \left(\mathbf{I} + \mathbf{\Psi}_{E}^{Q} - \mathbf{\Psi}_{E_{\mu}}^{Q} \right)^{-1} \widetilde{\mathbf{H}}\mathbf{Q} \right| \tag{3.4}$$

where $\mathbf{E}_{\mu} = \mathrm{E}[\mathbf{E}]$. For convenience in both single- and multi-user analyses we use the shorthand $\mathbf{\Psi}_{\mathbf{V}}^{\mathbf{U}}$ to define the transform on some covariance matrix $\mathbf{U}$ with $\mathbf{V}$

$$\mathbf{\Psi}_{\mathbf{V}}^{\mathbf{U}} = \mathrm{E}\left[\mathbf{V}\mathbf{U}\mathbf{V}^{H} \right]. \tag{3.5}$$

In [25] it was shown that (3.4) is a tight bound for zero mean, i.i.d. channel error and most values of SNR and number of antennas, though no assumption is made about the distribution of channel estimation errors in this current work. Throughout this chapter, maximization of (3.4) will be referred to as an achievable rate of the channel or a capacity loss when compared with the true capacity of the channel.

A parameter that arises with outdated CSI, and needs to be evaluated in order to calculate capacity loss, is the weighted correlation matrix of the estimation error $\mathbf{\Psi}_{E}^{Q}$. This quantity represents the self-interference caused by using outdated CSI at the receiver and can be estimated using the measured data. With a small abuse of notation, consider the error term doubly indexed over the starting distance n in addition to the differential displacement Δ_{n}

$$\mathbf{E}(\Delta_{\mathrm{n}}) = \mathbf{E}(\Delta_{\mathrm{n}}, n) = \mathbf{H}(n + \Delta_{\mathrm{n}}) - \mathbf{H}(n). \tag{3.6}$$

Using (3.5) and (3.6) the correlation for the error term can be written as

$$\mathbf{\Psi}_E^Q = \mathrm{mat}\left\{ \frac{1}{N-\Delta_\mathrm{n}} \left(\sum_{n=1}^{N-\Delta_\mathrm{n}} \mathbf{E}^*(\Delta_\mathrm{n}, n) \otimes \mathbf{E}(\Delta_\mathrm{n}, n) \right) \mathrm{vec}(\mathbf{Q}) \right\} \tag{3.7}$$

where $\otimes$ is the matrix Kronecker product, n is an integer representing channel sample index and the output quantity is implicitly a function of Δ_n. The function $\mathrm{vec}(\cdot)$ is the matrix column stacking operator while $\mathrm{mat}(\cdot)$ is its inverse (e.g. $\mathrm{mat}(\mathrm{vec}(\mathbf{A})) = \mathbf{A}$). To reiterate, (3.7) is implicitly a function of node displacement but will be not written so in order to preserve clarity in future expressions.

The separation of the random error with the input covariance in (3.7) is justified by using a property of the Kronecker product $\mathrm{mat}(ABC) = \mathrm{mat}([C^T \otimes A]\mathrm{vec}(B))$ and the linearity of expectation. This is extremely useful as the error statistics can be calculated offline without any foreknowledge of future input covariance values. Though (3.7) is a function of distance, it will be assumed that the receiver knows the statistics for each possible displacement in the dataset. Further note that (3.7) and (3.5) are not equivalent due to the non-stationarity of the data and finite sample sizes, though they share the same notation in order to avoid confusion in the capacity expressions.

Similar to (3.7), the mean of the channel error can also be estimated from the channel samples. This is accomplished for some node displacement n with

$$\mathbf{E}_\mu = \frac{1}{N/n} \sum_{j=0}^{N/n-1} \mathbf{H}_i([n+1]j+n+1) - \mathbf{H}_i([n+1]j+1). \tag{3.8}$$

Again, (3.8) is not equivalent to the expected value of the error, but will be used for convenience in working with the measured data; the user indices can be dropped for the single-user channel.

It should be stated that knowledge of (3.7) and (3.8) is necessarily more information than simply CSI; however, this analysis is focused on determining the time variation of achievable rates and not necessarily the feasibility of achieving these rates. In order to achieve the following bounds additional methods of channel knowledge acquisition would need to be employed; such topics are beyond the scope of this work.

3.1.1 Transmit CSI Delay (TCD)

Transmit CSI delay (TCD) measures the change in mutual information when attempting to perform optimal signaling based on erroneous channel estimates at the transmitter and perfect CSIR. The mutual information expression (3.4) defined in the previous section is "maximized" according to the nodes' belief in, and availability of, their channel information. For TCD, it is assumed that the receiver has perfect CSI while the transmitter is unaware of the current channel or the statistics of the channel error. In other words, TCD will affect the input covariance matrix $\mathbf{Q}$ but will not have self-interference at the receiver: $\mathbf{\Psi}_E^Q = \mathbf{\Psi}_{E_\mu}^Q = 0$ in (3.4). It is interesting to note that TCD does not necessarily degrade from the capacity at the initial displacement. For example, if the channel estimate occurs at the end of a fade, then the TCD capacity is likely to be greater as the nodes move and the channel improves. However, the average trend with TCD is a reduction in achievable rate. The distance at which the achievable rate of outdated CSIT approaches the capacity of the uninformed transmitter is called d_{T}.

3.1.2 Receive CSI Delay (RCD)

Receive CSI delay (RCD) affects the loss in achievable information rate as nodes move and CSI at both the transmitter and the receiver becomes outdated. For this case, the transmitter will perform suboptimal signaling since knowledge of the channel is outdated and knowledge of the interference is unavailable. Such knowledge is necessary in order to maximize the mutual information even with outdated CSIT. The receiver will cause self-interference by attempting to decode the signal with a channel estimate that does not match the current channel realization: $\mathbf{\Psi}_E^Q \geq 0$. The distance at which the capacity drops to 50% of maximum is defined as d_R.

3.1.3 Effectiveness of Precoding U_{T}

Both TCD and RCD will be used to describe the sensitivity of throughput to channel knowledge in single- and multi-user channels. However, it is worthwhile to first examine the effectiveness of transmit precoding in the single-user channel which is determined by the contributing factors of: node mobility, transmit power, number of transmit antennas N_{t}, number of receive antennas N_{r}, and so on. This effectiveness of CSIT can be written, using the defined capacity metrics, as

$$U_{\mathrm{T}} = \frac{C_{\mathrm{T}}}{C_{UT}} - 1 \tag{3.9}$$

where, for the single-user case, the numerator comes from (3.2) and the denominator from (3.3). Equation 3.9 will be zero when channel knowledge does not increase capacity over the uninformed transmitter and $U_{\mathrm{T}} = 1$ when the available rate is doubled. Equation 3.9 can also become negative when the outdated channel knowledge is such that using it is actually detrimental and lowers the capacity below C_{UT}.

Figure 3.2 plots single-user U_{T} in the Indoor, Outdoor, and Urban environments for perfect CSIT and delayed CSIT at SNRs of 3 and 20 dB, respectively. The plots in Fig. 3.2(a) use perfect CSIT while Fig. 3.2(b) results show performance loss when transmitters use CSIT displaced by approximately three wavelengths or a fraction of a meter. This outdated CSIT is equivalent to erroneous CSIT and hence the effectiveness of channel knowledge drops. Note that for all environments the effectiveness of CSIT is reduced as the the number of available receiver antennas increases. This satisfies intuition since receive nodes with more degrees of freedom are better able to recover the signal and obviate the need for CSI at the transmitter. Conversely, more antennas at the transmitter provides mode possible spatial processing thus increasing the utility of CSIT as long as accuracy can remain high. CSIT is more important for power constrained systems which is confirmed by noting that the optimal input covariance matrix approaches the scaled identity (i.e. equivalent optimal input covariance for the uninformed transmitter) as power is increased. Environmentally, the LOS, Outdoor channel has more effective CSIT than the other locations due to the low variability in the

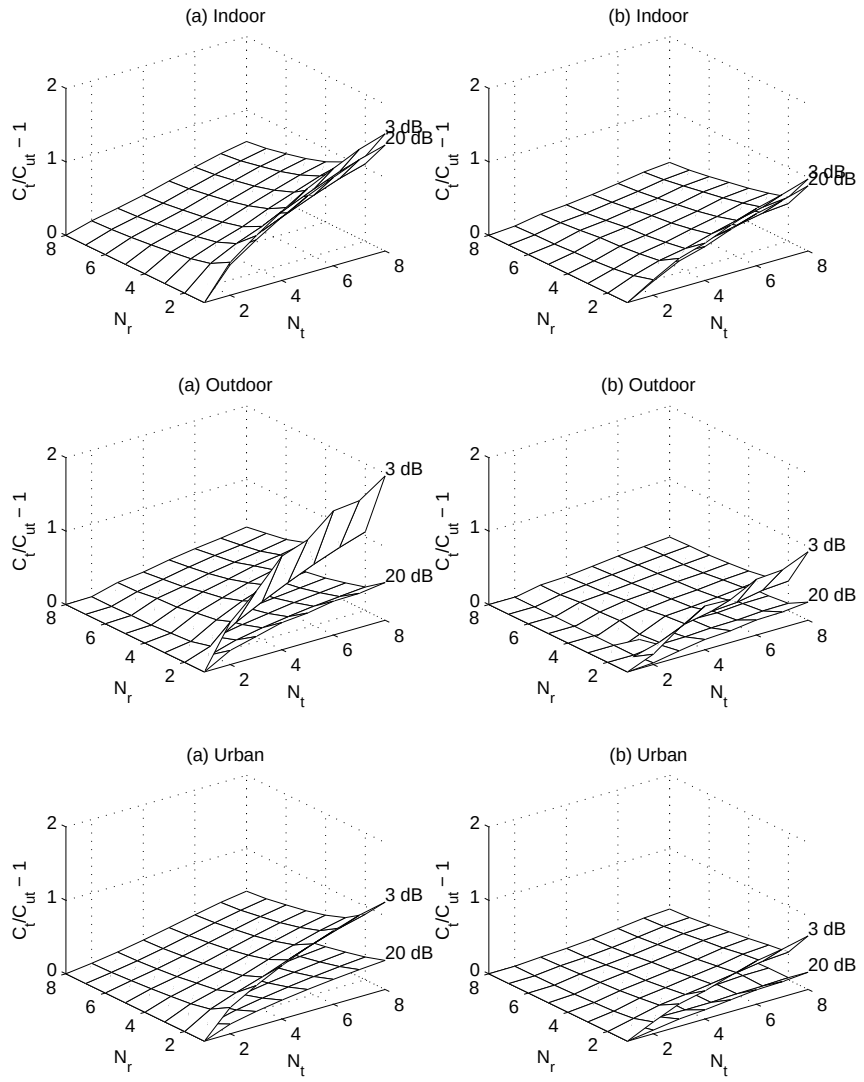

Figure 3.2: Effectiveness of transmit precoding, U_{T}, when using capacity-achieving input covariance matrices for (a) perfect CSIT at zero displacement and (b) CSIT delayed by three wavelengths for N_{t} transmit antennas and N_{r} receive antennas.

channel even with large lags.

3.2 Multi-User Analysis

Multi-user channels promise additional gains over the single-user channel by adding an additional dimension of user selection and multiple, concurrent channel access to the system. For the MIMO BC, a precoding technique so-called "dirty-paper coding" (DPC) maximizes the sum-capacity of the BC [2, 27] for stationary applications. DPC is a non-linear algorithm that is considered computationally complex for standard systems [28] though is optimal in a sum-rate sense. Conversely, successive-interference cancellation (SIC) is an optimal detection scheme for the MIMO MAC but suffers from possible error propagation if a user is decoded incorrectly. As suggested in Chapter 1, these schemes have an intuitive sensitivity to outdated CSI that will be analyzed in this chapter.

3.2.1 BC with DPC

Nonlinear dirty-paper coding [2] is optimal in the sense that it maximizes the sum mutual information (and therefore sum capacity) when the transmitter and receivers have perfect CSI. DPC is often considered infeasible in practice [28] but will be analyzed as a benchmark for other precoding algorithms throughout this work.

The impact of channel estimation error in a two-user SISO channel using DPC was analyzed in [26]. As an extension, consider the case of DPC in a MIMO channel when user ordering is not optimized at the transmitter, where user 1 is encoded first, user 2 second, and so on. At the transmitter, the DPC algorithm attempts to successively presubtract interference from previously encoded users, while the receiver uses its delayed channel knowledge for detection. In [26] the authors refer to DPC as "naive" when only presubtracting interference with the given channel estimates; this same naive approach to DPC will be used for the

MIMO case. As an example, consider the received vector for the first encoded user

$$\mathbf{y}_1^{\mathrm{DPC}} = \widetilde{\mathbf{H}}_1\mathbf{x}_1 + \mathbf{E}_1(\Delta_{\mathrm{r}})\sum_{i=1}^{K}\mathbf{x}_i + \widetilde{\mathbf{H}}_1\sum_{i=2}^{K}\mathbf{x}_i + \boldsymbol{\eta}_1 \tag{3.10}$$

where $\boldsymbol{\eta}_1$ is AWGN at the first receiver and channel and error terms are as defined by the single-user case (3.1) with the addition of indices indicating the specific user. Note that the first interference term is caused strictly by having erroneous CSIR while the second interference term is a direct result of being encoded first in the DPC scheme (all other users' messages will interfere with user 1). The received vector for the second user becomes

$$\mathbf{y}_2^{\mathrm{DPC}} = \widetilde{\mathbf{H}}_2\mathbf{x}_2 + \mathbf{E}_2(\Delta_{\mathrm{r}})\sum_{i=2}^{K}\mathbf{x}_i + \mathbf{E}_2(\Delta_{\mathrm{t}})\mathbf{x}_1 + \widetilde{\mathbf{H}}_2\sum_{i=3}^{K}\mathbf{x}_i + \boldsymbol{\eta}_2 \tag{3.11}$$

where the additional interference arises from the transmitter only being able to remove the known portion of the signal encoded for user 1.

Continuing in a similar manner, for a precoded transmit vector $\mathbf{x}_j$ destined for the jth user, the resulting receive vector for the jth user can be written as

$$\mathbf{y}_j^{\mathrm{DPC}} = \widetilde{\mathbf{H}}_j\mathbf{x}_j + \overbrace{\mathbf{E}_j(\Delta_{\mathrm{r}})\sum_{i=j}^{K}\mathbf{x}_i}^{\text{outdated CSIR}} + \overbrace{\mathbf{E}_j(\Delta_{\mathrm{t}})\sum_{i=1}^{j-1}\mathbf{x}_i}^{\text{outdated CSIT}} + \widetilde{\mathbf{H}}_j\sum_{i=j+1}^{K}\mathbf{x}_i + \boldsymbol{\eta}_j. \tag{3.12}$$

Since we cannot assume that the transmitter knows any information about $\mathbf{E}_j(\Delta_{\mathrm{n}})$, we consider the worst-case scenario where it is modeled as a zero mean Gaussian matrix whose variance grows with delay Δ_{t} or Δ_{r}. Despite the fact that time indices are dropped for clarity, it is important to recognize that the received vector is a function of the delay in channel feedback and/or error in channel estimation. Eq. (3.12) highlights those portions of the interference in the received signal that are caused by delayed channel knowledge.

The exact mutual information for the transmit and received vectors in (3.12) is unknown, and therefore the lower bound suggested in [25] will be adapted for use in the broadcast channel to include the additional interference terms shown in Eq. (3.12). Details of this analysis appear in Appendix B, with the result that the

mutual information for user j is bounded by

$$\begin{aligned} I^{\mathrm{DPC}}(\mathbf{x}_j;\mathbf{y}_j|\widetilde{\mathbf{H}}_1\ldots\widetilde{\mathbf{H}}_K) &\geq \log\left|\mathbf{I}+\widetilde{\mathbf{H}}_j^H\left(\mathbf{I}+\mathbf{Z}_j\right)^{-1}\widetilde{\mathbf{H}}_j\mathbf{Q}_j\right| \\ \mathbf{Z}_j &= \boldsymbol{\Psi}_{\mathbf{E}_{\mathrm{r},j}}^{\sum_{i=j}^{K}\mathbf{Q}_i}+\boldsymbol{\Psi}_{\mathbf{E}_{\mathrm{t},j}}^{\sum_{i=1}^{j-1}\mathbf{Q}_i}+\boldsymbol{\Psi}_{\widetilde{\mathbf{H}}_j}^{\sum_{i>j}\mathbf{Q}_i} \end{aligned} \tag{3.13}$$

where $\mathbf{x}_j$ are assumed to be independent Gaussian inputs and $\mathbf{E}_{\mathrm{t},j}=\mathbf{E}_j(\Delta_{\mathrm{t}})$ are used for simplicity as explained in Appendix B. The sum mutual information used for analysis in this work is then

$$C^{\mathrm{DPC}}(\Delta_{\mathrm{r}},\Delta_{\mathrm{t}})=\sum_{j=1}^{K}I_{\mathrm{DPC}}\left(\mathbf{x}_j;\mathbf{y}_j|\widetilde{\mathbf{H}}_1\ldots\widetilde{\mathbf{H}}_K\right) \tag{3.14}$$

where $C_{\mathrm{DPC}}(\Delta_{\mathrm{r}},\Delta_{\mathrm{t}})$ is implicitly a function of the input covariance matrices $\mathbf{Q}_j$. For the simulations in this work, the input covariance matrices are found by naively applying iterative water-filling using the duality of the multiple-access channel and broadcast channel [2] based on the known portions of CSIT. This implies that when $\Delta_{\mathrm{t}}=\Delta_{\mathrm{r}}=0$ (i.e. no channel error or delay), (3.14) reduces exactly to the sum capacity of the broadcast channel, but when $\Delta_{\mathrm{t}},\Delta_{\mathrm{r}}\geq 0$ additional performance loss will be seen in the system due to suboptimal input covariances.

3.2.2 MAC with SIC

The MAC or uplink channel consists of K users transmitting simultaneously to a single receiver. Analogous to DPC at the transmitter, the receiver can successively cancel interference (SIC) after a user has been decoded as long as that user is transmitting below its per-user capacity. Thus the ith user will see no interference from the jth user for $i>j$. The received signal vector for the MAC, $\mathbf{y}^{\mathrm{MAC}}$, when using SIC is the superposition of all transmitted signals, self-interference, and noise

$$\mathbf{y}_j^{\mathrm{MAC}}=\widetilde{\mathbf{H}}_j\mathbf{x}_j+\overbrace{\sum_{i=1}^{K}\mathbf{E}_i(\Delta_{\mathrm{r}})\mathbf{x}_i}^{\text{partial removal}}+\overbrace{\sum_{i=j+1}^{K}\widetilde{\mathbf{H}}_i\mathbf{x}_i}^{\text{uncanceled}}+\boldsymbol{\eta} \tag{3.15}$$

where the subscript j corresponds to the virtual received signal for the jth user after SIC has been performed on all previous users. In order to maximize throughput

and successfully decode all users the receiver needs to know the channel of all transmitting users as well as statistics of the error terms. Given the received signal (3.15), the same approach taken for finding the bound on mutual information in the BC, found in Appendix B, can be used for the MAC with SIC

$$\begin{aligned} I^{\mathrm{MAC}}(\mathbf{x}_j;\mathbf{y}_j|\widetilde{\mathbf{H}}_1\ldots\widetilde{\mathbf{H}}_K) &\geq \log\left|\mathbf{I}+\widetilde{\mathbf{H}}_j^H\left(\mathbf{I}+\mathbf{Z}_j\right)^{-1}\widetilde{\mathbf{H}}_j\mathbf{Q}_j\right| \\ \mathbf{Z}_j &= \sum_{i=1}^{K}\mathbf{\Psi}_{\mathbf{E}_{\mathrm{r},i}}^{\mathbf{Q}_i}+\sum_{i=j+1}^{K}\mathbf{\Psi}_{\widetilde{\mathbf{H}}_i}^{\mathbf{Q}_i} \end{aligned} \tag{3.16}$$

where the same assumptions are made in finding the bound. For completeness the sum-rate of the system for outdated CSI becomes

$$C^{\mathrm{MAC}}(\Delta_{\mathrm{r}},\Delta_{\mathrm{t}})=\sum_{j=1}^{K}I^{\mathrm{MAC}}\left(\mathbf{x}_j;\mathbf{y}_j|\widetilde{\mathbf{H}}_1\ldots\widetilde{\mathbf{H}}_K\right) \tag{3.17}$$

where $C^{\mathrm{MAC}}(\Delta_{\mathrm{r}},\Delta_{\mathrm{t}})$ is also implicitly a function of the input covariance matrices $\mathbf{Q}_j$ and channel estimates for all users.

The metrics defined in [12] and reiterated in the previous section can easily be extended to the multi-user channel by merely changing single-user capacity to sum-rate or sum-capacity. However, multi-user channels introduce an added dimension to the time-variation problem which produce interesting results for capacity degradation with nodal displacement. For example, simple suboptimal encoding schemes can out perform optimal transmission at small displacements. This implies that a single encoding/decoding strategy is not sufficient to fully characterize the time variation of the multi-user channels. Since the focus of this work is also on the sensitivity of optimum transmission policies, we will focus on suboptimal solutions as well for analysis purposes.

3.2.3 Linear Processing (LP)

Though a detailed discussion on beamforming would be out-of-place this early it the discussion, it is worthwhile to examine a suboptimal transmission/detection scheme that uses the spatial degrees of the channel, rather than specific coding, in

order to reduce MAI via linear processing (LP). For this suboptimal scheme, all users will be interfered with by all other users and no pre- or post-subtraction of the signal will be used at either transmitter or receiver in either the MAC or BC. Specifically, we want to look at the effect that CSIT has on the transmitter in the BC and the dual effect of CSIR in the MAC. The BC achievable rate with this approach proceeds by simply removing the successive subtraction of interference that DPC provides

$$C^{\text{BC-LP}} = \sum_{i=1}^{K} \log \frac{\left|\mathbf{I} + \mathbf{H}_i^H \left(\sum_{j=i}^{K} \mathbf{Q}_j\right) \mathbf{H}_i\right|}{\left|I + \mathbf{H}_i^H \left(\sum_{j\neq i}^{K} \mathbf{Q}_j\right) \mathbf{H}_i\right|} \tag{3.18}$$

where there are no error terms as a consequence of perfect CSIR; all performance degradation is directly a result of suboptimal input covariance values.

Similarly, the analysis of interest is the effect of outdated CSIR on MAC decoding. Using the same approach as BC-LP of removing all canceling interference terms, the lower bound on mutual information with outdated CSIR and linear processing becomes

$$C^{\text{MAC-LP}} = \log \frac{\left|\mathbf{I} + \sum_{i=1}^{K} \left(\mathbf{\Psi}_{\widetilde{\mathbf{H}}_i}^{\mathbf{Q}_i} + \mathbf{\Psi}_{\mathbf{E}_{\text{r},i}}^{\mathbf{Q}_i}\right)\right|^K}{\prod_{i=1}^{K} \left|\mathbf{I} + \sum_{j=1,j\neq i}^{K} \mathbf{\Psi}_{\widetilde{\mathbf{H}}_i}^{\mathbf{Q}_j} + \sum_{k=1}^{K} \mathbf{\Psi}_{\mathbf{E}_{\text{r},k}}^{\mathbf{Q}_k}\right|}. \tag{3.19}$$

This expression for mutual information considers all signals besides the desired signal as interference for the current decoded signal.

Equations (3.19) and (3.18) are non-convex functions and need to be solved numerically. For the purpose of this analysis, these expressions are maximized suboptimally assuming the input covariances represent water-filling solutions of their respective virtual channels by including MAI from all other signals.

3.2.4 Time-Sharing (TS)

Perfect time-sharing (TS) completely removes MAI by forbidding users to access the channel at the same time. In fact, the optimal TS policy only allows the single user with the best channel to ever transmit - with potential of producing

an unbalanced and severely delay-constrained network. In this study, we instead look at "fair" TS where each user is given an equal amount of time accessing the channel. Since TS is essentially a SUC averaged over all users, the achievable rates for the MAC and BC are similar in form

$$C^{\text{BC-TS}} = \frac{1}{K}\sum_{i=1}^{K}\log\left|\mathbf{I}+\mathbf{H}_i^H\hat{\mathbf{Q}}_i\mathbf{H}_i\right| \tag{3.20}$$

$$C^{\text{MAC-TS}} = \frac{1}{K}\sum_{i=1}^{K}\log\frac{\left|\mathbf{I}+\mathbf{\Psi}_{\tilde{\mathbf{H}}_i}^{\mathbf{Q}_i}+\mathbf{\Psi}_{\mathbf{E}_i}^{\mathbf{Q}_i}\right|}{\left|\mathbf{I}+\mathbf{\Psi}_{\mathbf{E}_i}^{\mathbf{Q}_i}\right|} \tag{3.21}$$

where MAC-TS (3.21) is the average single-user channel with outdated CSIR/CSIT and BC-TS (3.20) is the average rate with perfect CSIR and outdated CSIT. The performance resulting from these expressions should not be compared with each other since outdated CSIR will obviously cause a more drastic capacity loss. The BC-TS mutual information (3.20) is instead intended to be used as a benchmark on which to compare DPC and BF. Furthermore, the TCD distance d_{T} will be redefined for the BC as the distance in which DPC capacity drops below TS or BF for either channel.

3.3 Performance Loss Results

The results in this section are derived from measurements taken from the custom-built MIMO channel sounder at BYU as described in Chapter 2. In Fig. 3.3 the effects on capacity loss are shown for the single-user, Urban channel with (a) outdated CSIT, (b) outdated CSIR and both cases versus increasing power. For perfect CSIR, an increase in power leads to growth in capacity, as expected, even when channel knowledge at the transmitter is not perfect. This is not true, however, for outdated CSIR resulting from node movement or other environmental changes discussed in the previous chapter. The achievable rate drops quickly regardless of power and approaches some asymptotic value far below the true capacity. In fact, at certain displacements, the capacity actually *decreases* with power. To further exacerbate the problem, the RCD distance d_R is a decreasing

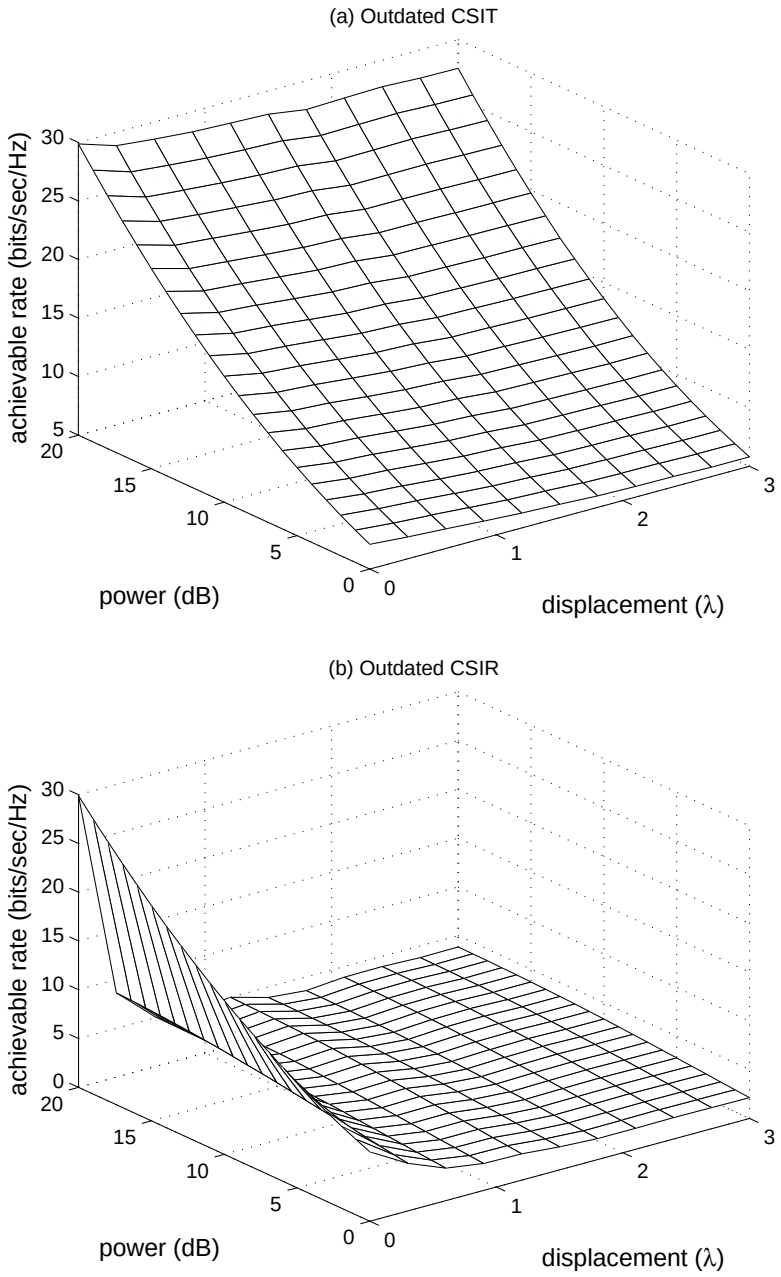

Figure 3.3: Maximum achievable rate for outdated (a) CSIT and (b) CSIR with varying available power in the single-user channel. In (b), at a displacement of 1λ, the rate at 20dB power is less than at 10dB.

function versus power, meaning link efficiency will degrade faster for higher power. Knowledge of the time-scale at which additional power is not beneficial is essential for transmitters to preserve the scarce resources of the network.

For MAC and BC experimental analysis the use of measured data for a three-user network (four nodes total) is used. Fig. 3.4 displays achievable rate for the three-user broadcast channel with various environments and precoders analyzed in this chapter. For the LP curve a suboptimal algorithm is used that attempts to maximize (3.19) constrained to water-filling matrices as explained in Section 3.2.3. For the Urban and Indoor environments, at fractions of a wavelength the optimal transmission strategy, DPC, is outperformed by both suboptimal BC-LP and BC-TS even when CSIR is perfect. Though not shown, the inclusion of outdated CSIR would result in a TCD distance that is much smaller showing additional sensitivity to mobility.

Fig. 3.5 demonstrates the capacity degradation versus displacement for the MAC when either CSIT is outdated or channel knowledge is outdated at both transmitter and receiver. Again, it is important to note that the MAC-LP curves do not represent optimum beamforming, rather, they consider the case when SIC is not used at the receiver and are included in the analysis to demonstrate the loss of optimal precoding. The MAC exhibits a similar behavior in performance loss versus distance for CSIT and CSIR as the SUC. However, a distinction between the MAC and SU behavior is the distance at which partial CSIT is beneficial to the overall throughput; using some sort of CSIT is almost always better than uninformed transmissions. It is interesting to note that SIC always outperforms MAC-BF and MAC-TS regardless of the delay in CSIR or CSIT. This suggests that in MAC situations the receiver should always attempt to perform optimum decoding. Fig. 3.6 shows the same CSIR curves as the number of users increases from one (single-user channel) to three users. The RCD metric distance tends to decrease with number of users, implying that the throughput efficiency of the system may drop to unacceptable levels for small node mobility. It should be noted that, in this case, the absolute sum-capacity is still greater for a higher number of users, though the efficiency is less.

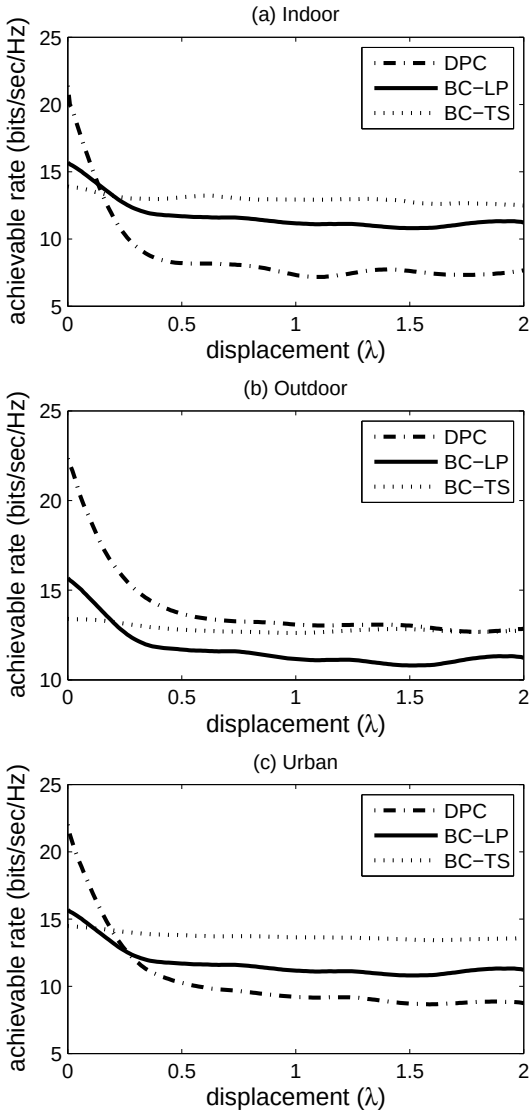

Figure 3.4: $K = 3$ user broadcast channel with $N_r = N_t = 8$ antennas and capacity degradation for DPC, BC-LP, and BC-TS as CSIT goes out-of-date and CSIR remains perfect. The metric d_{T} is the distance at which the optimum scheme DPC falls below TS.

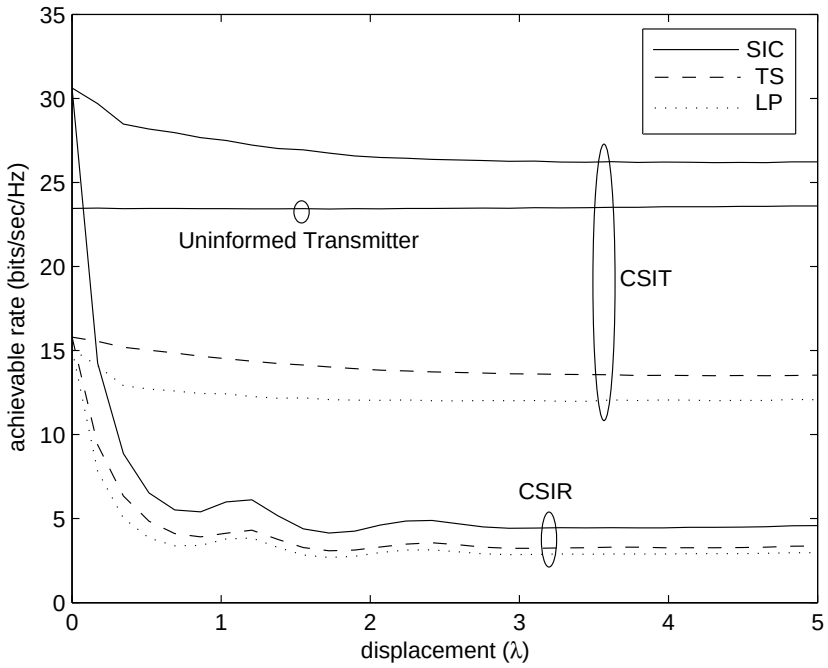

Figure 3.5: $K = 3$ user multiple-access channel with $N_r = N_t = 8$ antennas as CSIT and CSIR go out-of-date.

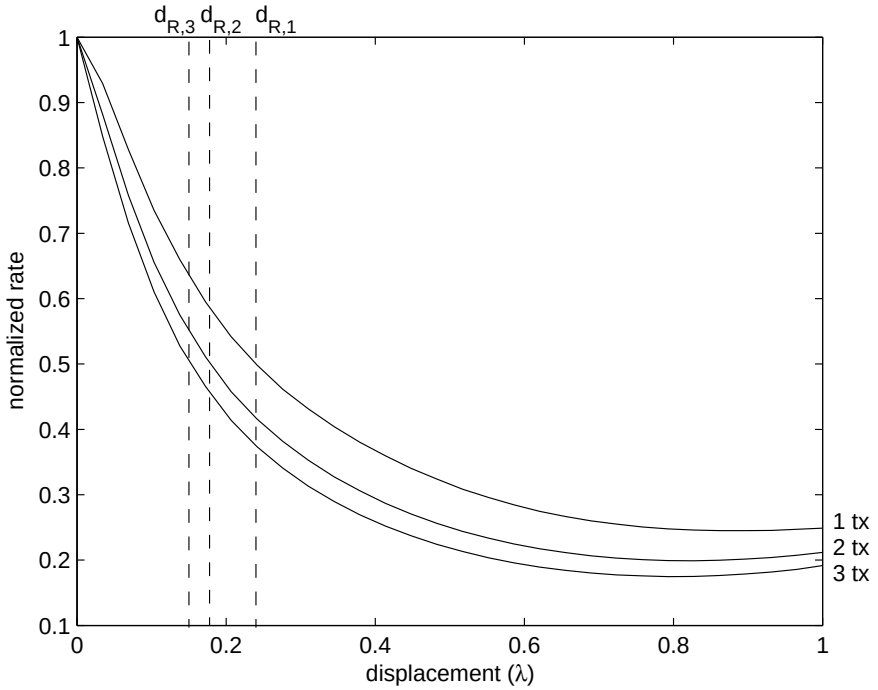

Figure 3.6: Vertical lines denote the RCD distances $d_{R,i}$ in which the achievable rate drops to 50% of capacity for $i = 1, 2, 3$ transmitters, respectively, in the multiple-access channel. The single-user case is $i = 1$.

The concluding message of this chapter is apparent - bad CSI almost always forces poor results in single- and multi-user channels in any environment. Specifically, the optimal coding strategies for the BC and MAC result in severe rate loss when naively assuming the channel is perfect at all nodes. If a node is forced to use CSI without knowledge of its' datedness then performance loss in inevitable. The next chapters focus on novel approaches to pre- and post-processing on the signal in order to provide stable performance with some initial loss in maximum throughput. The channel spatial correlation and statistical characterization of the MIMO channel will play an important role in these techniques.

The work presented in this chapter, in part, was originally published in the following papers, of which the author was also the main contributor: A. L. Anderson, J. R. Zeidler, and M. A. Jensen, "Reduced-feedback linear precoding with stable performance for the time-varying MIMO broadcast channel," *IEEE Journal on Selected Areas of Communications, (Special Issue on Limited Feedback)*. Vol. 26, No. 8, 11 pages, October, 2008; A. L. Anderson, J. R. Zeidler, and M. A. Jensen, "Performance of transmit precoding in time-varying point-to-point and multi-user MIMO channels," in *Conference Record of the IEEE Asilomar Conference on Circuits, Systems and Computers*, Nov. 2006.

Chapter 4

Stable Transception in the MIMO Broadcast Channel

As results from the time-varying MIMO channel analysis showed, though temporal diversity gains enabled by channel time variation further increase system performance, this temporal variation typically implies that outdated CSI estimates are used to construct the signaling strategy, resulting in capacity degradation [11,12] that is analogous to that created by channel estimation errors [25,26]. These same effects of channel estimation errors and Doppler sensitivity in practical precoding systems were shown in [29,30] to contribute significantly to performance loss. These observations motivate the development of transmission schemes which are robust to physically-realistic channel variations. Regarding this effort to reduce the sensitivity to CSI quality, recent research has suggested the formation of transmit beamformers using channel distribution information (CDI) at the transmitter (CDIT) [31, 32], a strategy which is optimal in an ergodic capacity sense under certain antenna correlation conditions. An adaptive beamformer that uses both CSI and CDI is suggested in [33] where capacity degradation from outdated CSI occurs in a time division duplex (TDD) MIMO system with a spatially correlated Jakes' channel.

Similar work for the multi-user MIMO channel has focused more on the

effects of channel estimation errors than the impact of outdated CSI created by channel time variation. For example, for the SISO broadcast channel, a scheduling strategy was proposed in [34] to combat the effects of channel estimation error. Furthermore, capacity regions for the MIMO broadcast channel with erroneous CSIT and CSIR are found in [35] using the duality between the broadcast and multiple-access channels [36]. The work in [26] uses error statistics for the sum-capacity-optimal DPC [2] to determine when time-sharing outperforms DPC in the MISO broadcast channel. A similar study for erroneous CSIT was also performed for the computationally simpler zero-forcing DPC (ZF-DPC) in [37] using capacity bounds similar to those presented in [25].

This chapter builds on the existing understanding to study the behavior of different CSIT-based transmit precoding techniques [28] in the time-variant multi-user BC. The study considers DPC, linear beamforming, and time-sharing techniques. While numerous beamforming algorithms exist for various design criteria [28, 38, 39] we focus on the beamforming algorithm that maximizes capacity for a MIMO broadcast channel (for linear precoding) as defined in [28] which is an extension of the algorithm in [40] for MISO channels. The TS scheme removes MAI and the need for CSIT by assigning each user a unique time slot for channel access and using the optimal signaling strategy for an uninformed transmitter. The analysis of these schemes begins with simulations based on accepted models for the spatially-correlated time-variant channel [16,20]. However, since these models may not capture the complex physical structure of the multi-user time-variant MIMO channel [41], the results obtained using the models are reinforced using simulations with experimentally-obtained channels [9] taken in an outdoor environment on the Brigham Young University (BYU) campus [6, 12]. Motivated by the performance degradation observed for the existing signaling schemes, this chapter develops and analyzes an iterative beamforming algorithm that has similar performance to the capacity optimal beamformer when used with CSIT and provides stable throughput performance when constructed with CDIT. The stable performance offered by this algorithm implies the existence of slowly-varying subspaces in the time-varying multi-user MIMO channel.

4.1 Regularized Channel Inversion (RCI)

Linear transmit precoding, or beamforming, uses linear preprocessing to mitigate multi-user interference in an effort to optimize various communication parameters [28]. Because this chapter considers techniques which maximize the sum mutual information, we will consider the rate-maximizing RCI technique found in [28, 42]. This algorithm assumes a single data stream is transmitted to each user unless the user has been excluded from channel access. Allowing multiple streams per user is straightforward and only adds complexity to the beamforming algorithm; however, for the "square" systems (equal number of transmit and receive antennas) considered in this work, the beamformers almost always choose a single stream per user even when given the option of multiple streams. Including these multiple streams does provide additional performance; however, multi-stream gains are marginal for the channels considered and will therefore be omitted for clarity. The received signal vector for user j is then

$$\mathbf{y}_j = \mathbf{H}_j \mathbf{b}_j(\Delta_\mathrm{t}) \mathbf{x}_j + \mathbf{H}_j \sum_{i \neq j}^{K} \mathbf{b}_i(\Delta_\mathrm{t}) \mathbf{x}_i + \boldsymbol{\eta}_j \tag{4.1}$$

where $\mathbf{b}_j(\Delta_\mathrm{t})$ is the transmit beamforming vector calculated using the RCI algorithm from the channel knowledge delayed by Δ_t samples. It is assumed that each user only has knowledge of their individual channel matrix and the transmit weights assigned to all streams; thus, receive beamforming weights $\mathbf{w}_j(\Delta_\mathrm{r})$ are calculated at each node using the MMSE criterion based on the channel knowledge delayed by Δ_r samples and transmit weights delayed by Δ_t samples. The significance of this formulation is that all error introduced by inaccurate CSI is contained within the transmit and receive beamforming vectors taking on suboptimal values.

Application of this linear processing reduces the system to a single stream per user with mutual information given by

$$I^{\mathrm{BF}}(\mathbf{x}_j; \mathbf{y}_j | \rho_j) = \log\left(1 + \rho_j\right) \tag{4.2}$$

where

$$\rho_j = \frac{|\mathbf{w}_j^H \mathbf{H}_j \mathbf{b}_j|^2}{1 + \sum_{i \neq j} |\mathbf{w}_j^H \mathbf{H}_j \mathbf{b}_i|^2} \tag{4.3}$$

where noise power is assumed unity and throughput degradation arises from using outdated beamforming vectors on the current channel. When the RCI algorithm excludes a user from the channel, the weight vector $\mathbf{b}_i$ becomes zero and equivalently $\rho_i = 0$. For completeness with all the other precoding strategies examined thus far, one can write the total expected rate given the outdated beamforming weights as

$$C^{\mathrm{BF}} = \sum_{j=1}^{K} I^{\mathrm{BF}} \left[\mathbf{x}_j; \mathbf{y}_j | \rho_j\right]. \tag{4.4}$$

It is shown in [42] that the weights which maximize the sum-rate from (4.4) in a broadcast channel with linear preprocessing have the form

$$\mathbf{B} = \left(\frac{\mathrm{tr}(\mathbf{D})}{P}\mathbf{I} + \mathbf{H}^{*}\mathbf{D}_j\mathbf{H}\right)^{-1}\mathbf{H}^{*}\mathbf{\Lambda}$$

where $\mathbf{B} = [\mathbf{b}_1, \ldots, \mathbf{b}_K]$ is the matrix of beamforming weights for each user, $\mathbf{\Lambda}$ and $\mathbf{D}$ are diagonal weighting matrices [42], and each row of $\mathbf{H}$ represents the channel for each of the individual MISO channels. An iterative procedure was shown in [42] that guarantees convergence to a local maximum of the sum-rate. Note that the only input parameter to the RCI algorithm is the channel transfer matrix for each user.

Some comments are necessary regarding the capacity maximizing MISO RCI beamforming algorithm. In [28], this technique was used with multiple receive antennas by iteratively performing the algorithm while updating the receiver beamformer with MMSE weights, although no proof of optimality was made. Indeed, varying the initial condition of the diagonal weight vectors can produce different solutions. Since the beamforming weights are, in form, capacity optimal for the MISO channel and have the structure of a regularized channel inversion, it will be used as the rate-maximizing beamformer for the MIMO channel with linear processing.

Performance comparisons between different transmit precoders can be made by examining how total throughput scales with the number of network nodes [28]. Consider the standard Rayleigh flat-fading channel scenario where there is no lag

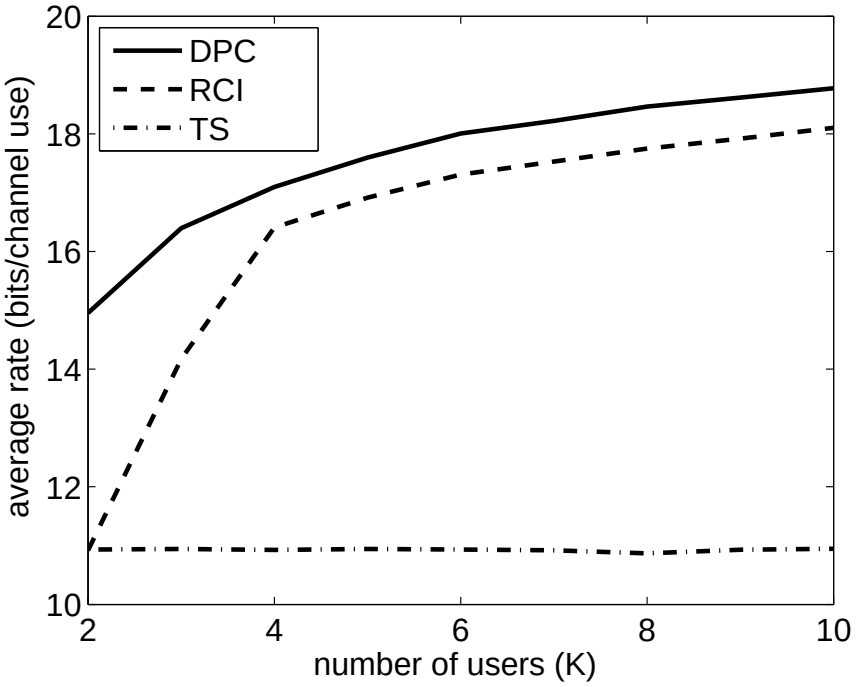

Figure 4.1: Average rate versus number of users for fixed $N_{\mathrm{r}} = N_{\mathrm{t}} = 4$ antennas and $P = 10$ in Rayleigh, flat-fading channel model. All nodes have perfect channel knowledge for all realizations of the channel.

between CSIR and CSIT (e.g. $\Delta_t = 0$) and all nodes have error-free estimates of the channel. Figure 4.1 shows throughput scaling as the number of users increases for each of the transmit precoding techniques discussed. The system is fixed at $N_t = 4$ transmit antennas, $N_r = 4$ receive antennas per user, and a total power constraint of $P = \sum_i \mathrm{tr}\{\mathbf{Q}_i\} = 10$. The channel model used is the standard Rayleigh and spatially-white model discussed in Chapter 2. While these results reveal the optimality of DPC, they also show that BF captures the majority of available throughput for larger networks and that the TS performance does not scale appreciably with increasing network size because it uses no CSIT or multi-access to the channel.

4.2 Optimization Objective Functions

Assessing the performance of the algorithms under consideration requires definition of meaningful metrics which capture the performance degradation created by outdated CSIT. Naturally, many different metrics could be defined, with the conclusions drawn ultimately depending on these definitions. However, since the goal of DPC and RCI is to maximize the sum mutual information, it is logical that the performance metrics used in this work depend on this quantity. One excellent metric which describes the maximum rate at which error-free transmission is theoretically possible for a given channel type is the ergodic channel capacity [2]. However, computing this quantity requires an expectation over an infinite set of channel realizations, which is not possible using a finite set of measured data, and is not strictly defined for outdated CSI.

Given the difficulties associated with the ergodic capacity for this application, metrics used in this study are based on the sample average rate (SAR) which is the expected error-free throughput for the channel as a function of the delay $n - n_0$ where precoding or detection is based off the channel at time n_0 after propagation through the channel at time n. We perform a time average over all possible initial displacements n_0, so that the SAR for a displacement $\Delta_t = n - n_0$

is defined as

$$S_{\mathcal{X}}(\Delta_{\mathrm{t}}) = \frac{1}{N_{\max} - \Delta_{\mathrm{t}}} \sum_{m=0}^{N_{\max}-\Delta_{\mathrm{t}}} C^{\mathcal{X}}(m, m + \Delta_{\mathrm{t}}) \tag{4.5}$$

where sum-rate expressions are written explicitly as functions of time, $N_{\max}$ is the total number of samples in the dataset, and the subscript $\mathcal{X}$ is a member of the set of specified precoders {DPC, BF, TS}. Note that for $\Delta_{\mathrm{t}} = 0$, Eq. (4.5) represents the time-average expected system throughput. Since this chapter considers temporal channel variation exclusively, and not coefficient estimation, it is assumed that the channel estimates $\mathbf{H}_j(n)$ and $\mathbf{H}_j(n_0)$ known respectively at the receiver and transmitter are error free.

It is noteworthy that $C^{\mathcal{X}}(n_0, n_0+\Delta_{\mathrm{t}})$ is not necessarily a decreasing function of Δ_{t}. For example, if the channel estimate occurs at the end of a fade, the sum mutual information is likely to be greater as the nodes move and the channel improves. However, because the SAR in Eq. (4.5) represents an average behavior, it generally decreases with increasing Δ_{t}. Figure 4.2 plots the SAR versus the *spatial* displacement $\Delta = \Delta_{\mathrm{t}} T_s v$, where T_s and v represent respectively the sample interval and the receiver velocity, for each of the transmit precoders assuming Jakes' channel model and a normalized Doppler frequency of $f_d = 0.0086$ chosen based upon T_s and v. The system parameters include $K = 5$ users each equipped with $N_{\mathrm{r}} = 4$ antennas, a transmitter with $N_{\mathrm{t}} = 4$ antennas, and a total power constraint of $P = 10$. The maximum displacement Δ is limited to 3λ since the transient behavior of throughput degradation happens within this interval. Note that both DPC and RCI experience a reasonably rapid degradation in throughput as a result of outdated CSIT.

While plots of the SAR such as that in Fig. 4.2 reveal detailed information regarding performance degradation due to outdated CSIT, it is useful to derive simple quantitative measures from the SAR that allow single-number comparison of the behavior for different environments. The remainder of this section outlines two metrics based on the SAR which help quantify the stability of the transmit precoding algorithms and motivate the new algorithms defined in Sections 4.3.2 and 4.4.1.

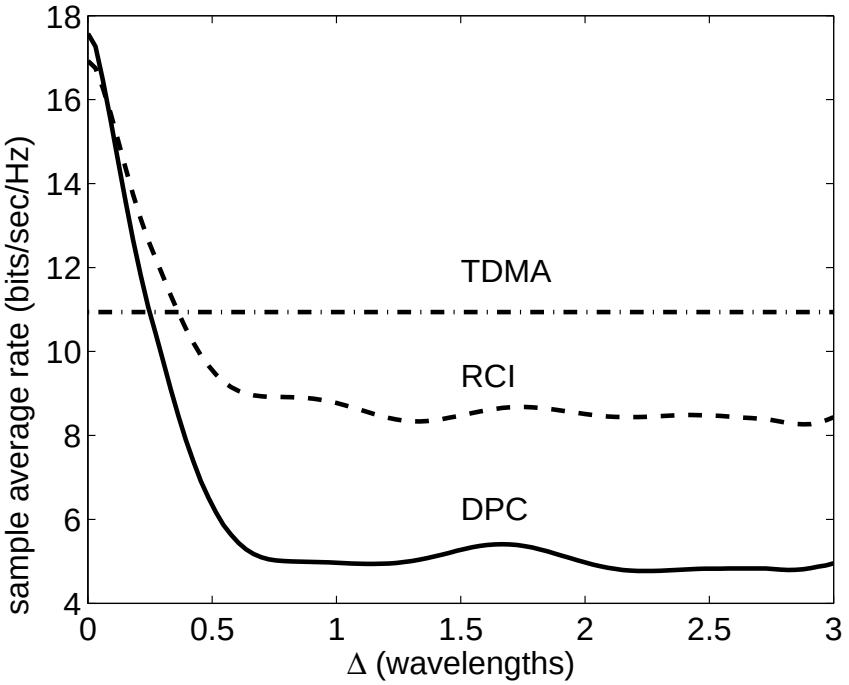

Figure 4.2: Sample average rate (SAR) as a function of delay for a network with parameters $N_{\mathrm{t}} = N_{\mathrm{r}} = 4$, $K = 5$, and $P = 10$ given various transmit precoding schemes in the spatially-white, Jakes' channel model with a normalized Doppler frequency of $f_d = 0.0086$.

4.2.1 Sample Average Rate (SAR) Cross-Over Distance

As shown in Fig. 4.2, there is a displacement at which the average rate drops below that for TS. This displacement, denoted as d_T, is referred to as the SAR cross-over distance and quantifies the displacement beyond which CSIT is no longer useful (i.e. beyond this displacement, TS, which uses no CSIT, offers higher throughput). Small values of d_T suggest that a given precoding algorithm is highly sensitive to channel temporal variations and will perform poorly in practical systems. In Fig. 4.2, $d_T = 0$ for TS, $d_T \approx 0.25\lambda$ for DPC, and $d_T \approx 0.4\lambda$ for RCI beamforming.

4.2.2 Expected Sample Average Rate (ESAR)

While the SAR cross-over distance gives an indication of how quickly the performance degrades with node displacement, it clearly provides only limited insight into the behavior. This fact motivates another performance metric which incorporates the throughput over all displacements. The Expected Sample Average Rate (ESAR) is defined by

$$\bar{S}^{\mathcal{X}}(M) = \frac{1}{M} \sum_{d=0}^{M-1} S^{\mathcal{X}}(d) \tag{4.6}$$

where M represents the extent of displacements in the region of interest. From Fig 4.2, the normalized ESAR values $\bar{S}_{\mathcal{X}}/\bar{S}_{\text{TS}}$ are 1, 0.89, and 0.55 for TS, RCI, and DPC, respectively.

Some important observations from Fig. 4.2 can be made regarding the performance metrics and their effects on transmission stability. The distance d_T is meaningful in that it defines the sensitivity of an algorithm to node movement but is not practical as an optimizable variable. For example, maximizing d_T will not necessarily result in a stable transmission policy since the majority of available throughput may be lost in the first few fractions of a wavelength. In fact, Fig. 4.2 indicates that the most stable transmission scheme is TS which maximizes the ESAR. These observations will be used to motivate a more stable transmit precoder

in the following section.

4.3 Broadcast Channel Stable Transmission: Perfect CSIR

As shown in the previous sections, attempting to transmit with either the optimal non-linear transmit precoding scheme (DPC) or linear beamforming on the optimal subspaces (RCI) results in significant performance loss with even small node displacement. This observation suggests that a signaling strategy which is insensitive to node displacement must use transmission on suboptimal subspaces that remain constant for longer periods of time. Motivated by this fact, we present an iterative beamforming algorithm that has similar performance to RCI beamforming when used with CSIT and stable performance when used with CDIT. While the complexity of this algorithm is higher than that of RCI, it enables a significantly reduced frequency at which the transmitter BF weights must be updated.

4.3.1 MMSE-CSIT Beamforming

Our goal is to define a beamforming algorithm that achieves the capacity-optimal performance of RCI when used with CSIT but can be extended for use with CDIT. We apply the standard coordinated transmitter/receiver beamforming algorithm suggested in [28] where weights at the transmitter and receiver are updated in an iterative manner. To motivate the steps at each iteration of the algorithm, the following observations are considered:

- The metric of interest is maximizing the total mutual information (capacity) of the system with linear beamforming (Section 4.1),
- MMSE beamforming at the receiver is capacity optimal [36],
- There exists a duality between transmit and receive beamforming [2, 36].

For the following, the optimization variable is indexed over the current sample index n and the index n_0 at which the transmitter acquires CSI. This indexing is for convenience when we address CDI beamforming, while for CSI beamforming the transmitter assumes $n_0 = n$ for all time (i.e. the transmitter only calculates a single set of beamforming weights).

Unit norm transmit beamforming weights $\mathbf{b}_i(n_0)$ are initialized for a given number of data streams N_s using the singular vectors of a random matrix, similar to the random beamforming algorithm [43], with the powers for all streams initially equal. Given transmit weights and powers, each receiver calculates a set of N_s MMSE beamforming weights, one for each of the N_s streams. For unit receiver noise variance and assuming linear receiver processing (so that multiple streams destined for the same user will interfere with each other), the resulting received SINR of the ith stream to the jth user for the MISO broadcast channel is written as

$$\rho_{i,j}(n_0, n) = \frac{p_i(n_0)\mathbf{b}_i^H(n_0)\mathbf{H}_j^H(n)\mathbf{H}_j(n)\mathbf{b}_i(n_0)}{1 + \sum_{k \neq i} p_k(n_0)\mathbf{b}_k^H(n_0)\mathbf{H}_j^H(n)\mathbf{H}_j(n)\mathbf{b}_k(n_0)} \tag{4.7}$$

where $p_i(n_0)$ is the power allocated to the ith stream and $\sum_i p_i(n_0) \leq P$.

The next step within the iteration is to assign a single user to each stream. This is accomplished by sequentially moving through each of the N_s streams and assigning to it the user which achieves the highest value of $\rho_{i,j}(n_0, n_0)$. If $\pi(i)$ represents the user index for the ith stream, this process is represented mathematically as

$$\pi(i) = \arg\max_j \rho_{i,j}(n_0, n). \tag{4.8}$$

It is important to note that while the stream mapping policy $\pi(i)$ may result in nodes without an assigned stream at a given iteration, these nodes may recapture a stream at a future iteration.

Once streams have been mapped to users, MMSE receiver beamforming weights are computed using

$$\mathbf{w}_{i,j}(n_0, n) = \left\{ \mathbf{I} + \mathbf{H}_j(n) \sum_{k=1}^{K} p_k(n_0)\mathbf{b}_k(n_0)\mathbf{b}_k^H(n_0)\mathbf{H}_j^H(n) \right\}^{-1} \mathbf{H}_j(n)\mathbf{b}_i(n_0)p_i(n_0). \tag{4.9}$$

Each receiver then "transmits" using its set of beamforming weights over the reciprocal channel $\mathbf{H}_j^H(n_0)$, and for each stream the transmitter computes updated MMSE beamforming weights $\mathbf{b}_i(n_0)$. For a given set of transmitter and receiver beamforming weights, the quasiconvexity of the single-input single-output SINR function enables a straightforward numerical optimization of the power coefficients $p_i(n_0)$ to increase the expected system rate. The sample average rate based on the beamforming weights and power allocations using

$$C_{\text{MMSE-CSIT}}(n_0, n) = \sum_{i=1}^{N_s} \log\left(1 + \rho_{i,\pi(i)}(n_0, n)\right) \tag{4.10}$$

where Eq. (4.7) is modified to include transmit weights. The final solution corresponds to the weights $\mathbf{w}_i(n_0)$ associated with the value of N_s that maximizes Eq. (4.10). The complete algorithm for maximizing the sample throughput through linear processing, referred to as MMSE-CSIT, is summarized in Table 4.1. Note that since the algorithm is performed with $n = n_0$, Table 4.1 drops sample indices from the variable matrices.

Figure 4.3 compares RCI and MMSE-CSIT beamforming for $N_{\text{t}} = 6$, $N_{\text{r}} = 1$, $P = 10$, and a variable number of receiver nodes for perfect CSI. The channel coefficients were generated using the standard Rayleigh, flat-fading model for the multi-user channel. Figure 4.3 also shows the optimal non-linear DPC precoder as a performance reference. Note that, with power optimization, RCI and MMSE-CSIT perform almost identically, which is the intended result. When Step 4 is dropped from the algorithm, equal power is used for each data stream and only a small loss in throughput is seen as the number of users increases. Figure 4.4 shows the convergence with the number of iterations for RCI and MMSE-CSIT. Note that the trend for both algorithms is a longer convergence time as the number of users is increased. Though not shown, a similar behavior is observed as the number of antennas is increased for either the transmitter or receiver. It is noteworthy that both the RCI and MMSE-CSIT algorithms only guarantee convergence to a local maximum when used in the MIMO broadcast channel, therefore allowing the situation where one algorithm outperforms the other. From a computational complexity standpoint, at each iteration the complexity of the RCI algorithm is

Table 4.1: Iterative beamforming for maximization of sample average rate

1. Assume an initial set of N_s random transmit weights $\mathbf{b}_i$
with equal power allocation $p_i = P/N_s$
2. Calculate the MMSE *receiver* beamforming weights
for all streams to all users
$$\mathbf{w}_{i,j} = (\mathbf{I} + \mathbf{H}_j \left(\sum_k p_k \mathbf{b}_k \mathbf{b}_k^H\right) \mathbf{H}_j^H)^{-1} \mathbf{H}_j \mathbf{b}_i p_i$$
3. Find the survivor streams using SINR
$$\pi(i) = \arg\max_j \rho_{i,j}$$
4. Numerically optimize the powers p_i assigned to each stream
5. Update the MMSE *transmitter* beamforming weights
$$\mathbf{b}_i = \left(\mathbf{I} + \sum_k p_k \mathbf{H}_{\pi(k)}^H \mathbf{w}_{k,\pi(k)} \mathbf{w}_{k,\pi(k)}^H \mathbf{H}_{\pi(k)}\right)^{-1} \mathbf{H}_{\pi(i)} \mathbf{w}_{i,\pi(i)} p_i$$
6. Repeat 2-5 until convergence
7. Repeat 1-6 for $N_s = 1 \ldots K$
8. Use $\mathbf{w}_{i,\pi(i)}$ corresponding to the value of N_s that maximizes
$$C_{\text{MMSE-CSIT}} = \sum_{i=1}^{N_s} \log\left(1 + \rho_{i,\pi(i)}\right)$$

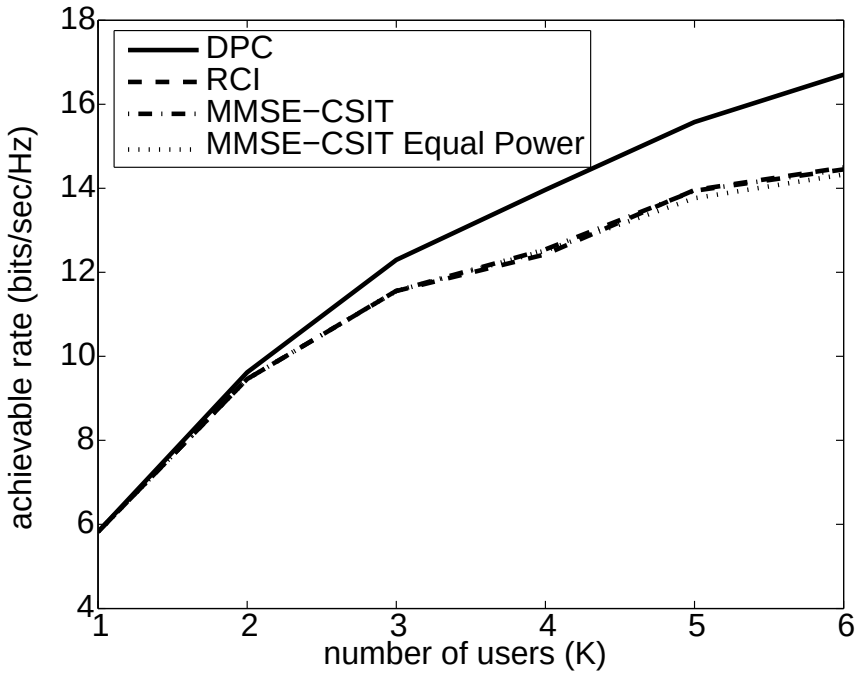

Figure 4.3: Comparison of optimal transmit beamforming RCI and MMSE-CSIT beamforming for $N_{\mathrm{t}} = 6$, $N_{\mathrm{r}} = 1$, and $P = 10$ in a Rayleigh flat-fading channel. The optimal non-linear preprocessing (DPC) is also shown for comparison.

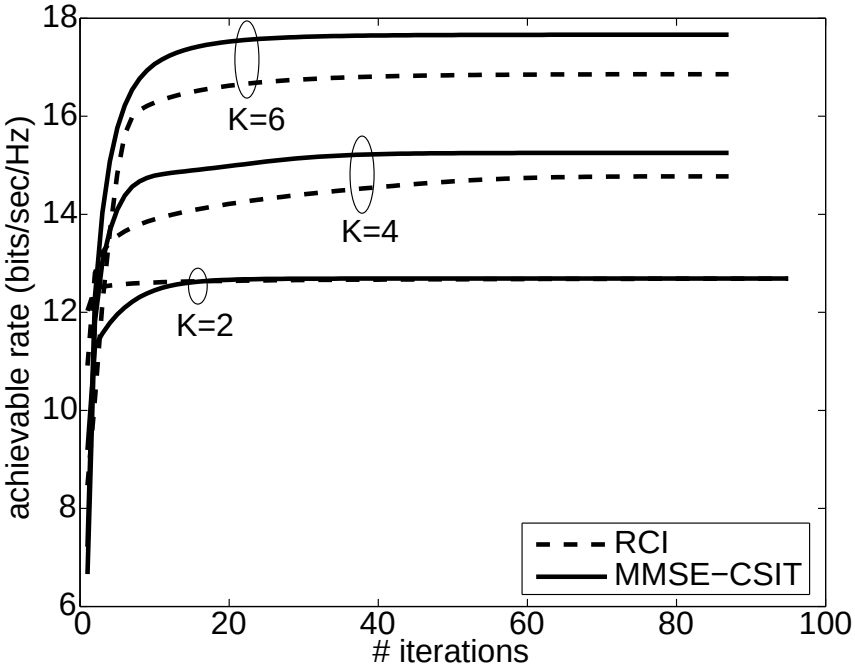

Figure 4.4: Convergence of RCI and MMSE-CSIT beamforming algorithms for $N_{\mathrm{t}} = 4$, $N_{\mathrm{r}} = 4$, $P = 10$, and different number of users for a channel realization from the measured data.

dominated by the cost of taking the inverse of a single $N_\mathrm{t} \times N_\mathrm{t}$ and K $N_\mathrm{r} \times N_\mathrm{r}$ matrices, with an asymptotic cost of $O(N_\mathrm{t}^3 + KN_\mathrm{r}^3)$. In contrast, the complexity of the MMSE-CSIT algorithm requires taking the inverse of approximately K $N_\mathrm{t} \times N_\mathrm{t}$ and K^2 $N_\mathrm{r} \times N_\mathrm{r}$ matrices, which is roughly K times the cost of the RCI scheme.

4.3.2 MMSE-CDIT Beamforming

As observed at the end of Section 4.2.2 and shown in Fig. 4.2, stable transmission is achieved by the scheme that maximizes the ESAR of the channel rather than instantaneous throughput. We therefore reformulate the beamforming problem to maximize the average of Eq. (4.10) over some window size M, or

$$\bar{C}_{\text{MMSE-CSIT}}(n_0, M) = \frac{1}{M} \sum_{m=0}^{M-1} \sum_{i=1}^{N_s} \log\left(1 + \rho_{i,\pi(i)}(n_0, n_0+m)\right). \tag{4.11}$$

While direct maximization of Eq. (4.11) with no CSIT appears difficult, under ideal conditions the average throughput can be upper and lower bounded by (see Appendix C for discussion on bounds)

$$\bar{C}^{\text{upper}}(n_0, M) = \sum_{i=1}^{N_s} \log(1 + \bar{\rho}_{i,\pi(i)}(n_0, M)) \tag{4.12}$$

$$\bar{C}^{\text{lower}}(n_0, M) = \sum_{i=1}^{N_s} \log\left(1 + \tilde{\rho}_{i,\pi(i)}(n_0, M)\right) \tag{4.13}$$

where

$$\bar{\rho}_{i,\pi(i)}(n_0, M) = \frac{1}{M} \sum_{m=0}^{M-1} \frac{\text{num}\{\rho_{i,\pi(i)}(n_0, n_0+m)\}}{\text{den}\{\rho_{i,\pi(i)}(n_0, n_0+m)\}} \tag{4.14}$$

$$\tilde{\rho}_{i,\pi(i)}(n_0, M) = \frac{\frac{1}{M}\sum_{m=0}^{M-1} \text{num}\{\rho_{i,\pi(i)}(n_0, n_0+m)\}}{\frac{1}{M}\sum_{m=0}^{M-1} \text{den}\{\rho_{i,\pi(i)}(n_0, n_0+m)\}} \tag{4.15}$$

and num$\{\cdot\}$ and den$\{\cdot\}$ return the numerator and denominator, respectively, of the argument. Equation (4.14) is the average SINR (ASINR) while Eq. (4.15) is the ratio of the average signal power to the average interference plus noise powers (ASAINR). Analogous to the instantaneous throughput of Eq. (4.10), the bounds on average throughput Eqs. (4.12) and (4.13) can each be considered

instantaneous throughputs assuming the SNR is given by the average quantities ASINR and ASAINR, respectively.

Since, as shown in Appendix C, the lower bound on ESAR is tighter than the upper bound, we will use this bound as the objective function for maximization. The ASAINR can be expanded generically as

$$\begin{aligned}
\tilde{\rho}_{i,j}(n_0, M) &= \frac{\frac{1}{M}\sum_{m=0}^{M-1} \mathrm{num}\{\rho_{i,j}(n_0, n_0+m)\}}{\frac{1}{M}\sum_{m=0}^{M-1} \mathrm{den}\{\rho_{i,j}(n_0, n_0+m)\}} \\
&= \frac{\frac{1}{M}\sum_{m=0}^{M-1} p_i(n_0)\mathbf{b}_i^H(n_0)\mathbf{H}_j^H(n_0+m)\mathbf{H}_j(n_0+m)\mathbf{b}_i(n_0)}{1+\frac{1}{M}\sum_{m=0}^{M-1}\sum_{k\neq i} p_k(n_0)\mathbf{b}_k^H(n_0)\mathbf{H}_j^H(n_0+m)\mathbf{H}_j(n_0+m)\mathbf{b}_k(n_0)} \\
&= \frac{p_i(n_0)\mathbf{b}_i^H(n_0)\sqrt{\mathbf{R}_{\mathrm{t},j}(n_0,M)}^H\sqrt{\mathbf{R}_{\mathrm{t},j}(n_0,M)}\mathbf{b}_i(n_0)}{1+\sum_{k\neq i} p_k(n_0)\mathbf{b}_k^H(n_0)\sqrt{\mathbf{R}_{\mathrm{t},j}(n_0,M)}^H\sqrt{\mathbf{R}_{\mathrm{t},j}(n_0,M)}\mathbf{b}_k(n_0)} \qquad (4.16)
\end{aligned}$$

where $\mathbf{R}_{\mathrm{t},j}(n_0, M)$ is the transmit correlation matrix from Eq. (2.2). Note that Eq. (4.16) is in the exact form of Eq. (4.7) used for maximizing throughput with CSIT when the transmit correlation matrices are exchanged for channel realizations. Thus, the same beamforming algorithm used to maximize instantaneous throughput can also be used to maximize the lower bound on average throughput by simply swapping CDIT for CSIT. Table 4.2 shows the beamforming algorithm that utilizes CDIT (MMSE-CDIT) with power optimization removed for computational savings.

An important discrepancy between the MMSE-CSIT and MMSE-CDIT beamformers is the use of channel duality when updating the beamformer weights. With MMSE-CSIT beamforming, the dual of the downlink channel is simply the matrix Hermitian of the uplink and vice versa. However, for MMSE-CDIT beamforming, the receive correlation matrix is *not* generally the Hermitian of the transmit correlation matrix. For example, if the transmitter is closely obstructed by interferers or contains tightly spaced antennas then Eq. (2.2) will reflect more correlation than Eq. (2.3) and duality will not hold. For this algorithm, however, SINR equality is only required when the transmitter and receiver change roles, and this is satisfied when using $\mathbf{R}_{\mathrm{t},j}^H(n_0, M)$ as the dual "channel" for MMSE-CDIT.

This result suggests that the beamforming weights produced by the MMSE-

Table 4.2: Iterative beamforming for maximization of ESAR lower bound

1. Assume an initial set of N_s random transmit weights $\mathbf{b}_i$
   with equal power allocation $p_i = P/N_s$
2. Calculate the *receiver* beamforming weights for all streams to all users
   $$\mathbf{w}_{i,j} = (\mathbf{I} + \sqrt{\mathbf{R}_{\mathrm{t},j}} \left(\sum_k p_k \mathbf{b}_k \, \mathbf{b}_k^H\right) \sqrt{\mathbf{R}_{\mathrm{t},j}}^H)^{-1} \sqrt{\mathbf{R}_{\mathrm{t},j}} \mathbf{b}_i p_i$$
3. Find the survivor streams by using
   $$\pi(i) = \arg\max_j \tilde{\rho}_{i,j}$$
4. Update the *transmitter* beamforming weights
   $$\mathbf{b}_i = \left(\mathbf{I} + \sum_k p_k \mathbf{R}_{\mathrm{t},\pi(k)}^H \mathbf{w}_{k,\pi(k)} \mathbf{w}_{k,\pi(k)}^H \mathbf{R}_{t,\pi(k)}\right)^{-1} \mathbf{R}_{\mathrm{t},\pi(i)} \mathbf{w}_{i,\pi(i)} p_i$$
5. Repeat 2-4 until convergence
6. Repeat 1-5 for $N_s = 1 \ldots K$
7. Use $\mathbf{w}_{i,\pi(i)}$ corresponding to the value of N_s that maximizes
   $$C_{\text{MMSE-CDIT}} = \sum_{i=1}^{N_s} \log\left(1 + \tilde{\rho}_{i,\pi(i)}\right)$$

CDIT algorithm reside in stable subspaces within the multi-user time-varying MIMO channel. This stability can be seen by noting that the throughput as a function of SINR and delay is only based on the single set of beamformer weights produced at zero delay and not adapted to channel conditions and variations. It is also interesting to note that the SAR cross-over distance d_T for the RCI beamformer in this spatially-correlated channel is larger than that observed for the spatially-white Jakes' channel considered in Fig. 4.2. This observation suggests that spatial correlation provides an innate robustness to channel temporal variation when used with linear beamforming even when the correlation is not explicitly used in the computation of the beamforming weights.

Some comments regarding the MMSE-CDIT beamforming algorithm are necessary. First, it is important to reinforce that for simulation purposes, the weights found from the iterative MMSE-CDIT algorithm are treated like standard beamforming weights of RCI. In other words, the algorithm is used to find a single set of weights, and these weights are fixed as the nodes move throughout the system. No adaptive beamforming is considered for either case. Second, one might

consider using CDIT knowledge directly with either DPC or RCI. However, we have observed that the resulting performance is lower than that obtained from either the MMSE-CDIT beamformer or TS, and therefore these approaches are not considered further in this work.

4.3.3 Stable Transmission Results

Full assessment of the performance of the algorithms considered in this chapter requires sweeping over a large number of independent parameters, including available power at the transmitter, number of transmit and receive antennas, node velocities, channel spatial correlation, number of users, and type of scattering environment. For measured channel data, certain parameters (number of antennas, transmit power) can be altered to some degree while others (scattering environment, node velocities, number of users) are determined by the operational environment. In this section, the SAR is examined for a fixed number of antennas and transmit power level. The following conditions are imposed on the simulations undertaken:

- Although the ordering of users could be optimized in order to maximize information throughput [2], this chapter is focused on the performance degradation due to channel time-variation for a specified ordering, and therefore user signal encoding is performed in a fixed order.
- The measured data can accommodate a maximum of six users in the broadcast channel.
- Prior to node movement both transmitter and receiver share perfect (i.e. channel estimation error-free) knowledge of the channel. As nodes move, the receiver is assumed to always have the current CSI while the transmitter only has the initial channel state. This assumption suggests embedded training symbols in the transmitted signal and error-free channel estimation at the receiver with limited feedback to the transmitter.

- When spatial correlation is used with the modeled channel, the transmit correlation matrix is taken from estimates generated by the measured channel. Although results in this section are focused on the measured data, we also provide results in a later chapter for the modeled channel (i.e. spatially-correlated Jakes' model) which allows for some contrast between the two.

Figure 4.5 shows the SAR of the four transmit precoders examined in this work, namely non-linear optimal DPC, linear optimal BF (RCI), the iterative beamformer presented in this chapter (MMSE-CDIT), and time-sharing (TS) each of which will be normalized by the TS sum-rate to describe precoding effectiveness as defined for the single-user channel 3.9. The simulation uses the measured data with $N_{\mathrm{t}} = 4$ transmit antennas and $K = 3$ users each with $N_{\mathrm{r}} = 4$ antennas. The total available power is fixed at $P = 10$ and nodes are displaced at a constant pedestrian velocity. These results reveal that while DPC has the highest possible throughput, it is also the most sensitive to outdated CSIT as measured by the decrease in effectiveness. Optimal CSIT beamforming achieves an initial performance that is near that of DPC and has a more graceful loss in performance as nodes move. MMSE-CDIT beamforming throughput performance is initially suboptimal, but remains constant throughout the length of the simulation and is always more effective than TS. It is clear that the SAR cross-over distance for MMSE-CDIT is beyond the simulation region and is much larger than that of any other precoder. As a reference, the SAR cross-over distance (d_T) and normalized ESAR ($\bar{S}_{\mathcal{X}}/\bar{S}_{\mathrm{TS}}$) for each of the transmit precoders and channel models are provided in Table 4.3. The differences between the results for the various environments demonstrate the fundamental spatial characteristics of the channels. Despite these differences, the results for the channel types suggest the same performance trends, with the most notable one being that MMSE-CDIT beamforming outperforms all other schemes for the metrics presented given sufficient delay between channel acquisition and channel use. Furthermore, it appears that linear precoding even with outdated CSI provides some robustness to channel temporal variations for the given antenna correlations while the self-interference caused by nonlinear precoding significantly degrades the system.

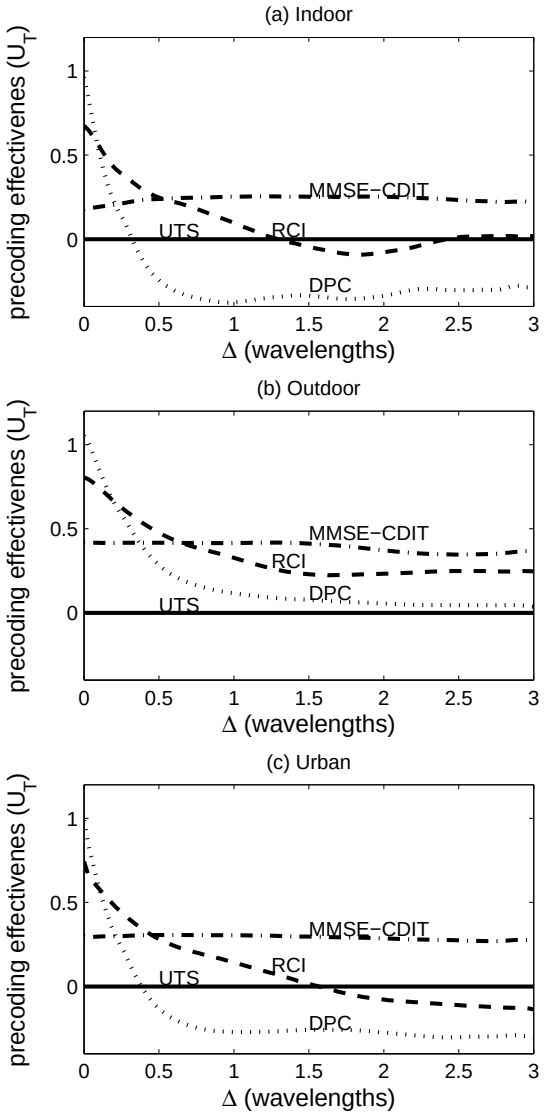

Figure 4.5: Precoding effectiveness U_{T} in the MIMO broadcast channel with $K = 3$ users, $N_{\mathrm{r}} = N_{\mathrm{t}} = 4$ antennas, and $P = 10$ power constraint. Results are shown for the (a) Indoor, (b) Outdoor, and (c) Urban environments.

Table 4.3: Performance Metrics for DPC, RCI, and TS in Indoor, Outdoor, and Urban Environments

	DPC		RCI		MMSE-CDIT	
Indoor	$.32\lambda$	.75	1.292λ	1.1	$> 3\lambda$	1.17
Outdoor	$> 3\lambda$	1.167	$> 3\lambda$	1.33	$> 3\lambda$	1.38
Urban	0.383λ	0.81	1.57λ	1.08	$> 3\lambda$	1.27
	d_T	$\frac{\bar{S}_{\text{DPC}}}{S_{\text{TS}}}$	d_T	$\frac{\bar{S}_{\text{RCI}}}{S_{\text{TS}}}$	d_T	$\frac{\bar{S}_{\text{MMSE-CDIT}}}{S_{\text{TS}}}$

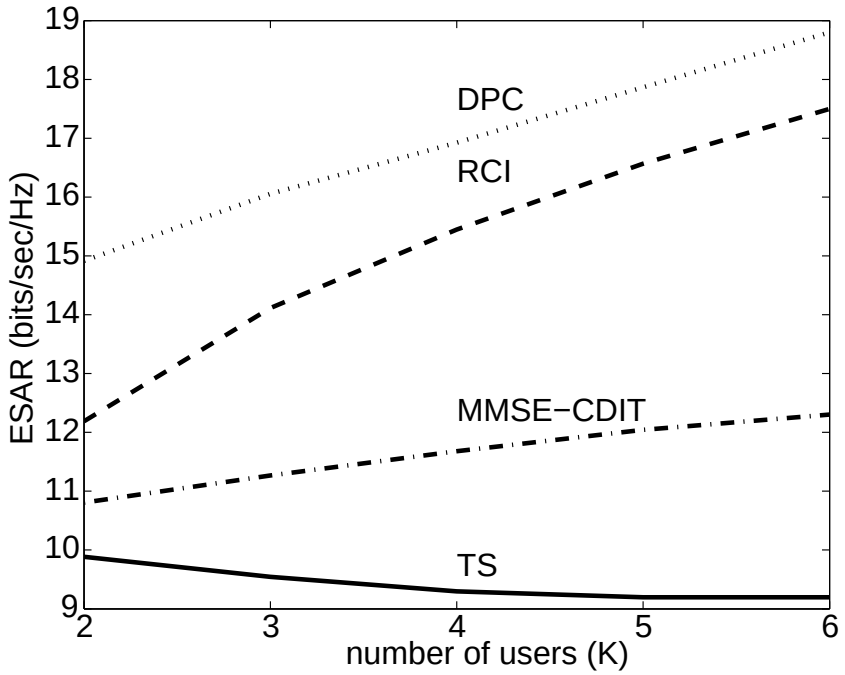

Figure 4.6: Sample average rate versus number of users for $N_{\text{t}} = N_{\text{r}} = 4$ and $P = 10$ in the measured channel. There is no lag between channel acquisition and use.

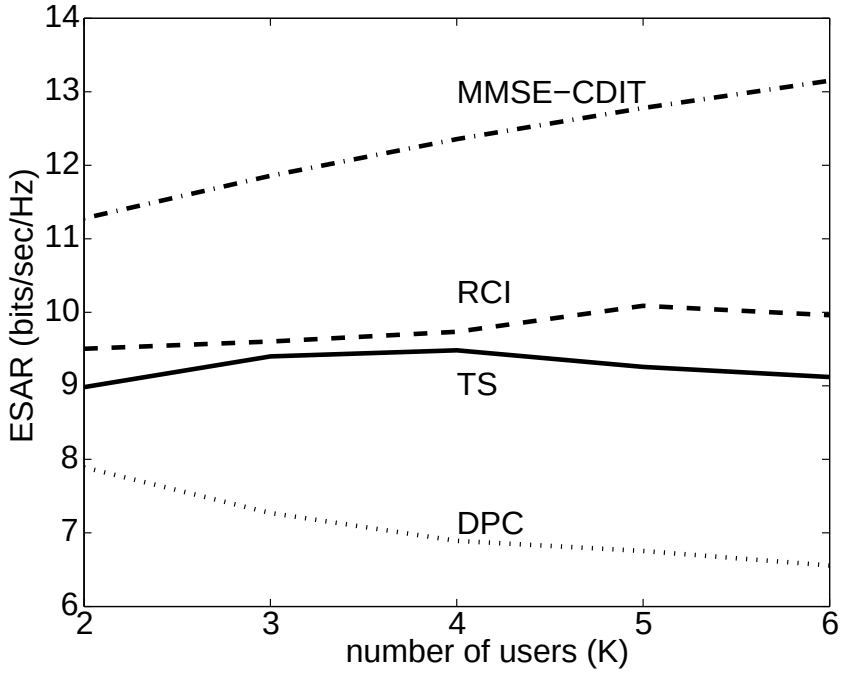

Figure 4.7: Sample average rate versus number of users for $N_{\mathrm{t}} = N_{\mathrm{r}} = 4$ and $P = 10$ in the measured channel. There is a lag of 1.5λ between channel acquisition and use.

Figure 4.6 demonstrates scalability of the network for different types of precoding when both transmitter and receiver are equipped with perfect channel knowledge. The simulation uses measured data with $N_{\mathrm{t}} = N_{\mathrm{r}} = 4$ and $P = 10$ with a variable number of receivers. These results confirm the finding from Fig. 4.1 that all schemes that use some form of channel knowledge scale in throughput versus the number of users. Figure 4.7 shows the results of the same simulation performed with a displacement of $\Delta = 1.5\lambda$ between channel update and transmission. This intriguing result reveals that the performance degradation for DPC worsens as the network size increases. MMSE-CDIT beamforming is impervious to mobility in the network within the channel stationarity time and is the only precoder that provides significant increase in performance with the number of nodes for outdated transmit channel information.

4.4 Broadcast Channel Stable Reception: Erroneous CSIR

The severe loss in rate with outdated CSIT observed in the prior section will be magnified by outdated CSI at the receiver and poses a more difficult problem. Therefore, we will use a combination of the approaches outlined in [21] of maximizing the *lower bound* on an idealized average sum-rate, and [42] of deriving the *form* of the maximizing beamformer weights. The general steps followed for finding the beamforming weights that maximize the approximate sum-rate are: 1) define the sum-rate objective function as a function of the beamforming vectors, 2) solve for the weights that provide maxima to the objective function, and 3) define an iterative algorithm that finds the weights given some initial condition.

4.4.1 Regularized Channel Distribution Inversion (RCDI)

Consider the sum-rate approximation given linear processing as described in Appendix C. Under this constraint of linear preprocessing, the objective function

is written as

$$\bar{C} = \sum_{j=1}^{K} \log\left(1 + \frac{\bar{n}_j}{\bar{d}_j}\right) \tag{4.17}$$

where $\bar{n}_j = \mathrm{E}[\mathrm{num}(\rho_j)]$, $\bar{d}_j = \mathrm{E}[\mathrm{den}(\rho_j)]$, and $\mathrm{num}(\cdot)$ and $\mathrm{den}(\cdot)$ return the numerator and denominator of the argument, respectively. The optimization problem is then to construct transmit and receive beamforming vectors to maximize this quantity, or

$$\max_{\mathbf{w}_j, \mathbf{b}_j} \bar{C} \tag{4.18}$$

with power constraints imposed on the input beamforming vectors.

The details of the maximization process can be found in Appendix D. The resulting regularized channel distribution inversion (RCDI) beamformer matrix $\mathbf{B}$, each column of which represents the transmit beamformer $\mathbf{b}_j$ for the jth user, is given as

$$\mathbf{B} = \left(\frac{\mathrm{tr}(\mathbf{D})}{P}\mathbf{I} + \sum_{i=1}^{K} \mathbf{D}_{i,i}\bar{\mathbf{H}}_j\right)^{-1} \mathbf{\Lambda} \tag{4.19}$$

where the definitions for $\mathbf{D}$, $\mathbf{\Lambda}$, and $\bar{\mathbf{H}}_j$ can be found in Appendix D. It is interesting that the form of (4.19) is similar to that in (4.5) for the RCI beamformer (see also [42]). However, because RCI depends on CSI, the required feedback frequency for RCI is on the order of the channel coherence time. In contrast, since RCDI depends on CDI, feedback is only required when the channel correlation structure changes appreciably.

Since $\mathbf{B}$ appears on both sides of (4.19) (both $\mathbf{\Lambda}$ and $\mathbf{D}$ are functions of $\mathbf{B}$), an iterative solution must be used to obtain the final solution. Using a combination of the steps suggested in [21, 28, 42] results in the iterative RCDI beamforming algorithm shown in Table 4.4 where steps 1-6 update the transmit weights while step 7 updates the receive weights using an MMSE criterion on the average signal to average interference plus noise ratio (ASAINR). Whereas the channel matrix is the only required input for the RCI algorithm, $\mathbf{S}_{\mathrm{t},j}$ and $\mathbf{S}_{\mathrm{r},j}$, which are nonlinear permutations of the full spatial correlation matrix for each user, are the only inputs required for the RCDI algorithm. Furthermore, the RCDI algorithm gives the

Table 4.4: Iterative beamforming for MIMO regularized channel distribution inversion (RCDI)

Calculate $\mathbf{S}_{\mathrm{t},j} = \mathrm{E}[\mathbf{H}_j^T \otimes \mathbf{H}_j^H]$ and $\mathbf{S}_{\mathrm{r},j} = \mathrm{E}[\mathbf{H}_j^* \otimes \mathbf{H}_j]$

Initialize $\mathbf{D}$ and $\mathbf{\Lambda}$

Repeat until convergence:

1. $\bar{\mathbf{H}}_j = \mathrm{mat}(\mathbf{S}_{\mathrm{t},j}\mathrm{vec}(\mathbf{w}_j\mathbf{w}_j^H))$
2. $\mathbf{B} = (\frac{\mathrm{tr}(\mathbf{D})}{P}\mathbf{I} + \sum_{i=1}^{i=K} \mathbf{D}_{i,i}\bar{\mathbf{H}}_i)^{-1}\mathbf{\Lambda}$
3. $\bar{n}_j = \mathbf{B}_{:,j}\bar{\mathbf{H}}_j\mathbf{B}_{:,j}^H$
4. $\bar{d}_j = 1 + \sum_{i \neq j} \mathbf{B}_{:,i}\bar{\mathbf{H}}_j\mathbf{B}_{:,i}^{\mathbf{H}}$
5. $\mathbf{\Lambda} = \left[\frac{(\bar{\mathbf{H}}_1\mathbf{B})_{:,1}}{\bar{d}_1}, \ldots, \frac{(\bar{\mathbf{H}}_K\mathbf{B})_{:,K}}{\bar{d}_K}\right]$
6. $\mathbf{D} = \mathrm{diag}\left(\frac{\bar{n}_1}{\bar{d}_1(\bar{d}_1+\bar{n}_1)}, \ldots, \frac{\bar{n}_K}{\bar{d}_K(\bar{d}_K+\bar{n}_K)}\right)$
7. Update $\mathbf{w}_j$ using $\mathbf{S}_{\mathrm{r},j}$ and the MMSE criterion on ASAINR

end

same results as the RCI algorithm when the expectation operator is removed (i.e. $\mathbf{S}_{\mathrm{t},j} = \mathbf{H}_j^T \otimes \mathbf{H}_j^H$).

Because of the nonconvex nature of the beamforming capacity expression, both RCI and RCDI algorithms only guarantee convergence to a local maximum, and they therefore may not produce the true sum capacity of the broadcast channel with linear precoding [42]. The implication of this observation is that the performance depends on the initial values of $\mathbf{D}$ and $\mathbf{\Lambda}$. For RCI, the beamformer created from the regularized pseudo-inverse of the channel offers a good starting point. However, since an analogous initial condition for the RCDI algorithm has not yet been discovered, we will use several starting points and select the result which gives the highest bound on the average sum-rate.

4.4.2 Stable Reception Results

The performance of using the described algorithm will be analyzed using measured channel data. While modeled channel analysis could be insightful, the

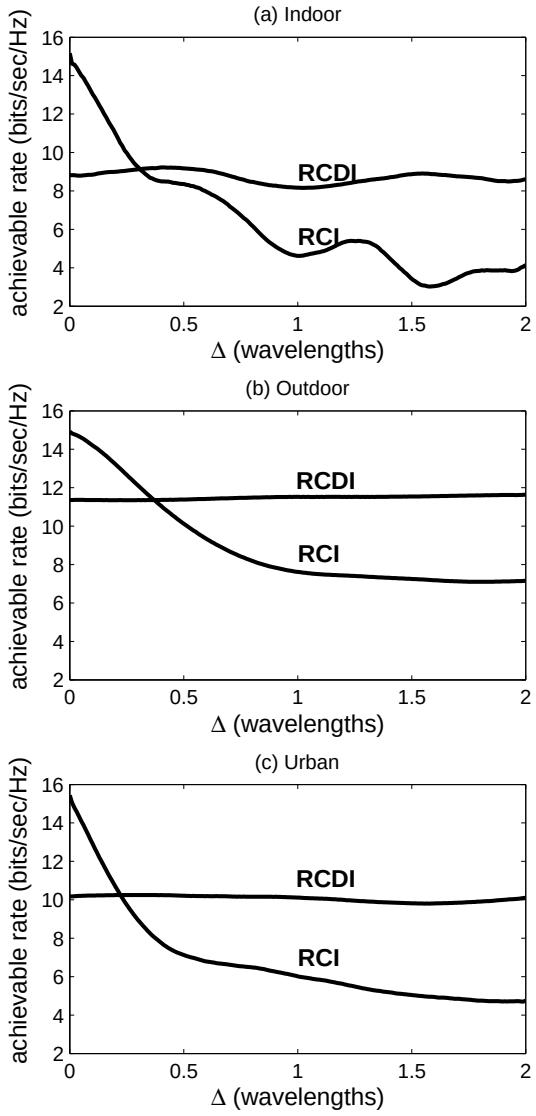

Figure 4.8: Average sum-rate of RCI and RCDI versus displacement for $K = N_{\mathrm{r}} = N_{\mathrm{t}} = 4$ and $P = 10$. The receiver and transmitter share equally delayed knowledge of that channel given by Δ (wavelengths) from the current channel. Shown are the (a) Indoor, (b) Outdoor, and (c) Urban environments.

difficulty lies in the fact that many models impose wide sense stationarity and spatial structure on the channel realizations, which is a characteristic that will favor CDI-based techniques especially when such techniques exploit *a priori* knowledge of the model. Our goal in using measured data is to show that the CDI-based schemes with reduced feedback requirements work well in realistic channels when stationarity or structure is not artificially imposed. Furthermore, multiple measurement campaigns were adopted in the simulations in order to confirm the algorithmic performance over a wide variety of spatial structures.

Fig. 4.8 compares RCI and RCDI performance as a function of displacement for Indoor, Outdoor, and Urban measurements. For these simulations, it is assumed the transmitter has the full spatial correlation matrix for all users. The elements of the full correlation matrix estimated using (2.4) are appropriately arranged to construct the matrices $\mathbf{S}_{\mathrm{t},j}$ and $\mathbf{S}_{\mathrm{r},j}$ required for the RCDI implementation. Once RCDI beamforming vectors have been found, each user is assumed to have knowledge of their transmit and receive weights which they use for all time independent of the time variations in the channel. The results in Fig. 4.8 confirm that while the performance of RCDI is lower than that of RCI with recent CSIT and CSIR, its throughput remains stable over large node displacements where the slight fluctuations in performance are artifacts of using measured data. The stability of RCDI implies that the feedback frequency for the RCDI algorithm is much lower than that required by the RCI approach to maintain a specified throughput. Furthermore, as shown in Fig. 4.8(a) for the Indoor environment, spatial structures introduced on the channel due to the environment directly affect the possibility of effectively using CDI as a precoding resource. For a spatially-white channel, the RCDI algorithm could not make any distinction between users and no gains would be possible over outdated CSI.

Results presented in this chapter suggest possibilities in combating the channel time-variation difficulties that were observed in Chapter 3 and which directly motivated this work. Two beamforming algorithms were established to this end. By simply exchanging CSI for CDI in the form of one-sided correlation matrices, with the assumption of perfect CSIR, MMSE-CDIT beamforming provides a sim-

ple manner of providing stability. With outdated CSIR, the RCDI algorithm can be used to provide more complete robustness at the cost of suboptimality in the initial performance. When channel estimates are poor the correlation-based beamformers are the only examined precoding techniques that enjoy significant network throughput scaling.

The work presented in this chapter, in part, was originally published in the following papers, of which the author was also main contributor: A. L. Anderson, J. R. Zeidler, and M. A. Jensen, "Reduced-feedback linear precoding with stable performance for the time-varying MIMO broadcast channel," *IEEE Journal on Selected Areas of Communications, (Special Issue on Limited Feedback)*. Vol. 26, No. 8, 11 pages, October, 2008; A. L. Anderson, J. R. Zeidler, and M. A. Jensen, "Stable transmission in the time-varying MIMO broadcast channel," *EURASIP Journal on Advances in Signal Processing*, 2008, Article ID 617020, 14 pages, 2008. doi:10.1155/2008/617020.

Chapter 5

Stable Transception in the MIMO Multiple-Access Channel

As developed in the previous chapter, when CSI is available at the transmitter in the BC the optimal, rate-maximizing beamformer is found in [42] for the MISO channel or in [28] for the MIMO channel. This current chapter takes the approach found in [22] in order to maximize the sum-rate of the MAC using linear processing and either channel state information in the form of estimated channel matrices or channel distribution information which will take the form of spatial correlation matrices.

Though significant gains are guaranteed when CSI is perfectly known, significant loss will also occur in the MAC when assumed channel estimates are erroneous at the receiver or additional delay occurs when beamforming weights are fed back to the transmitters. Such errors in the channel can occur when limited training is used for channel estimation or when node mobility happens with infrequent training and feedback. This channel error has the possibility to significantly degrade the performance of the entire system [21] and negate the theoretical rates given for the MIMO MAC as shown in this current work. The same method of combating the effects of erroneous CSI developed for the BC is adapted for the MAC - beamforming techniques that use no CSI for processing [22]. In addition

to deriving the rate-maximizing beamformer with CSI in the MAC, this chapter also introduces a beamforming method that attempts to maximize the average sum-rate thus circumventing the loss seen by channel errors.

5.1 Regularized Channel Inversion in the MAC (RCI-MAC)

Consider the scenario where the receiver estimates the channel to all users and uses some algorithm to calculate transmit and receive beamforming vectors for all desired data streams. After this processing, the data transmission phase begins where the received signal for user j in the K-user MAC with linear beamforming at the transmitters and receiver is written as

$$\mathbf{y}_j = \mathbf{w}_j^H \mathbf{H}_j \mathbf{b}_j x_j + \mathbf{w}_j^H \sum_{i \neq j}^{K} \mathbf{H}_i \mathbf{b}_i x_i + \mathbf{w}_j^H \boldsymbol{\eta}_j$$

where $\mathbf{w}_j$ and $\mathbf{b}_j$ are the beamforming vectors, x_j is the transmitted Gaussian symbol, and $\boldsymbol{\eta}_j$ is an $N_r \times 1$ AWGN noise vector. Again, time indices are dropped as the channel is considered stationary over the data detection phase; lag due to time variation in the channel and mobile users is taken into account through the channel estimation error (2.13).

In order to account for per-user power constraints and users that are excluded from the channel, the transmitted signals are normalized as

$$\mathbf{y}_j = \frac{\mathbf{w}_j^H \mathbf{H}_j \mathbf{b}_j \mathbf{x}_j}{\max(||\mathbf{b}_j||, 1)} + \mathbf{w}_j^H \sum_{i \neq j}^{K} \frac{\mathbf{H}_i \mathbf{b}_i \mathbf{x}_i}{\max(||\mathbf{b}_i||, 1)} + \mathbf{w}_j^H \boldsymbol{\eta}_j. \tag{5.1}$$

The normalized received vector (5.1) is valid for all users whether or not they access the channel and also valid for any weight of the transmit vector $\mathbf{b}_j$. If $||\mathbf{b}_j|| = 0$ then the user is considered "off" and will provide no interference to other users nor have any signal gain at the receiver. For, $||\mathbf{b}_j|| > 0$ the user is "on" and accessing the channel at the same transmit power as all other transmitting users; thus, the

normalization in (5.1) accounts for the per-user power constraint and user selection at each transmitter.

Given this normalized expression for received signals the instantaneous SINR can be written for each received signal and consequently rate equations that describe the achievable throughput of the MAC as a function of the SINR [44]

$$r_j = \log\left(1 + \frac{|\mathbf{w}_j^H \mathbf{H}_j \mathbf{b}_j|^2}{\sigma_n^2 ||\mathbf{w}_j||^2 \delta_j + \sum_{i \neq j} \frac{\delta_j}{\delta_i} |\mathbf{w}_j^H \mathbf{H}_i \mathbf{b}_i|^2}\right) \tag{5.2}$$

where $\delta_j = \max(||\mathbf{b}_j||, 1)$. The sum of these rate equations becomes the total possible throughput of the system given linear precoding and detection. Ultimately, the rate expression will be used for optimization purposes in order to find the form of the rate maximizing beamformer; however, the δ_j terms which contain the max-valued functions provide for difficult manipulation. These rate expressions can be simplified by separating the data streams into "on" or "off" regions which leads to

$$r_j = \begin{cases} \log\left(1 + \frac{|\mathbf{w}_j^H \mathbf{H}_j \mathbf{b}_j|^2}{\sigma_n^2 ||\mathbf{b}_j||^2 + \sum_{i \neq j} |\mathbf{w}_j^H \mathbf{H}_i \mathbf{b}_i|^2}\right) & \text{, "on"} \\ \log\left(1 + \frac{|\mathbf{w}_j^H \mathbf{H}_j \mathbf{b}_j|^2}{\sigma_n^2 + \sum_{i \neq j} |\mathbf{w}_j^H \mathbf{H}_i \mathbf{b}_i|^2}\right) & \text{, "off"} \end{cases} \tag{5.3}$$

where receive vectors are normalized to unity. It is straightforward to confirm that (5.3) describes the same rate as (5.2) when $||b_j||^2 \in 1, 0$ as is the case for the final, power-constrained, solution.

The rate maximizing beamformer for the MISO BC was found in [42] and used in the MIMO channel in [28]. For distinction between the various types of beamforming algorithms discussed in this chapter, the method from [28] will be referred to as the regularized channel inversion in the broadcast channel (RCI-BC) algorithm. It is noteworthy to mention that the RCI-BC algorithm may be used in the MAC when coupled with the duality between BC/MAC where transmitters and receivers exchange roles but keep the same beamforming vectors and power allocations [44]. This duality ensures that the achievable rate in the BC is the same as the MAC; however, since the BC only has a sum-power constraint users may be allocated more or less of the total available power contrary to the MAC where, in this work, all users are considered either silent or transmitting a single

stream at full power. However, for comparison purposes, this work allows illegal allocation of power when using RCI-BC and the channel duality; this method of beamformer construction is referred to as the RCI-BC→MAC algorithm.

As will be shown in this section, direct maximization of the MAC sum-rate also has the form of a regularized channel inversion and is referred to as RCI-MAC. The optimization problem is written as

$$\begin{array}{cc} \max\limits_{\mathbf{w}_j,\mathbf{b}_j} & \sum_j r_j \\ ||\mathbf{w}_j||^2 = 1 & ||\mathbf{b}_j||^2 \in \{1,0\} \end{array}$$

where r_j is found from the simplified expression (5.3). Note that the norm constraint on the transmit beamformer is used under the assumption that information streams are either "on" or "off".

In order to find the beamforming vectors that maximize the instantaneous rate of the MAC, a similar process is employed as that used for maximization in the BC. The partial derivative of the sum-rate (5.3) is taken with respect to each element of $\mathbf{b}_j$. Each partial derivative is set equal to zero and terms are gathered to create vectored-valued equations

$$\mathbf{b}_j = \begin{cases} \left(\frac{[\mathbf{D}]_{j,j}}{P}\mathbf{I} + \mathbf{H}_j^H\bar{\mathbf{D}}\mathbf{H}_j\right)^{-1}\mathbf{H}_j^H\mathbf{w}_j\Delta_j & , \text{ "on"} \\ \left(\mathbf{H}_j^H\bar{\mathbf{D}}\mathbf{H}_j\right)^{-1}\mathbf{H}_j^H\mathbf{w}_j\Delta_j & , \text{ "off"} \end{cases} \tag{5.4}$$

where the following organizational assignments are used for simplifying the expressions

$$\begin{aligned} r_j &= \log\left(1+\frac{n_j}{d_j}\right) \\ \mathbf{W} &= [\mathbf{w}_1 \dots \mathbf{w}_K] \\ \Delta_j &= (\mathbf{w}_j^H\mathbf{H}_j\mathbf{b}_j)^* \\ \mathbf{D} &= \operatorname{diag}\left(\frac{n_1}{d_1(n_1+d_1)} \dots \frac{n_1}{d_1(n_1+d_1)}\right) \\ \bar{\mathbf{D}} &= \mathbf{W}\mathbf{D}\mathbf{W}^H. \end{aligned}$$

Note that different beamformer expressions are used depending on whether a node is considered "on" or "off" which allows for user selection when the number of users

is greater than that sustainable by the receiver. Furthermore, $\mathbf{b}_j$ terms appear on each side of the vector equation leading to an iterative solution as described in [22]. The form of (5.4) also resembles a regularized channel inversion, and direct maximization of the sum-rate in the MAC beamforming algorithm is called RCI-MAC. It is also important to remark that though the RCI-MAC and RCI-BC beamformers have a similar structure, it is a non-trivial adaptation to go from one expression to the other due to the per-user versus sum power constraint of the respective systems. Finally, the RCI-MAC is a function of the *assumed* channel and performance loss will be seen when this input is erroneous.

As a comparison between RCI-BC→MAC and RCI-MAC consider generating temporally independent realizations of the spatially-white channel for each user. Figure 5.1 shows the resulting sum-rate of these realizations of the wireless MIMO channel when each technique is used for either (a) $K = 4$ or (b) $K = 6$ users with $N_t = N_r = 4$ antennas each. As a benchmark, the optimal non-linear processing [2] using successive interference cancellation (SIC) is also plotted. Note that for the situation described in (a) the RCI-MAC algorithm almost always equally divides power between the data streams resulting in RCI-BC→MAC having the same performance as RCI-MAC. However, when there are a greater number of users than sustainable streams, user selection and power allocation play a more significant role in throughput as shown in (b). In fact, under certain channel realizations, RCI-MAC outperforms the rate maximizing RCI-BC→MAC scheme even though there is a stricter rule on power allocations. For all simulations, the total power of the system was the same.

5.2 Average-Rate Maximizing Beamformer in the MAC (RCDI-MAC)

In the previous section it was shown that linear precoding in the MAC can achieve a significant portion of the total possible information throughput of the system under consideration when CSI is perfectly available at both the transmitters

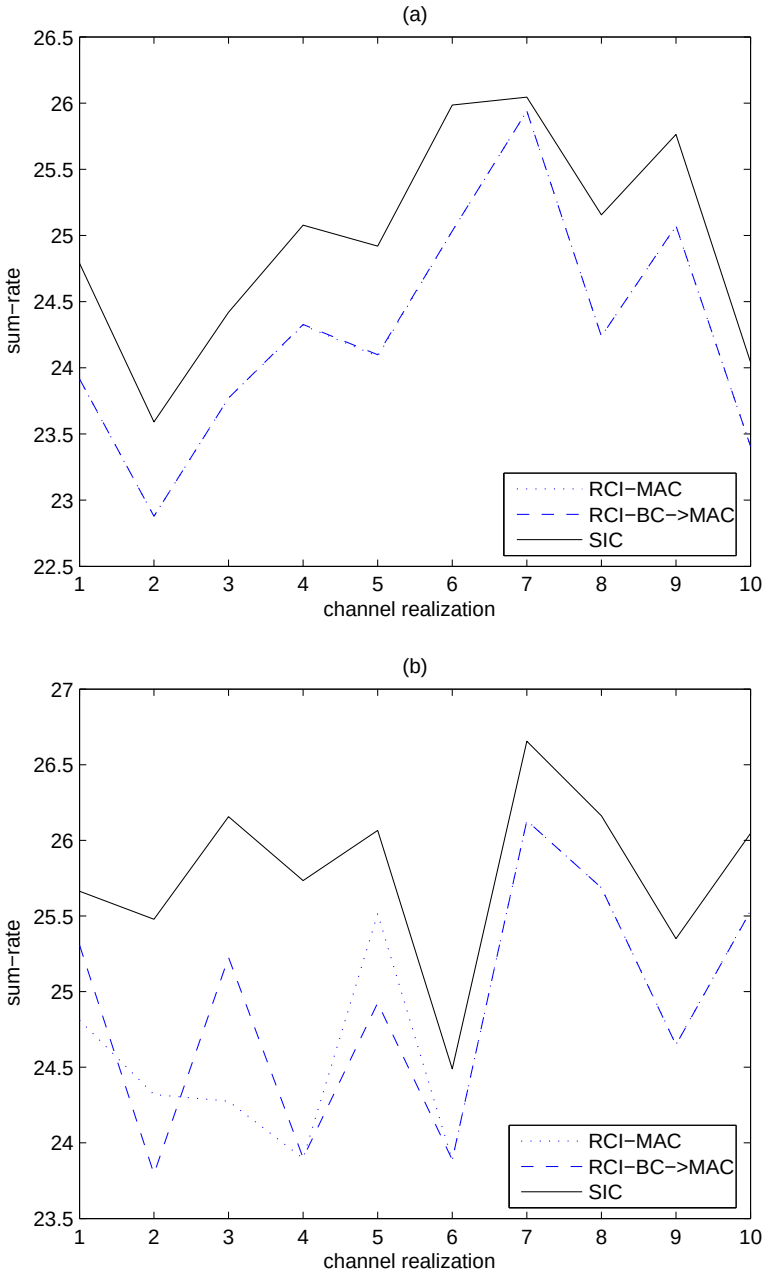

Figure 5.1: Instantaneous throughput for various precoding techniques and a channel size of $N_r = N_t = 4$, $P = 10$ and (a) $K = 4$ or (b) $K = 6$ users.

and receiver and a beamforming algorithm (RCI-MAC) was derived to directly achieve these throughputs. When the assumption of perfect CSI no longer holds, significant degradation was shown to occur in the BC [22] and will also influence rate loss in the MAC. To combat these detrimental effects of inaccurate CSI, a beamforming algorithm was derived in [22] that attempts to maximize the *average* sum-rate of the BC - referred to as regularized channel distribution inversion in the BC (RCDI-BC). This section shows a similar analysis in the MAC and presents results regarding performance loss with erroneous CSI.

In order to maximize the average sum-rate in the MAC, an approximation on the sum-rate will be used analogous to that used in Chapter 4. For clarity, this expression is reiterated here as

$$\bar{r}_j = \log\left(1 + \frac{\bar{n}_j}{\bar{d}_j}\right) \tag{5.5}$$

where $\bar{n}_j$ and $\bar{d}_j$ are the expected values of numerator and denominator, respectively, of (5.2) or analogously (5.3) when simplification is used on the rate equations. Given this approximation on the average per-user rate, the optimization problem becomes

$$\begin{array}{cc} \max\limits_{\mathbf{w}_j,\mathbf{b}_j} & \sum_j \bar{r}_j \\ ||\mathbf{w}_j||^2 = 1 & ||\mathbf{b}_j||^2 \in \{1, 0\} \end{array}$$

where the objective function is the approximation (5.5) derived from (5.3).

Using a similar approach to average sum-rate maximization in the BC, the RCDI-MAC beamforming weights are derived as

$$\mathbf{b}_j = \begin{cases} \left(\frac{[\mathbf{D}]_{j,j}}{P}\mathbf{I} + \sum_{i=1}^{i=K}[\mathbf{D}]_{i,i}\bar{\mathbf{R}}_{i,j}\right)^{-1}\boldsymbol{\Omega}_j & , \text{ “on”} \\ \left(\sum_{i=1}^{i=K}[\mathbf{D}]_{i,i}\bar{\mathbf{R}}_i\right)^{-1}\boldsymbol{\Omega}_j & , \text{ “off”} \end{cases}$$

where

$$\begin{aligned} \bar{\mathbf{R}}_{i,j} &= \text{mat}(\mathbf{R}_i \text{vec}(\mathbf{w}_j\mathbf{w}_j')) \\ \mathbf{D} &= \text{diag}\left(\frac{\bar{n}_1}{\bar{d}_1(\bar{n}_1+\bar{d}_1)}, \ldots, \frac{\bar{n}_1}{\bar{d}_1(\bar{n}_1+\bar{d}_1)}\right) \\ \boldsymbol{\Omega}_j &= \frac{\bar{\mathbf{R}}_{j,j}\mathbf{b}_j}{\bar{d}_j}. \end{aligned} \tag{5.6}$$

However, it is worthwhile to note that the RCDI-MAC can not be written directly from the RCDI-BC algorithm nor is it apparent how channel duality can be used with CDI beamforming; thus, only RCDI-MAC is analyzed to maximize the average rate approximation (i.e. no straightforward RCDI-BC→MAC mapping is available).

Figure 5.2 shows the performance of RCDI-MAC as well as the degradation of RCI-MAC when erroneous CSI is used to calculate the beamforming weights. Two specific cases are examined for comparison purposes. In Case A, the situation where the receiver has perfect CSI and the transmitters have either erroneous CSI feedback or perfect CDI feedback is examined. In practical MAC systems, the receiver will most likely calculate transmit beamforming weights for all users and simply feed the weights or a quantized version back to the transmitters. For Case A, the effect of lag and error in the feedback channel is simply modeled as if the transmitters calculated the beamforming weights with the given channel estimation error while the receiver has error-free CSI to calculate receive beamforming weights. Case B shows the opposite extreme when the feedback channel is assumed instantaneous and perfect while the transmitters and receiver possess equally-erroneous CSI as quantified by ρ_d and the error model (2.13) or perfect CDI from all users.

Figure 5.2 demonstrates that RCDI-MAC provides stable performance at the expense of lower rate compared to the CSI based scheme; however, RCI-MAC eventually has poorer performance when the error in the channel estimates becomes large enough (due to lag in this case). The results indicate the importance of obtaining accurate CSI at the receiver as the degradation is rapid as CSI accuracy lessens as displayed by Case B. Another interesting result, as shown in Case A, is the stability of using the RCDI-MAC vectors at the transmitters. A MAC receiver, aware of the mobility in the channel, may choose to instead feedback RCDI-MAC weights rather than RCI-MAC weights to provide for better performance against the time-varying channel. Environmentally, the Outdoor channel has a tighter spread between RCI-MAC and RCDI-MAC curves which follows the general trend seen throughout this dissertation.

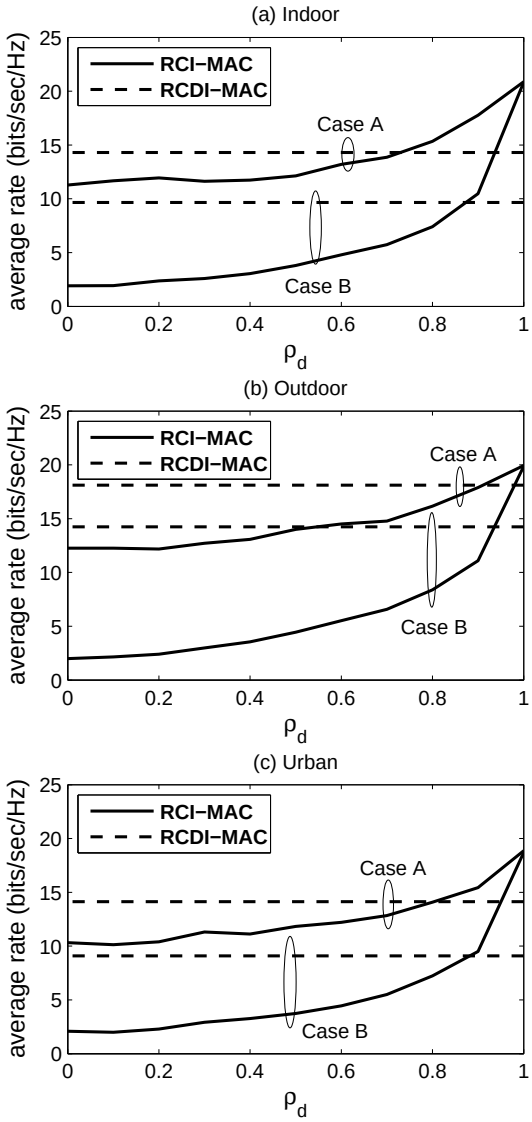

Figure 5.2: Achievable throughput for RCI-MAC and RCDI-MAC beamformers with $N_r = N_t = K = 4$ and $P = 10$. For the RCI-MAC beamformer CSI estimation error is fixed at $\sigma_e^2 = .1$.

The work presented in this chapter, in part, was originally published in the following paper, of which the author was also main contributor: A. L. Anderson, J. R. Zeidler, and M. A. Jensen, "Instantaneous and average rate maximization in MIMO multiple-access channels (MAC) with linear processing," in *42nd Asilomar Conf. Signals, Systems and Computers*, Pacific Grove, CA, Oct. 2008.

Chapter 6

Reduced Feedback RCDI Beamforming

As demonstrated in previous chapters, to limit the frequency of feedback, alternatively stable (yet suboptimal) communication performance may be obtained by signaling based on channel distribution information, often referred to as partial CSI, in the form of either channel mean (CMI) or covariance (CCI) information in both single-user and multi-user channels [2, 45, 46]. Combining various forms of partial CSI is also possible [47], [48] where both CQI and CDI are used to perform coarse channel acquisition for scheduling purposes in the broadcast channel. The work in [21] develops a signaling approach for the broadcast channel based on minimum mean squared error (MMSE) beamforming weights at the transmitter and receiver computed from CDI in the form of one-sided spatial correlation matrices under the assumption that the receiver possesses perfect CSIR. The algorithm is shown to provide stable communication performance for time-variant channels with low required feedback frequency.

In addition to limiting the frequency of feedback it is important to limit the *quantity* of required feedback for coding algorithms. One approach for mitigating these quantities in both single- and multi-antenna channels is to change the type or amount of information used to construct the precoder [49]. For example, a simple

method of limiting the quantity of feedback, often referred to as opportunistic or random beamforming [43,50], is for each user to simply return information regarding the signal-to-interference plus noise ratio (SINR) to the transmitter who can then determine user selection for the given beamforming vectors and scheduling algorithm. Variations on and comparisons to opportunistic or random beamforming can be found in [51, 52]. Another approach to limited feedback is to create quantized beamforming codebooks for either single-user [53] or multi-user [54,55] channels, which when known to transmitter and receiver(s), can reduce the feedback to simply an index into the predetermined codebook. Other methods of feedback quantization are also possible, as in [56] where feedback of normalized channel vectors is compared with standard beamforming codebooks or when information about the channel itself is quantized and fed back to the transmitter [57–59]. Other types of information, often generically referred to as channel quality information (CQI), can also be used for beamformer construction [44, 60, 61]. Though each of these methods can dramatically reduce the amount of feedback data required, the frequency of feedback must still remain high to compensate for time variations in the channel.

The RCDI algorithm was shown to limit the frequency of feedback in BC and MAC using linear processing on the channel statistics. The drawback of the algorithm, however, is that since it requires the full spatial covariance matrix, each user must feed back a significant amount of information to describe the spatial correlation compared to CSI-based schemes. This chapter therefore develops a method for parameterizing the required CDI using two commonly accepted channel models, namely the Kronecker [16] and Weichselberger [19] models, that can both be utilized to explicitly represent the spatial covariance structure. Simulations in realistic channels show that this parameterization reduces the feedback on par with CSI-based schemes with minor loss in throughput performance while significantly lowering the frequency of feedback.

6.1 Channel Distribution Parameterization

The prior chapters demonstrated that the RCDI algorithm enables good throughput performance with reduced feedback frequency in the time-varying broadcast or multiple-access channels. However, because the algorithm computation requires the full spatial correlation matrix

$$\mathbf{R} \;=\; \mathrm{E}[\mathrm{vec}(\mathbf{H})\mathrm{vec}(\mathbf{H})^H]$$

through the permutations $\mathbf{S}_\mathrm{t}$ and $\mathbf{S}_\mathrm{r}$, where the user index is dropped for convenience, the amount of data that must be fed back is significant. In fact, assuming M antennas per node, each user must feedback an $M^2 \times M^2$ matrix, or M^4 complex values, in contrast to the M^2 numbers that must be fed back for RCI implementation using the channel matrix. The goal of this section is to consider ways to parameterize $\mathbf{S}_\mathrm{t}$ and $\mathbf{S}_\mathrm{r}$ to reduce the required volume of feedback data. The approach taken is to explore the use of popular channel models, namely the Kronecker and Weichselberger models, which impose structure on the correlation matrix to allow its representation using smaller matrices. Throughout this development, we will make use of the properties $\mathbf{AB} \otimes \mathbf{CD} = (\mathbf{A} \otimes \mathbf{C})(\mathbf{B} \otimes \mathbf{D})$ and $(\mathbf{A} \odot \mathbf{B}) \otimes (\mathbf{C} \odot \mathbf{D}) = (\mathbf{A} \otimes \mathbf{C}) \odot (\mathbf{C} \otimes \mathbf{D})$ where $\otimes$ is the matrix Kronecker product and $\odot$ is the element-wise, matrix, Schur-product.

6.1.1 Kronecker Model

The Kronecker model [16] assumes separability between transmit and receive spatial correlation matrices. Assuming that $\mathbf{H}_w$ is an $M \times M$ matrix with zero-mean, unit variance, i.i.d. complex Gaussian entries, the correlated channel matrices can be realized using

$$\mathbf{H}_\mathrm{Kron} \;=\; \sqrt{\mathbf{R}_\mathrm{r}}\mathbf{H}_w\sqrt{\mathbf{R}_\mathrm{t}}$$

where the one-sided correlation matrices are calculated from $\mathbf{R}_\mathrm{r} = \mathrm{E}[\mathbf{H}\mathbf{H}^H]$ and $\mathbf{R}_\mathrm{t} = \mathrm{E}[\mathbf{H}^T\mathbf{H}^*]$ or estimated from the measured data using (2.2) and (2.3). As-

suming this structure leads to the RCDI input matrix

$$\begin{aligned}
\mathbf{S}_{\mathrm{t}}^{\mathrm{Kron}} &= \mathrm{E}[\mathbf{H}_{\mathrm{Kron}}^{T} \otimes \mathbf{H}_{\mathrm{Kron}}^{H}] \\
&= \mathrm{E}\left[(\sqrt{\mathbf{R}_{\mathrm{r}}}\mathbf{H}_{w}\sqrt{\mathbf{R}_{\mathrm{t}}})^{T} \otimes (\sqrt{\mathbf{R}_{\mathrm{r}}}\mathbf{H}_{w}\sqrt{\mathbf{R}_{\mathrm{t}}})^{H}\right] \\
&= \mathrm{E}\left[\widetilde{\mathbf{R}}_{\mathrm{t}}^{\mathrm{Kron}}\left(\mathbf{H}_{w}^{T} \otimes \mathbf{H}_{w}^{H}\right)\widetilde{\mathbf{R}}_{\mathrm{r}}^{\mathrm{Kron}}\right] \\
&= \widetilde{\mathbf{R}}_{\mathrm{t}}^{\mathrm{Kron}}\mathbf{I}_{\mathrm{t}}\widetilde{\mathbf{R}}_{\mathrm{r}}^{\mathrm{Kron}} \qquad (6.1)
\end{aligned}$$

where $\mathbf{I}_{\mathrm{t}} = \mathrm{E}[\mathbf{H}_{w}^{T} \otimes \mathbf{H}_{w}^{H}]$, $\widetilde{\mathbf{R}}_{\mathrm{t}}^{\mathrm{Kron}} = \sqrt{\mathbf{R}_{\mathrm{t}}}^{T} \otimes \sqrt{\mathbf{R}_{\mathrm{t}}}^{H}$, and $\widetilde{\mathbf{R}}_{\mathrm{r}}^{\mathrm{Kron}} = \sqrt{\mathbf{R}_{\mathrm{r}}}^{T} \otimes \sqrt{\mathbf{R}_{\mathrm{r}}}^{H}$. In a similar fashion we can construct

$$\mathbf{S}_{\mathrm{r}}^{\mathrm{Kron}} = \widetilde{\mathbf{R}}_{\mathrm{r}}^{\mathrm{Kron}}\mathbf{I}_{\mathrm{r}}\widetilde{\mathbf{R}}_{\mathrm{t}}^{\mathrm{Kron}} \qquad (6.2)$$

where $\mathbf{I}_{\mathrm{r}} = \mathrm{E}[\mathbf{H}_{w}^{*} \otimes \mathbf{H}_{w}]$. These results demonstrate that the feedback information is reduced to two $M \times M$ matrices for a total of $2M^2$ complex numbers.

6.1.2 Rank-1 Approximation Model

Computing $\mathbf{R}_{\mathrm{r}}$ and $\mathbf{R}_{\mathrm{t}}$ directly from the channel matrices and then using the Kronecker products to estimate the full correlation matrix can result in substantial modeling error. An alternate approach is to impose the Kronecker structure of the correlation matrix but compute estimates $\widehat{\mathbf{R}}_{\mathrm{t}}$ and $\widehat{\mathbf{R}}_{\mathrm{r}}$ from the optimization

$$\min_{\hat{\mathbf{R}}_{\mathrm{r}}, \hat{\mathbf{R}}_{\mathrm{t}}} ||\mathbf{R} - \hat{\mathbf{R}}_{\mathrm{t}} \otimes \hat{\mathbf{R}}_{\mathrm{r}}||^2. \qquad (6.3)$$

These estimates can be obtained using the solution discussed in [62], which is referred to as the rank-1 approximation. These matrices can be fed back to the transmitter and used in (6.1) and (6.2). This approach also results in a feedback complexity of $2M^2$ complex numbers.

6.1.3 Weichselberger Model

The Weichselberger model [19] was introduced in an effort to overcome some of the deficiencies discovered with the Kronecker model. The Kronecker model

deficiencies arise from imposing one-sided correlations on the spatial structure of the channel which result in underestimation of the channel capacity [18]. Under the Weichselberger model, channel matrix realizations are represented as

$$\mathbf{H}_{\text{Weichs}} = \mathbf{U}_{\text{r}}(\check{\mathbf{\Omega}} \odot \mathbf{H}_w)\mathbf{U}_{\text{t}}^T$$

where $\check{\mathbf{A}}$ is the element-wise square root on the matrix $\mathbf{A}$ and the matrices $\mathbf{U}_{\text{r}}$ and $\mathbf{U}_{\text{t}}$, respectively, contain the eigenvectors of $\mathbf{R}_{\text{r}}$ and $\mathbf{R}_{\text{t}}$ from the Kronecker model. Under this representation we can write

$$\begin{aligned}
\mathbf{S}_{\text{t}}^{\text{Weichs}} &= \text{E}[\mathbf{H}_{\text{Weichs}}^T \otimes \mathbf{H}_{\text{Weichs}}^H] \\
&= \text{E}\left[(\mathbf{U}_{\text{r}}(\check{\mathbf{\Omega}} \odot \mathbf{H}_w)\mathbf{U}_{\text{t}}^T)^T \otimes (\mathbf{U}_{\text{r}}(\check{\mathbf{\Omega}} \odot \mathbf{H}_w)\mathbf{U}_{\text{t}}^T)^H\right] \\
&= \text{E}\left[\widetilde{\mathbf{U}}_{\text{t}}^{\text{Weichs}} \left\{(\check{\mathbf{\Omega}} \odot \mathbf{H}_w) \otimes (\check{\mathbf{\Omega}} \odot \mathbf{H}_w)\right\} \widetilde{\mathbf{U}}_{\text{r}}^{\text{Weichs}}\right] \\
&= \widetilde{\mathbf{U}}_{\text{t}}^{\text{Weichs}} \left\{(\check{\mathbf{\Omega}}^T \otimes \check{\mathbf{\Omega}}) \odot \mathbf{I}_{\text{t}}\right\} \widetilde{\mathbf{U}}_{\text{r}}^{\text{Weichs}}
\end{aligned} \tag{6.4}$$

where $\widetilde{\mathbf{U}}_{\text{t}}^{\text{Weichs}} = \mathbf{U}_{\text{t}}^T \otimes \mathbf{U}_{\text{t}}^H$, and $\widetilde{\mathbf{U}}_{\text{r}}^{\text{Weichs}} = \mathbf{U}_{\text{r}}^T \otimes \mathbf{U}_{\text{r}}^H$. Similarly,

$$\mathbf{S}_{\text{r}}^{\text{Weichs}} = \widetilde{\mathbf{U}}_{\text{r}}^{\text{Weichs}} \left\{(\check{\mathbf{\Omega}}^* \otimes \check{\mathbf{\Omega}}) \odot \mathbf{I}_{\text{r}}\right\} \widetilde{\mathbf{U}}_{\text{t}}^{\text{Weichs}}. \tag{6.5}$$

This result indicates that the RCDI implementation requires feedback of three $M \times M$ matrices for a feedback complexity of $3M^2$ complex numbers. Details on estimation of these matrices from the data can be found in [19].

6.2 Parameterization Results

Prior to examining the performance of each parameterization technique, it is worthwhile to first note the resulting modeling error that each technique introduces if it were used to model channel capacity. Fig. 6.1 examines this modeling error by way of normalized capacity with respect to the full correlation model. For this plot, the measured data is used to estimate the various parameters necessary for each model. In other words, the full correlation matrix and its Rank-1 approximation is calculated as well as the left- and right-sided correlation matrices for the Kronecker

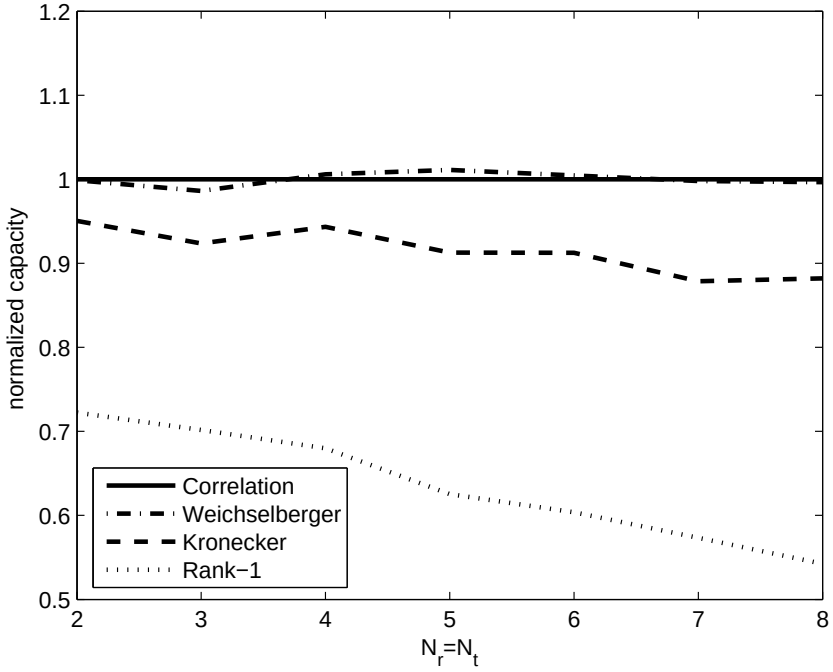

Figure 6.1: Model capacity versus $N_r = N_t$ in the single-user channel where each value is normalized by the full correlation model capacity. Power is constrained to $P = 10$.

model and the coupling matrix for the Weichselberger model. Once estimated, new channels are realized for each of these models, Eqs. (2.5) (6.1) (6.4), and the resulting uninformed capacity is found and normalized by the capacity found under the full correlation model. Note that the results are similar to those presented in other work [18]; namely, the Kronecker model produces higher error with more antennas while the Weichselberger model provides for a good model of the spatial correlation. The Rank-1 approximation of the Kronecker model results in a poor model of the channel capacity since the framework used places constraints on minimizing the norm of the correlation error but does not address the modeling error directly.

The performance of the RCDI implementation for the different parameterizations is examined in Fig. 6.2 for various environments in the BC. For this plot, the power is held constant at $P = 10$ while the number of antennas and users was swept assuming $N_{\mathrm{r}} = N_{\mathrm{t}} = K$. Similar results are available for the MAC in Fig. 6.3. Parameterizing the spatial correlation is less beneficial in the MAC as the receiver can just feed back the beamforming weights rather than the entire or parameterized correlation matrix. However, these results are still applicable in larger network settings when other users may invoke knowledge of the receiver spatial properties for their own transmissions. Notice that the results in Fig. 6.3 mirror a similar trend as shown in Fig. 6.2 for the BC.

These results show that when an appropriate parameterization is used, the impact of parameterization on the overall performance is relatively small. This is noteworthy, since this parameterization significantly reduces the quantity of feedback data. As an example, for $M = 6$ antennas at all nodes feedback of the full correlation matrix requires communication of 1296 complex numbers per user compared to only 108 and 72 complex numbers using parameterizations based on the Weichselberger and rank-1 models, respectively. These results also show that while the Kronecker structure for the correlation matrix is reasonable (as evidenced by the performance for the rank-1 model), it is critical that the matrices $\mathbf{R}_{\mathrm{t}}$ and $\mathbf{R}_{\mathrm{r}}$ be properly estimated. The deficiencies in the traditional Kronecker model for larger array sizes observed here appear supportive of other studies which have

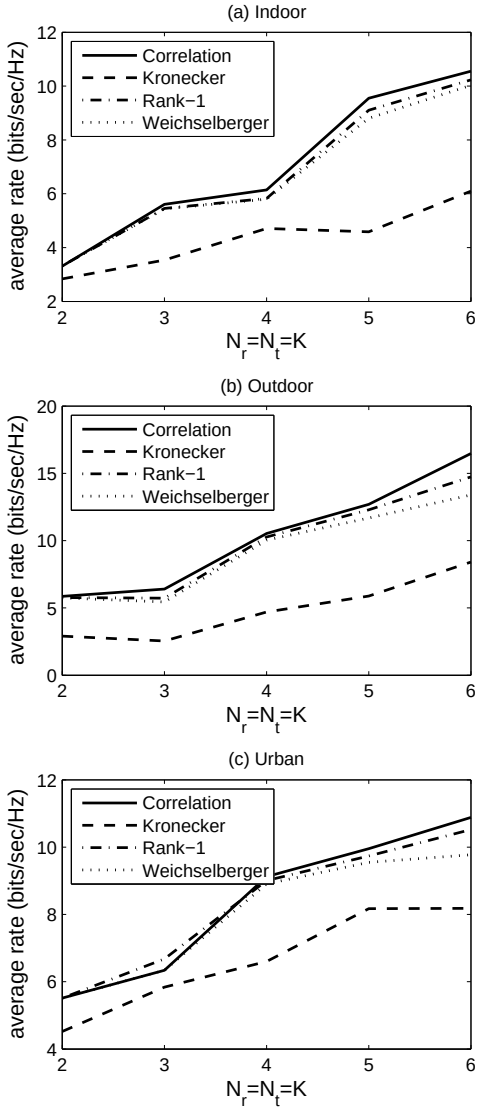

Figure 6.2: Average sum-rate versus system size when the matrices $\mathbf{S}_t$ and $\mathbf{S}_r$ are generated by using: the full correlation matrix, the Weichselberger model, the Kronecker model, and a rank-1 approximation. Shown are the (a) Indoor, (b) Outdoor, and (c) Urban environments.

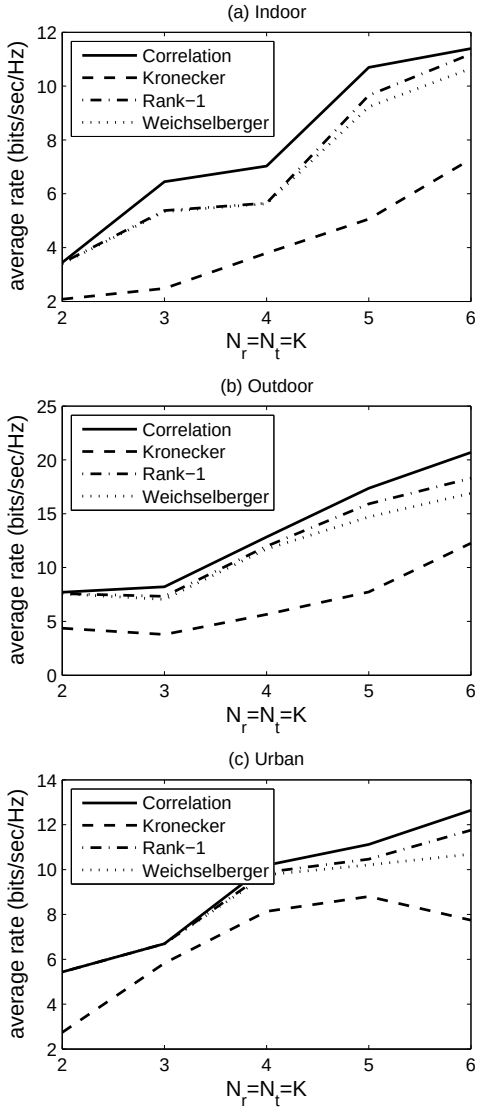

Figure 6.3: Average sum-rate versus system size when the matrices $\mathbf{S}_t$ and $\mathbf{S}_r$ are generated by using: the full correlation matrix, the Weichselberger model, the Kronecker model, and a rank-1 approximation. Shown are the (a) Indoor, (b) Outdoor, and (c) Urban environments.

shown that this model fails to accurately represent the channel spatial structure as the number of antennas increases [18].

The work presented in this chapter, in part, was originally published in the following papers, of which the author was also main contributor: A. L. Anderson, J. R. Zeidler, and M. A. Jensen, "Reduced-feedback linear precoding with stable performance for the time-varying MIMO broadcast channel," *IEEE Journal on Selected Areas of Communications, (Special Issue on Limited Feedback)*. Vol. 26, No. 8, 11 pages, October, 2008; A. L. Anderson, J. R. Zeidler, and M. A. Jensen, "Regularized channel distribution inversion and parameterization in the MIMO broadcast channel," in *Proc. 2008 IEEE 68th Veh. Technol. Conf.*, Calgary, Canada, Sept. 2008.

Chapter 7

Generalized Correlation-Based Beamforming

In this work MIMO antenna links have been shown to increase the link capacity in both single- and multi-user channels including the broadcast and multiple-access channels using either CSI or CDI. Such links promise future generation wireless *networks* increased reliability and throughput over standard single-input single-output links by exploiting the dimensionality gains of employing both multiple antennas per node and multiple nodes per channel. With this increased performance comes increased complexity at both the medium access control (MAC) layer and physical (PHY) layer where scheduling and allocation of correct link topologies [63–65] become an issue in large MANETs, and where optimal per-link transmission strategies require nonlinear precoding [2, 28, 66]. In this chapter, we examine the various possible link topologies in a MANET and also simple transmission strategies, in the form of sum-rate maximizing beamformers, to aid the MAC and PHY layers in finding the "best" possible combination of link schedules in a cross-layer fashion.

The net gain seen by MIMO links and capacity of MANETs is intimately connected to the precoding and detection schemes utilized by the transmitters and receivers as well as the link access algorithm. Significant work has been done on

analyzing the capacity regions of multi-user and ad hoc networks employing links from simple P2P to more complex interference and multiple-access links. In [67,68] fundamental limits on capacity of a network are examined for both SISO and MIMO channels. These limits are increased when additional assumptions about node capabilities are made such as multi-packet reception (MPR) [69] or more complex information dissemination [70]. Other work [71, 72] examines the ad hoc network capacity with emphasis on the available transport capacity regions for various network sizes and link topologies. Ultimately, capacity optimal analyses often require that nonlinear techniques be used at the transmitters and/or receivers which can further increase the complexity of the overall system [28].

As specific examples, such nonlinear coding techniques as dirty-paper coding (DPC) and successive interference cancellation (SIC) provide optimal performance at the cost of complexity and nonlinearity at the link nodes [27, 28, 66]. As focused within this work, beamforming, or linear processing, is a simpler form of transmission that sacrifices some performance in exchange for simplicity in its implementation. In [73] an iterative minimum mean-square error (MMSE) beamformer was suggested for optimization of a minimum power constraint in ad hoc networks. It is shown that linear beamforming for MANETs [74] is optimal when the interference is sufficiently large and CSI is available at all nodes. The rate-maximizing beamformers for both single-user channels as well as the broadcast [21, 40] and multiple-access channels [75] have been examined previously for both multiple-input single-output (MISO) and MIMO links. This current work extends these rate-maximizing beamforming algorithms in the context of network link topologies regardless of the type of scheduled channel. However, as these rate maximizing beamformers also require accurate knowledge of channel state information (CSI) at all nodes, performance loss is incurred due to erroneous CSI caused by numerous factors, including: limited training, channel estimation errors, delayed feedback from network overhead, quantization effects, and so on.

Each of these loss factors for erroneous CSI are quantized into a single value in Chapter 2 that demonstrates instability of the CSI-beamformers, as analyzed in this work, and also shows severity of lost throughput based on the link type.

To alleviate the problem of obtaining accurate CSI and combating the effects of erroneous CSI, the approach found in [22] is adapted to the channels analyzed in this work. In [22] a beamforming algorithm based exclusively on CSI or CDI, depending on the available information, is derived that results in stable performance in the broadcast channel with feedback limited to a single transmission of the spatial correlation matrices given the assumption of statistically-stationary channels. A more general form of this beamformer is presented in this work that will be useful in analyzing the stability gains for *all* links in a MANET. Given this form of beamforming and for the simulation scenarios examined in this work, it is shown that each channel can maintain roughly 70-80% of the optimal CSI-based average sum-rate but with the advantage of being immune to time variations in the channel and CSI acquisition overhead. Thus, the CDI-beamformers equalize the differential time-scales between the MAC and PHY layers mitigating the overhead required for all nodes within a multi-user channel to share information. This approach allows the MAC layer to perform truly cross-layer optimization in the network as the MAC and PHY layers share common information about link throughput.

7.1 Notation and Definitions

As any work focusing on MIMO MANETs range in scope from large N-node networks down to a single data transmission between nodes at the PHY layer it is important to specifically define the terminology that may have ambiguous meaning depending on the context. For example, traditionally a "link" may refer to two nodes communicating with one another via a single P2P data stream while in this work a link has a different meaning depending on the type of single- or multi-user channel that has been scheduled for access. Consider the following definitions for different partitions of the network:

- ***Network*** - For this work, the terminology MANET and network will be interchangeable in describing a group of N mobile nodes each consisting of $N_r = N_t$ antennas and some power constraint P per node. All nodes

are considered within transmission range to all other nodes meaning any simultaneous transmission, without further partitioning, will interfere with all other transmissions.

- ***Subnetwork*** - A subdivision or partition of the larger network is referred to as a subnetwork. These subnetworks consist of $K \leq N$ users which are orthogonally separated from other subnetworks - whether via time, code, or frequency is unimportant for this analysis. As working with subnetworks reduces the complexity and simulation time of performance results, the focus of this work will be on the smaller subnetworks for these practical reasons.

- ***Link*** or ***Schedule*** - Refer to one of the various possible types of topologies available to the MAC layer for access scheduling. Links can consist of any number of data streams and may also contain multiple transmit and receive nodes all transmitting and receiving at the same time while also interfering with on another. From Chapter 1, Fig. 1.5 shows examples of the possible single- and multi-user links or channels examined in this work. As defined, a single link in a MIMO subnetwork can consist of both multiple data streams and users all of which can be used for optimization purposes in the subnetwork or full network throughput.

- ***Sublink*** or ***Stream*** - Each of the possible links in Fig. 1.5 consists of one or more sublinks representing a single data stream from one transmitting user to one receiving user. If a link contains multiple sublinks then each sublink will cause interference to all receivers attempting to decode. For example, the MAC link shown in Fig. 1.5(c) consists of three sublinks.

- ***Channel*** - As the five single- and multi-user channels have been defined as links with appropriate acronyms, the term "channel" will be used primarily as the $N_r \times N_t$ channel transfer matrix $\mathbf{H}_{\{m,n\}}$ between the mth and nth users.

For notational purposes throughout the analysis, scalars are written in either unbold-face lower- or upper-case, while vectors and matrices are written as

bold-face in lower- or upper-case, respectively. Standard matrix operations of transpose, conjugate, and conjugate-transpose are defined as $\{\cdot\}^T$, $\{\cdot\}^*$, and $\{\cdot\}^H$, respectively. The function vec$(\cdot)$ is the matrix column stacking operator while mat$(\cdot)$ is its inverse (e.g. mat(vec$(\mathbf{A})) = \mathbf{A}$). Finally, $\otimes$ is the matrix Kronecker product.

7.2 Network Partitioning and Scheduling

Prior to any analysis on an N-node MANET it is important to determine the complexity that scheduling algorithms will encounter given the allowed types of PHY layer links. The end goal of this work is to find the optimal beamformers for each of five different types of single- and multi-user channels, as defined in Section 7.1, with any number of sublinks per channel. The total number of possible links given the network or subnetwork size will directly determine the complexity in finding the network rate-maximizing beamforming weights.

Consider first a full-duplex N-node network represented by a fully-connected graph which models the case when all nodes are in transmission range of all other nodes. If full duplexing is allowed then nodes are allowed to simultaneously transmit and receive, and each possible sublink in the connected graph can be described by a single-digit 4-ary number representing the relationship between two nodes: transmit, receive, transmit and receive, or silent. The total number of sublinks in the connected graph is $\binom{N}{2}$ leading to a total number of unique, duplex network topologies

$$L^{DUP}(N) = 4^{\binom{N}{2}} \tag{7.1}$$

where $\binom{1}{2}$ is assumed identically zero. Though this work will not address the question of duplexity on wireless links, the number of different duplex sublinks $L^{DUP}(N)$ will be used as a comparison in complexity with the number of half-duplex sublinks determined in this paper.

In [71] it was shown that the total number of different multiple-access topologies for the standard MAC link given an N-node network can be written

as

$$L^{MA}(N) = 1 + \sum_{i=1}^{B(N)} \prod_{j=1}^{L_i} b_j^i \tag{7.2}$$

where B(N) is the Bell number of the network which gives the total number of ways the network can be divided into subnetworks, b_j^i represents the ith Bell partition of size j, and L_i is the number of active links. Similarly, it is possible to find the total number of P2P (or IC) links $L^{P2P}(N)$ [71, 72] given the size of the network and excluding duplex links.

However, the ultimate goal of this work is to find the number of *all* possible half-duplex link schedules (i.e. all the links defined in Section 7.1) in a network or subnetwork without constraint to a specific type. It is straightforward to arrive at this solution and is facilitated by considering the network as an irreducible bipartite graph where users are placed in one of two sets representing transmit or receive nodes (but not both). We can then sum over all possible number of transmit nodes $N_{tx} = 1, 2, \ldots, N-1$ and $N_{rx} = N - N_{tx}$ receive nodes where each user takes a turn as transmitter or receiver with a unique set of other transmitting or receiving nodes. With this approach it is assumed that all nodes in the transmit set must transmit but nodes in the receive set do not need to be a part of any link (i.e. not all nodes who are not transmitting will necessarily have information destined for themselves).

Using the simplification that the sum of binomial coefficients can be written as $\sum_{i=0}^{K} \binom{K}{i} = 2^K$, the total number of possible half-duplex links at any given realization of the channel in an ad hoc network with N nodes is written as

$$L(N) = 1 + \sum_{i=1}^{N-1} \binom{N}{i} (2^{N-i} - 1)^i. \tag{7.3}$$

As any valid link can be considered a subset of the HC link, $L(N)$ gives the total number of HC links as well. In brief, the resulting values of $L(N)$ represent the total number of possible schedules that the MAC layer is allowed to work with in the MIMO MANET of size N. Note that validating (7.3) is possible for small values of N by performing an exhaustive search over all possible sublink configurations, though for $N > 8$ the search time becomes quite large.

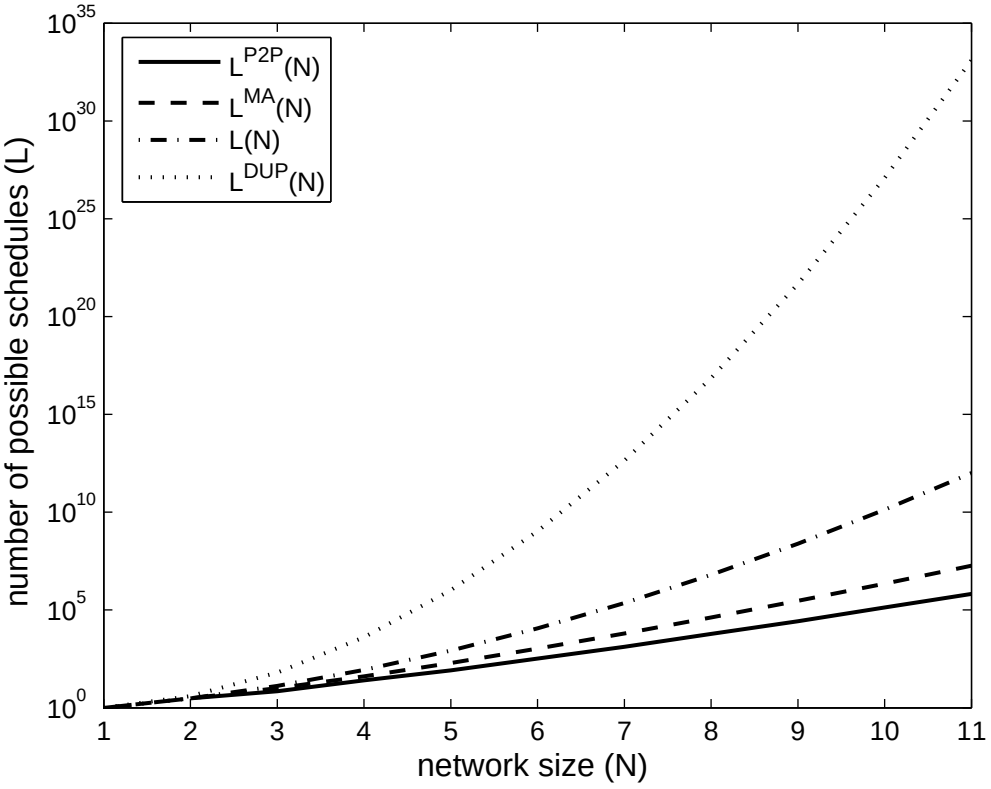

Figure 7.1: Number of possible schedules given various link constraints in an N-node ad hoc network.

Table 7.1: Number of possible unique schedules using point-to-point, MA/BC, half-duplex, and duplex links.

N	$L^{P2P}(N)$	$L^{MA}(N)$	$L(N)$	$L^{DUP}(N)$
1	1	1	1	1
2	3	3	3	4
3	7	10	13	64
4	25	41	87	4096
5	81	196	841	1048576
6	331	1057	11643	–
7	1303	6322	227893	–
8	5379	41393	6285807	–
9	26785	293608	–	–
10	133651	2237921	–	–

Though (7.3) is a number representative of the total complexity for MAC layer scheduling if all possible half-duplex links are considered viable, it is worthwhile and informative to also determine the specific number of each type of link as well. Using the same approach as above, and for completeness, the topologies for multiple-access links only can be written as

$$L^{MA}(N) = 1 + \sum_{i=1}^{N-1} \binom{N}{i} (N-i)^i. \tag{7.4}$$

Thus (7.2) and (7.4) are equivalent expressions which also give the total number of BC links as well. In a similar fashion, the expressions for the number of P2P topologies, which includes both SUC and IC links, becomes

$$L^{P2P}(N) = 1 + \sum_{i=1}^{N-1} \binom{N}{i} \binom{N-i}{i} i!. \tag{7.5}$$

Note that all topology sizes for $L^{DUP}(N)$, $L(N)$, $L^{MA}(N)$, and $L^{P2P}(N)$ contain the "zero" topology where no transmission takes place between any set of nodes - all nodes are silent.

Table 7.1 lists the resulting values of L for the various link topologies depending on constraints placed at the PHY layer. Missing values in Table 7.1 represent extremely large numbers while these same results are represented graphically in Fig. 7.1 on a logarithmic scale to show the general trend for large values of $L(N)$. This plot also helps to get an intuitive feel for the schedule complexity growth as a function of network size even for small networks. Note that only allowing simple SUC/IC links has a similar trend in growth as MA/BC links while allowing HC links has a significant increase in complexity.

Given the complex nature of possible link schedules, this work will focus on subnetworks of size $K = 4$ for a possible $L(4) = 87$ unique topologies (ranging from the "zero" topology to the almost fully-connected HC link) in order to keep the results tractable. It needs to be reiterated, however, that though we limit the network in this manner for ease in presenting results, the following work is valid for all possible values of K or N. Furthermore, dividing a larger network into smaller orthogonal subnetworks (such as $K = 4$) is related to the task of clustering MANETs into smaller partitions (see [76] for a tutorial on MANET clustering).

7.3 Network Model and Performance Metric

In the previous section, the total number of subnetwork topologies was found for a MANET or subnetwork that allows any type of half-duplex link at the PHY layer. In this section, these specific links will be analyzed and the model used to represent the time variation and spatial correlation of the wireless channel as well. Finally, the performance metric used for optimization purposes will be the sum-rate of each given link as a function of the SINR under the assumption of effective SISO sublinks via transmit and receive beamforming weights. This metric sum-rate will be used exclusively throughout the analysis.

For organizational purposes, assume that each possible schedule can be written as a set $\mathcal{L}$ consisting of sublink duples representing input and output nodes for the schedule under question. For example, the HC link shown by Fig. 1.5(e) can

be written as the set of sublinks $\mathcal{L} = [\{1,2\},\{1,4\},\{3,4\}]$ where the first number of each duple represents the transmit node, the second number the receive node, and the cardinality of $\mathcal{L}$ represents the total number of simultaneous streams occurring for the current schedule. Thus for the $K = 4$ subnetwork under examination there are a total of 87 unique sets $\mathcal{L}$ consisting of cardinalities ranging from zero (i.e. no transmissions) to four (i.e. HC with two BC and two MAC sublinks).

Consider the kth sublink defined as the duple $\{m,n\}$ of the topology defined by $\mathcal{L}$ where the received signal can be written as

$$\mathbf{y}_{\{m,n\}} = \mathbf{H}_{\{m,n\}}\mathbf{b}_{\{m,n\}}x_{\{m,n\}} + \sum_{\{i,j\}\neq\{m,n\}}^{\mathcal{L}} \mathbf{H}_{\{i,n\}}\mathbf{b}_{\{i,j\}}x_{\{i,j\}} + \boldsymbol{\eta}_{\{m,n\}} \tag{7.6}$$

where $\mathbf{H}_{\{m,n\}}$ is the $N_r \times N_t$ channel transfer matrix from user m to user n, $\mathbf{b}_{\{m,n\}}$ is the transmit beamformer for each link that attempts to transfer a single stream of information represented by the Gaussian symbol $x_{\{m,n\}}$, $\boldsymbol{\eta}_{\{m,n\}}$ is additive white Gaussian noise (AWGN) with variance σ_n^2, and all other sublinks are considered interference to the desired stream. A power constraint is placed upon each transmitting node such that no power is shared between users $\sum_{\{m,j\}\in\mathcal{L}} ||\mathbf{b}_{\{m,j\}}||^2 = P$ for the $\{m,n\}$ sublink. However, nodes acting as a BC can allocate power to individual sublinks as power optimization dictates.

In addition to the transmit beamforming vector $\mathbf{b}_{\{m,n\}}$, for each sublink received vector given by (7.6), there will be an associated received beamforming vector given by $\mathbf{w}_{\{m,n\}}$ used for detection purposes. Given this received vector and assumption that all sublinks will interfere with one another, the signal-to-interference plus noise ratio (SINR) can be calculated for each channel realization. Given the per-sublink SINR values, the total available sum-rate of the link [44] can be written as

$$C = \sum_{\{m,n\}}^{\mathcal{L}} \log\left(1 + \frac{|\mathbf{w}_{\{m,n\}}^H \mathbf{H}_{\{m,n\}}\mathbf{b}_{\{m,n\}}|^2}{\sigma_n^2 \sum_{\{m,j\}\in\mathcal{L}} ||\mathbf{b}_{\{m,j\}}||^2 + \sum_{\{i,j\}\neq\{m,n\}} |\mathbf{w}_{\{m,n\}}^H \mathbf{H}_{\{i,n\}}\mathbf{b}_{\{i,j\}}|^2}\right) \tag{7.7}$$

where it is assumed that $||\mathbf{w}_{\{m,n\}}||^2 = 1$. Without losing generality of power allocation, (7.7) assumes unit-average power constraints for all beamforming vectors

which is ensured for the $\{m, n\}$ stream by the normalizing factor in the denominator of the SINR value [75].

Finally, the spatial correlation of the channel matrices $\mathbf{H}_{\{m,n\}}$ will play an important role in providing the throughput/stability tradeoff for the MANET MAC layer. Modeling spatial correlation in the multi-user MIMO channel is facilitated by measurements taken by Brigham Young University [12]. For MIMO channel measurements, the receiver testbed is placed at a specific location in a given environment while the channel is sampled as the receiver traverses a fixed path. The receiver measurement equipment is then moved to a another location and the measurement process is repeated. In this manner, realizations of the multiple-user, multiple-antenna, time-varying channel can be created. Post-processing on the dataset is then performed to estimate the full spatial correlation matrix for the $\{m, n\}$ link

$$\mathbf{R}_{\{m,n\}} = \frac{1}{M} \sum_{i=1}^{M} \text{vec}\left(\widetilde{\mathbf{H}}_{\{m,n\}}(i)\right) \text{vec}\left(\widetilde{\mathbf{H}}_{\{m,n\}}(i)\right)^{H} \tag{7.8}$$

where the integer index i represents samples into the measured channel $\widetilde{\mathbf{H}}_{\{m,n\}}$ and M is the estimation window size. Once $\mathbf{R}_{\{m,n\}}$ has been estimated for each sublink, sublink channels can be realized using a random matrix model with the measured, full correlation matrix

$$\mathbf{H}_{\{m,n\}} \quad = \quad \text{mat}\left\{\sqrt{\mathbf{R}_{\{m,n\}}}\text{vec}(\mathbf{H}_w)\right\} \tag{7.9}$$

where $\mathbf{H}_w$ is an $N_r \times N_t$ matrix with unit-variance, complex Gaussian entries and $\sqrt{\cdot}$ is the matrix square root operator (i.e. $\sqrt{\mathbf{A}}\sqrt{\mathbf{A}} = \mathbf{A}$). This full correlation model (7.9) coupled with statistically measured samples from (7.8) allow for realistic correlation values while also providing a simplified method of channel realizations for statistical analysis.

7.4 Regularized Channel Inversion in Hybrid Channels (RCI-HC)

Priori knowledge of the available sum-rate per link per channel realization would provide the MAC layer with an invaluable tool in optimizing the overall network throughput. In order to provide this type of information to the MAC layer, the sum-rate maximizing beamforming vectors need to be found for all possible links as a function of the current channel realization. In [77], the sum-rate of a noncooperative, fully-informed HC link is examined by decomposing the channel into two noninterfering BC or MAC links. The algorithm from [42] was derived to maximize the sum-rate of a MISO broadcast channel with perfect CSI at the transmitter and receivers and is referred to as regularized channel inversion (RCI) in this work. This section details the steps taken to generalize the RCI beamformer and maximize the sum-rate of any link consisting of: single-user, broadcast, multiple-access, interference, or hybrid channels with nodes equipped with MIMO antennas. Since the HC represents the most complex channel topology - all other links can be considered subsets of the HC link - we will refer to the generic beamforming algorithm of this section as RCI-HC regardless of the actual channel it is used in (i.e. the RCI-HC algorithm will be used for SUC/IC/MAC/BC links as well).

To bring the MIMO channel into context and in order to incorporate multiple antennas at the receivers, an effective MISO channel can be created by initializing each sublink with a receive beamforming vector. Furthermore, to simplify the steps taken while deriving the rate maximizing beamformer, the following notation

is defined:

$$\begin{aligned}
\mathcal{N}_{\{m,n\}} &= \text{num}\{\rho_{\{m,n\}}\} \\
\mathcal{D}_{\{m,n\}} &= \text{den}\{\rho_{\{m,n\}}\} \\
\mathbf{A}_{\{l,m,n\}} &= \mathbf{H}_{\{l,n\}}^{H}\mathbf{w}_{\{m,n\}}\mathbf{w}_{\{m,n\}}^{H}\mathbf{H}_{\{l,n\}} \\
\mathbf{\Lambda}_{\{m,n\}} &= \frac{\mathbf{A}_{\{m,m,n\}}^{H}\mathbf{b}_{\{m,n\}}}{\mathcal{D}_{\{m,n\}}} \\
d_{\{m,n\}} &= \frac{\mathcal{N}_{\{m,n\}}}{\mathcal{D}_{\{m,n\}}\left(\mathcal{N}_{\{m,n\}}+\mathcal{D}_{\{m,n\}}\right)}
\end{aligned} \tag{7.10}$$

where $\rho_{\{m,n\}}$ is the $\{m,n\}$ sublink SINR used to calculate rate (7.7) and num$(\cdot)$ and den$(\cdot)$ return the numerator and denominator of the argument, respectively.

The sum-rate (7.7) can be rewritten and expanded as

$$C = \sum_{\{m,n\}}^{\mathcal{L}} \log\left(\mathcal{N}_{\{m,n\}}+\mathcal{D}_{\{m,n\}}\right) - \log\left(\mathcal{D}_{\{m,n\}}\right) \tag{7.11}$$

where the notation found in (7.10) is used for convenience. In order to find the maximum value of C the partial derivative must be taken against each element of all transmit and receive beamforming vectors. The partial derivative of the sum-rate with respect to $\mathbf{b}_{\{m,n\}}$ is first written as

$$\begin{aligned}
\frac{\partial C}{\partial \mathbf{b}_{\{m,n\}}} = \frac{\mathcal{N}'_{\{m,n\}}}{\mathcal{D}_{\{m,n\}}} &+ \frac{-\mathcal{D}'_{\{m,n\}}\mathcal{N}_{\{m,n\}} - \mathcal{N}'_{\{m,n\}}\mathcal{N}_{\{m,n\}}}{\mathcal{D}_{\{m,n\}}(\mathcal{D}_{\{m,n\}}+\mathcal{N}_{\{m,n\}})} \\
&- \sum_{\{i,j\}\neq\{m,n\}}^{\mathcal{L}} \frac{\mathcal{D}'_{\{i,j\}}\mathcal{N}_{\{i,j\}}}{\mathcal{D}_{\{i,j\}}(\mathcal{D}_{\{i,j\}}+\mathcal{N}_{\{i,j\}})}
\end{aligned} \tag{7.12}$$

after rearranging and gathering terms. Prior to continuing with the derivation of finding the optimal beamforming weights, the solution is facilitated by finding the following partial derivatives

$$\begin{aligned}
\mathcal{N}'_{\{m,n\}} &= \mathbf{A}_{\{m,m,n\}}\mathbf{b}_{\{m,n\}}^{*} \\
\mathcal{D}'_{\{m,n\}} &= \sigma_n^2\mathbf{b}_{\{m,n\}}^{*} \\
\mathcal{D}'_{\{m,j\}} &= \mathbf{A}_{\{m,m,j\}}\mathbf{b}_{\{m,n\}}^{*} + \sigma_n^2\mathbf{b}_{\{m,n\}}^{*},\ j\neq n \\
\mathcal{D}'_{\{i,n\}} &= \mathbf{A}_{\{m,i,n\}}\mathbf{b}_{\{m,n\}}^{*},\ i\neq m
\end{aligned} \tag{7.13}$$

where each partial is taken with respect to $\mathbf{b}_{\{m,n\}}$. Inserting each of these values into (7.12) results in

$$\begin{aligned}\frac{\partial C}{\partial \mathbf{b}_{\{m,n\}}} &= \frac{\mathbf{A}_{\{m,m,n\}}\mathbf{b}^*_{\{m,n\}}}{\mathcal{D}_{\{m,n\}}} \\ &\quad - \left(\sigma_n^2\mathbf{b}^*_{\{m,n\}} + \mathbf{A}_{\{m,m,n\}}\mathbf{b}^*_{\{m,n\}}\right) d_{\{m,n\}} \\ &\quad - \sum_{\{i=m,j\neq n\}}^{\mathcal{L}} \left(\mathbf{A}_{\{m,m,j\}}\mathbf{b}^*_{\{m,n\}} + \sigma_n^2\mathbf{b}^*_{\{m,n\}}\right) d_{\{m,j\}} \\ &\quad - \sum_{\{i\neq m,j=n\}}^{\mathcal{L}} \mathbf{A}_{\{m,i,n\}}\mathbf{b}^*_{\{m,n\}} d_{\{i,n\}}.\end{aligned} \tag{7.14}$$

Finding the partial derivatives for all beamforming weights, setting each equation to zero, and then stacking each solution into matrix form leads to

$$\mathbf{\Lambda}_{\{m,n\}} - \sigma_n^2 \sum_{\{i=m,j\}}^{\mathcal{L}} d_{\{m,j\}}\mathbf{b}_{\{m,n\}} - \sum_{\{i,j\}}^{\mathcal{L}} d_{\{i,j\}}\mathbf{A}_{\{m,i,j\}}\mathbf{b}^*_{\{m,n\}} = 0 \tag{7.15}$$

with the final solution becoming

$$\mathbf{b}_{\{m,n\}} = \left(\sigma_n^2 \sum_{\{i=m,j\}}^{\mathcal{L}} d_{\{m,j\}}\mathbf{I} + \sum_{\{i,j\}}^{\mathcal{L}} d_{\{i,j\}}\mathbf{A}_{\{m,i,j\}}\right)^{-1} \mathbf{\Lambda}_{\{m,n\}}. \tag{7.16}$$

It should be noted that (7.16) is not an explicit solution to the transmit beamforming weights; the vector $\mathbf{b}_{\{m,n\}}$ appears on each side of the equation through the definitions found in (7.10). Additionally, all other transmit vectors and all receive vectors were assumed fixed through the solution.

On the receive side, a similar result can be arrived at by fixing the transmit beamforming vectors and, with simple but necessary modifications, the form of the receive weight updates can be written as

$$\mathbf{w}_{\{m,n\}} = \left(\sigma_n^2 d_{\{m,n\}}\mathbf{I} + d_{\{m,n\}} \sum_{\{i,j\}}^{\mathcal{L}} \widetilde{\mathbf{A}}_{\{n,i,j\}}\right)^{-1} \widetilde{\mathbf{\Lambda}}_{\{m,n\}} \tag{7.17}$$

where

$$\begin{aligned}\widetilde{\mathbf{A}}_{\{l,m,n\}} &= \mathbf{H}^H_{\{m,l\}}\mathbf{b}_{\{m,n\}}\mathbf{b}^H_{\{m,n\}}\mathbf{H}_{\{m,l\}} \\ \widetilde{\mathbf{\Lambda}}_{\{m,n\}} &= \frac{\widetilde{\mathbf{A}}^H_{\{n,m,n\}}\mathbf{w}_{\{m,n\}}}{\mathcal{D}_{\{m,n\}}}.\end{aligned} \tag{7.18}$$

Since both transmit and receive vectors are implicitly functions of themselves, the iterative algorithm suggested in [22, 42] will be used for optimization purposes. As an overview, each node alternates updating $\mathbf{b}_{\{m,n\}}$ and $\mathbf{w}_{\{m,n\}}$ in a round-robin fashion until convergence or change in sum-rate is sufficiently small. After convergence, and with final solutions for $\mathbf{b}_{\{m,n\}}$ and $\mathbf{w}_{\{m,n\}}$ for all sublinks, the sum-rate for each link can be calculated using (7.7).

The performance of each possible link is of importance for scheduling purposes in the MAC layer and will be analyzed now. For these simulations it is assumed that given a type of link (i.e. SUC, BC, etc.) the best possible of all such links is used for each channel realization. For example, given a channel realization of the spatially-correlated fading model consider two (out of four total) distinctly possible MACs, $\mathcal{L}_1 = [\{1,2\},\{3,2\},\{4,2\}]$ and $\mathcal{L}_2 = [\{1,3\},\{2,3\},\{4,3\}]$. Both topologies contain three links with either node 2 or node 3 acting as the receiver. However, due to multi-user diversity in the channel one of these MAC links will have a higher throughput than the others. The average sum-rate calculated in this first analysis will choose the best possible link over all possible links of that same type given the current channel realization. Furthermore, only HC links that use all four streams will be classified as HC in order to provide distinction between the link types which are all subsets of HC. To enact some fairness, SUC is the only link allowed to transmit multiple streams from the same transmitter to the same receiver. In other words, with some small modifications to the RCI-HC algorithm $\mathcal{L} = [\{1,2\},\{1,2\},\{1,2\}]$ is a valid SUC link with multiple streams transmitted from user 1 to user 2. The average sum-rate for each of the link topologies using the RCI-HC algorithm is found in Table 7.2 with the following simulation procedures.

Two different simulations are performed in creating Table 7.2 which is divided into two respective columns representing per-node power equality (ENP) and equal total power (ETP). In ENP, each node has a power constraint $P = 10$ which gives advantage to nodes with multiple transmitters (higher total power in the network per channel use) but is realistic in an ad hoc setting where nodes cannot "share" power. The second column, or ETP simulation, shows the sum-rate

Table 7.2: Average sum-rate (bits/sec/Hz) for various links using CSI-Based Precoding

Link	Equal Per-Node Power (ENP)	Equal Total Power (ETP)
Single-User (SUC)	10.00	13.23
Broadcast (BC)	12.04	16.27
Multiple-Access (MAC)	16.16	16.24
Interference (IC)	12.76	13.76
Hybrid (HC)	16.33	18.07
Maximum Rate	16.77	18.12
Nonlinear Broadcast (DPC)	13.20	17.66

of each link when the per-node power is scaled such that the total power is the same over all links which is useful for providing theoretical conclusions by removing power advantages of certain links. For example, with ETP and the BC link, the transmitting node will be allowed to have triple the power of the MAC nodes (which remain at $P = 10$) while HC nodes have 1.5 times the power of MAC nodes in the network so that the total power for each link is constant for each channel realization. For both types of simulations the antenna configuration is fixed at $N_r = N_t = 3$ in the $K = 4$ subnetwork.

For comparison purposes Table 7.2 contains values for the maximum sum-rate over all beamformers and also the average sum-capacity when using the nonlinear DPC algorithm in the BC. The maximum sum-rate was chosen by scheduling the channel with the highest instantaneous sum-rate using linear beamforming with RCI-HC over all links. Note that this value is larger than any of the individual beamforming link values suggesting that no single channel exclusively dominates the throughput for all channel realizations for either ENP or ETP. The sum-rate

DPC value is used as a benchmark and "sanity" check for the RCI-HC beamforming algorithm in the BC. Since DPC is rate optimal it outperforms RCI-HC in the BC but the linear beamformer is able to capture a large portion of the available rate in the channel for both ENP and ETP simulations thus validating the RCI-HC algorithm. Furthermore, RCI-HC has similar performance to the decomposition scheme in [77]. The linear HC link outperforms DPC in the ETP simulation even with optimal nonlinear precoding versus beamforming because HC allows four simultaneous sublinks while DPC can only support three.

Table 7.2 provides several insightful observations into multi-user links. Even with only three antennas per node, HC allows up to four simultaneous sublinks to occur due to the additional benefit of multiple transmitters. Likewise, though not shown in Table 7.2, HC can support three streams with only $N_r = N_t = 2$ antennas available. MAC links for ENP only allow three streams per transmission but have more total power per channel use than any other link topology and are therefore beneficial to schedule in MANETs. When the power is equalized for the ETP simulations, HC has significant gains over MAC and all other links fortifying the importance of stream control in MANETs. For ETP, BC and MAC have the same average throughput which is a manifestation of channel duality [36].

Interesting and exploitable characteristics of MIMO MANETs are the gains available with having both multiple antennas *and* multiple users. As shown in Table 7.2, the use of multiple antennas allows for spatial reuse and the transmission of multiple and simultaneous data streams per channel use. However, Table 7.2 shows the best case scenario of the optimal link being chosen per topology for every channel realization. As shown in the previous section there are numerous links of the same type for even small $K = 4$ subnetworks. In fact, the variance between the highest and lowest sum-rate for a given channel can be significant as shown in Fig. 7.2. In this plot the average sum-rate is shown for each channel when all channel possibilities are first sorted from lowest to highest sum-rate. As an example, consider the SUC case. At each channel realization, for a $K = 4$ subnetwork, there are a total of 12 possible SUC links. The RCI-HC algorithm is used for each of the 12 possible link topologies and then sorted with the average

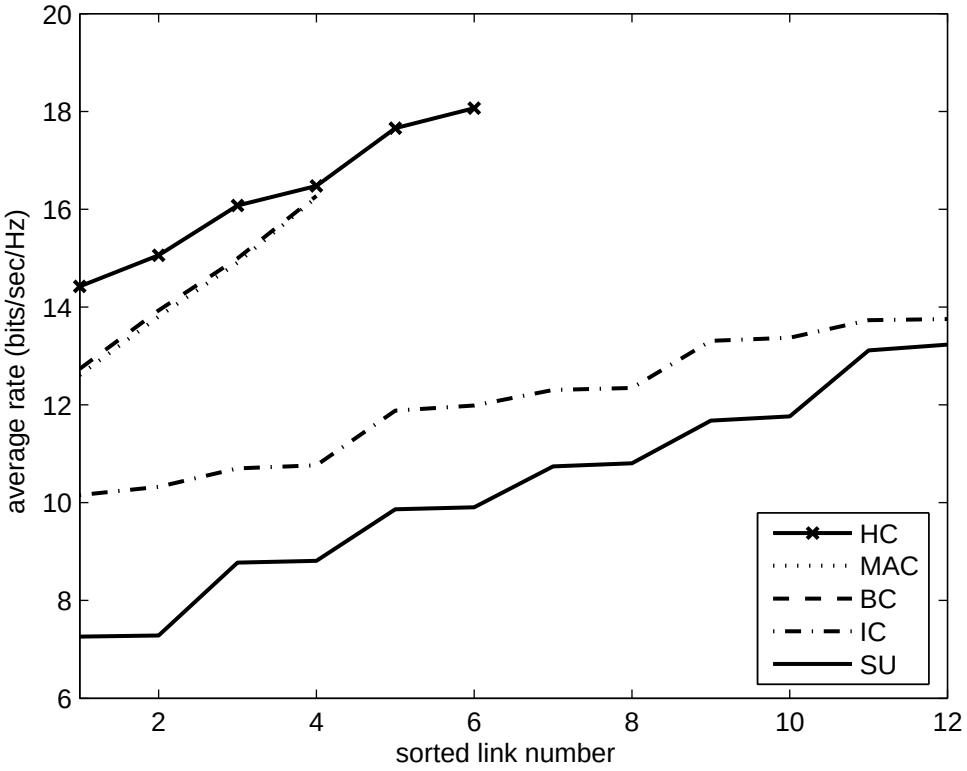

Figure 7.2: Average throughput for the ETP simulations with $N_r = N_t = 3$, $P = 10$, $K = 4$, and different link topologies. Links are sorted by instantaneous rate prior to averaging.

taken after sorting (keep in mind no single transmit-receive pair will always be the best or worst link). The step-like nature of the curves stress the reciprocity assumption of the wireless channel (i.e. $\mathbf{H}_{\{m,n\}} = \mathbf{H}^H_{\{n,m\}}$). Similarly, the duality between the MAC and BC [66] is evident when there is a total power constraint as shown by the same average throughput variance. In brief, Fig. 7.2 shows that the performance gains (or losses) can be quite significant when diversity gains from multi-user subnetworks are used (or unused).

7.5 Regularized Channel Distribution Inversion in Hybrid Channels (RCDI-HC)

The gains seen in the previous sections are all based on the strong assumption that perfect CSI is available. Providing CSI to all nodes in the network (even a small network) is often considered infeasible due to overhead costs and time variations of the channel. The results shown in Table 7.2 are for the best-case scenario of perfect CSI at all nodes and may not be feasible for even slowly time-varying mobile nodes when excessive handshaking becomes difficult. An important aspect of the RCI-HC beamformer is the performance loss seen by using imperfect CSI to calculate the RCI-HC beamforming weights.

Consider simplifying the model of erroneous CSI given from Chapter 2 as

$$\hat{\mathbf{H}}_{\{m,n\}} = \mathbf{H}_{\{m,n\}} + \mathbf{E}_{\{m,n\}} \tag{7.19}$$

where the channel error given by $\mathbf{E}_{\{m,n\}}$ is a zero-mean, Gaussian random matrix with i.i.d. entries of variance σ_e^2 which is a combination of channel delay and estimation error. Fig. 7.3 shows the loss in sum-rate when transmitting nodes use $\hat{\mathbf{H}}_{\{m,n\}}$ to calculate RCI-HC beamforming weights while the sum-rate is calculated with (7.7) and the actual channel $\mathbf{H}_{\{m,n\}}$. For these simulations it is assumed that the receivers maintain perfect CSI regardless of the state at the transmitters while CSI quality at the transmitters is measured by σ_e^2. Fig. 7.3 simulations assume the same linear processing subnetwork topologies as were used to calculate Table

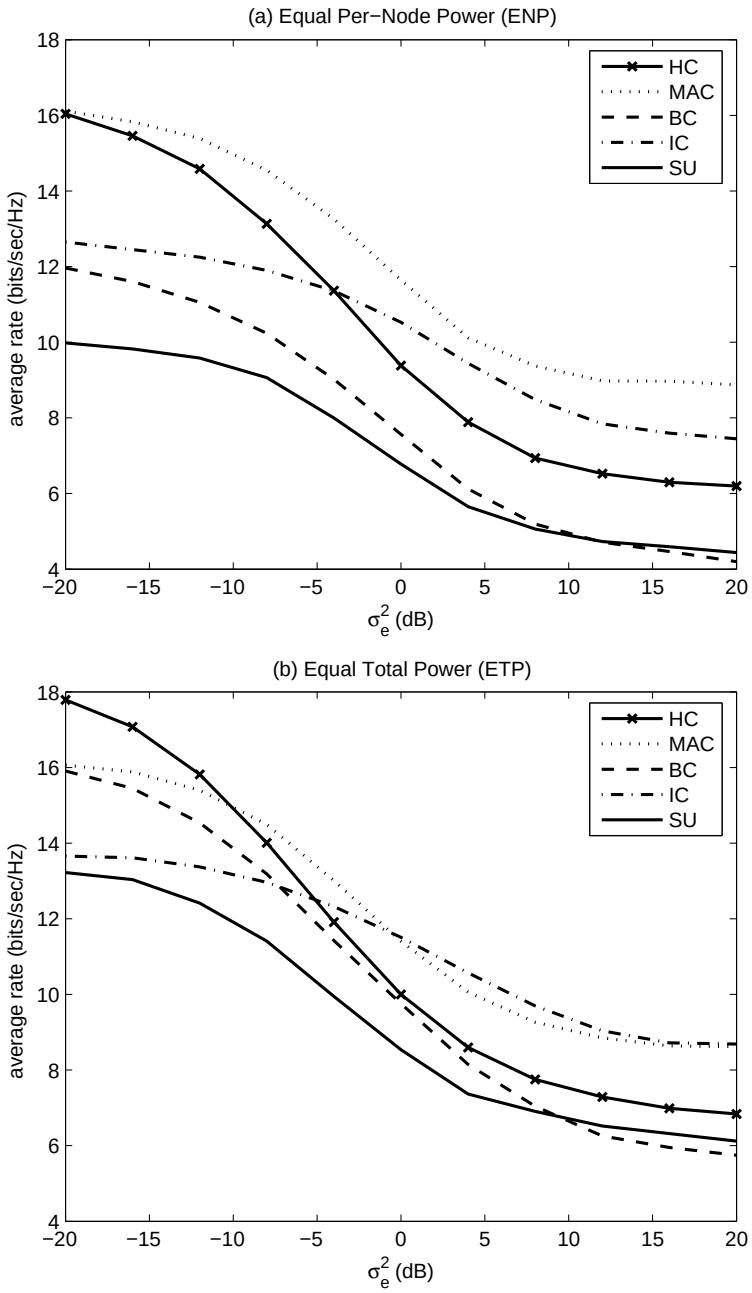

Figure 7.3: Instantaneous sum-rate throughputs for $N_r = N_t = 3$, $P = 10$, $K = 4$, and (a) ENP or (b) ETP simulations in various link topologies with erroneous CSI at the transmitter(s).

7.2 (i.e. $\sigma_e^2 = 0$ in Fig. 7.3 would have the same values as those shown in Table 7.2). Besides the general loss in sum-rate apparent as a function of channel error, it is interesting to note how each channel degrades differently depending on their dependence of CSI at the transmitter. The BC and HC (downlink) are much more susceptible to channel errors at the transmitter than the MAC (uplink) confirming the even higher importance of accurate CSI in downlink channels.

The loss in performance seen by RCI-HC beamforming as well as the general infeasibility of CSI at all nodes motivates a beamformer that requires no CSI and thus frees itself from all the difficulties that arise with such an assumption. In the previous section the RCI-HC algorithm was derived to maximize the sum-rate of a MIMO HC with perfect CSI at the transmitters and receivers for any topology at the link level. In this section the constraint on optimizing the instantaneous sum-rate is loosened in order to allow for more stable transmissions to occur at the cost of lower throughput. This beamformer will instead attempt to maximize the *average* sum-rate of the channel with no knowledge of CSI at the transmitters; rather, CDI is assumed. Thus we derive the so-called regularized channel distribution inversion beamformer for the hybrid channel (RCDI-HC).

In order to maximize the average sum-rate in the HC with no CSI, an approximation on the sum-rate expression in (7.7) will be used. Consider writing this approximation as

$$\bar{C} = \sum_{\{m,n\}}^{\mathcal{L}} \log\left(1 + \frac{\bar{\mathcal{N}}_{\{m,n\}}}{\bar{\mathcal{D}}_{\{m,n\}}}\right) \tag{7.20}$$

where $\bar{\mathcal{N}}_{\{m,n\}}$ and $\bar{\mathcal{D}}_{\{m,n\}}$ are the expected values of numerator and denominator, respectively, of the SINR values. Validity and motivation for using this approximation is discussed in [21] for the BC. Intuitively, this approximation can be considered a maximization on the average signal to average interference plus noise ratios (ASAINR) rather than the average sum-rate explicitly. Given (7.20) as the objective function for optimization purposes, it is straight forward to redefine a few input parameters of the RCI-HC algorithm in order to arrive at RCDI-HC.

The main difference between maximizing (7.7) and (7.20) is that the channel

$\mathbf{H}_{\{m,n\}}$ becomes a random quantity. However, because of the process used to maximize (7.7) coupled with the locations of the expectation operators in (7.20) it is a simple matter of redefining the input parameters of the RCI-HC algorithm in order to find RCDI-HC. Consider the definitions:

$$\begin{aligned}
\mathbf{S}_{\{m,n\}} &= \mathrm{E}\left[\mathbf{H}_{\{m,n\}}^{T} \otimes \mathbf{H}_{\{m,n\}}^{H}\right] \\
\tilde{\mathbf{S}}_{\{m,n\}} &= \mathrm{E}\left[\mathbf{H}_{\{m,n\}}^{*} \otimes \mathbf{H}_{\{m,n\}}\right] \\
\bar{\mathbf{A}}_{\{l,m,n\}} &= \mathrm{mat}\left(\mathbf{S}_{\{l,n\}}\mathrm{vec}\left(\mathbf{w}_{\{m,n\}}\mathbf{w}_{\{m,n\}}^{H}\right)\right) \\
\tilde{\bar{\mathbf{A}}}_{\{l,m,n\}} &= \mathrm{mat}\left(\tilde{\mathbf{S}}_{\{l,n\}}\mathrm{vec}\left(\mathbf{b}_{\{m,n\}}\mathbf{b}_{\{m,n\}}^{H}\right)\right)
\end{aligned} \tag{7.21}$$

where each definition represents "averaged" quantities of those input parameters defined for the transmit and receive RCI-HC weights. For example, by simply replacing $\mathbf{A}_{\{l,m,n\}}$ from (7.10) with $\bar{\mathbf{A}}_{\{l,m,n\}}$ the transmit beamforming vectors can be found that maximize the approximate average sum-rate (7.20) by using the RCI-HC algorithm. This resulting beamforming algorithm is referred to as RCDI-HC for distinction and clarity. The most important observation about RCDI-HC is that $\mathbf{H}_{\{m,n\}}$ us *not* an input parameter to the algorithm. Only the statistics of the channel in the form of the spatial correlation matrices $\mathbf{S}_{\{m,n\}}$ are required to calculate both transmit and receive beamforming weights.

With the same simulation parameters as those used in Table 7.2, the average sum-rates for the RCDI-HC beamformer are shown in Table 7.3. Note that for these simulations the sum-rate approximation (7.20) is only used to calculated transmit and receive beamforming weights. Once these are calculated, the actual sum-rate is found using (7.7) and the current channel. It is also assumed that all nodes share the spatial correlation matrices and that all receive nodes possess perfect CSI. With no knowledge of CSI at the transmitters, the best link per channel realization can not be chosen thus the "Maximum Rate" value does not appear in Table 7.3. Note that the trend seen in sum-rate performance is similar to that for RCI-HC with perfect CSI with the HC link providing the highest average rate for ETP simulations. Furthermore, RCDI-HC beamformers for each link perform at roughly 70-80% of their RCI-HC counterparts.

Table 7.3: Average sum-rate (bits/sec/Hz) for various links using RCDI-HC

Link	Equal Per-Node Power (ENP)	Equal Total Power (ETP)
Single-User (SUC)	7.22	9.98
Broadcast (BC)	8.47	11.37
Multiple-Access (MAC)	11.73	11.71
Interference (IC)	10.03	11.00
Hybrid (HC)	11.38	12.56

The most important conclusion of Table 7.3 needs to emphasize that the resulting sum-rates are *not* a function of CSI nor time variations in the statistically-stationary channel under consideration. The RCDI-HC beamformers will not suffer performance loss due to delay or overhead in acquiring CSI at each node as CSI does not appear in the RCDI-HC algorithm. Also, given that sufficient time has elapsed to accurately estimate the channel distribution, the assumption of perfect CDI is not unfounded compared to the constant updates that maintaining perfect CSI requires. The final result being that the values shown in Table 7.3 are constant for all values of σ_e^2 from Fig. 7.3 which emphasizes their stability in the MIMO channel. Thus the RCDI-HC beamformers provide a stability-throughput tradeoff by lowering the initial available sum-rate of a link but maximizing the time that the average sum-rate is valid. RCDI-HC beamformers provide truly cross-layer alternatives to CSI-based transmissions by allowing the MAC layer to have immediate knowledge of the PHY layer transmission scheme facilitating possible cross-layer optimizations on the network.

The work presented in this chapter, in part, was submitted to: A. L. Anderson, J. R. Zeidler, and M. A. Jensen, "Linear processing and link scheduling in MIMO mobile ad hoc networks (MANET)," submitted to *28th Conference on*

Computer Communications (INFOCOM 2008).

Chapter 8

Conclusions

The optimal linear and nonlinear precoders for the MIMO broadcast channel result in significant throughput loss when used with outdated or erroneous CSI, and therefore require frequent feedback to maintain high performance. This work has quantified this loss, and has adapted the sum-rate maximizing beamformer to use CDI in an effort to obtain an approach whose throughput performance remains stable in time-variant channels. Analysis of the throughput for this RCDI beamforming algorithm using measured channel data has demonstrated that it is robust to temporal variations and delay in the feedback channel and outperforms the optimal precoding techniques for node displacements that are just fractions of a wavelength. This suggests that the approach can be used to maintain good throughput with significantly reduced feedback frequency. Furthermore, simple parameterization of the channel correlation matrix using popular channel models allows significant reduction in the amount of data that must be fed back to the transmitter without resulting in significant performance loss.

This work has also addressed the dual multiple-access channel under thte same channel conditions as analyzed with the broadcast channel. When good estimates of CSI are available, the RCI-MAC beamformer provides performance on par with the rate maximizing beamforming algorithm in the dual broadcast channel. With channel errors caused by limited or infrequent training or feedback,

RCI-MAC beamforming degrades resulting in performance loss as demonstrated by the sum-rate degradation. For these scenarios, a beamformer was also found (RCDI-MAC) that attempts to maximize the average rate of the MIMO MAC using the channel distribution statistics in the form of spatial correlations. This beamformer provides the receiver with signaling options in order to combat the effects of estimation errors and mobility in multi-user MIMO networks.

As an extension to larger networks, this work has also derived and analyzed a linear beamforming technique (RCI-HC) for link-level use and all possible half-duplex configurations in a MIMO MANET. The RCI-HC beamformer works with point-to-point (P2P) links including the single-user (SUC) and interference channels (IC), standard multi-user broadcast (BC) and multiple-access channels (MAC), and even more complex topologies generally referred to as hybrid channels (HC). The impact of both rate-maximizing linear precoding and multi-user diversity was examined for each of these links with the RCI-HC beamforming algorithm. When the input information necessary to derive these optimal beamformers becomes outdated or erroneous, significant loss at the PHY layer is seen which would have a cascaded loss effect on the higher network layers. Motivated by this loss, another beamformer (RCDI-HC) based on channel distribution information was formulated in order to provide the medium access control layer with the option of a throughput-stability tradeoff by way of the type of information used to create beamforming weights. The RCDI-HC beamformer bridges the gap in time-scales between the PHY layer's channel coherence time when using CSI and the MAC layer's longer network time-scale.

Appendix A

Single-User Mutual Information Lower Bound

The expression used for capacity degradation from outdated CSI is based on the lower bound of mutual information for MIMO links with erroneous channel estimates [25]. The mutual information between input and output given the channel matrix and initial displacement is bounded by

$$\begin{aligned} I(\mathbf{x};\mathbf{y}|\widetilde{\mathbf{H}}) &= h(\mathbf{x}|\widetilde{\mathbf{H}}) - h(\mathbf{x}|\mathbf{y},\widetilde{\mathbf{H}}) \\ &\geq \log|\pi e\mathbf{Q}| - \log|\pi e\mathbf{R}_{x-\hat{x}}| \end{aligned} \tag{A.1}$$

assuming that x is Gaussian with covariance $\mathbf{Q}$, $\hat{x}$ is the MMSE estimate of x, and $\mathbf{R}_v = \mathrm{E}[\mathbf{v}\mathbf{v}^H]$ is the correlation matrix of the random vector $\mathbf{v}$. For the measured channel, the error statistics are assumed to be neither i.i.d. nor zero-mean leading to

$$\begin{aligned} \mathbf{R}_{x-\hat{x}} &= \mathrm{E}[(\mathbf{x}-\hat{\mathbf{x}})\mathbf{x}^H] \\ &= \mathbf{Q} - \mathbf{R}_{xy}\mathbf{R}_{yy}^{-1}\mathbf{R}_{yx} \\ &= \mathbf{Q} - \mathbf{Q}\tilde{\mathbf{H}}^H\mathbf{R}_{yy}^{-1}\tilde{\mathbf{H}}\mathbf{Q}^H \end{aligned} \tag{A.2}$$

where $\tilde{\mathbf{H}} = \hat{\mathbf{H}} + \mathbf{E}_\mu$. Equation (6.1) results is an upper-bound on the entropy

$$h(\mathbf{x}|\mathbf{y},\hat{\mathbf{H}}) \leq \log|\mathbf{Q} - \mathbf{Q}\tilde{\mathbf{H}}^H(\tilde{\mathbf{H}}\mathbf{Q}\tilde{\mathbf{H}}^H + \mathbf{\Psi}^E - \mathbf{\Psi}^{E_\mu} + \mathbf{I})^{-1}\tilde{\mathbf{H}}\mathbf{Q}|. \tag{A.3}$$

Using (A.1) and (A.2) with the matrix inversion lemma results in the lower bound on mutual information

$$I(\mathbf{x};\mathbf{y}|\widetilde{\mathbf{H}}) \geq \log \left| \mathbf{I} + \tilde{\mathbf{H}}^H \left(\mathbf{I} + \mathbf{\Psi}_E^Q - \mathbf{\Psi}_{E_\mu}^Q \right)^{-1} \tilde{\mathbf{H}}\mathbf{Q} \right|. \tag{A.4}$$

Appendix B

Multi-User Per-User Mutual Information Lower Bound

In order to obtain the lower bound on mutual information with measured data for the multi-user channels with optimal processing and outdated CSIR, the proof from [25] can be modified to include multiple users with channel error that is neither i.i.d. nor zero mean. For the jth user in the broadcast channel, the mutual information between input and output given the sum channel matrix and error mean is bounded by

$$\begin{aligned} I(\mathbf{x}_j; \mathbf{y}_j | \widetilde{\mathbf{H}}_1 \dots \widetilde{\mathbf{H}}_K) &= \mathrm{h}(\mathbf{x}_j | \widetilde{\mathbf{H}}_1 \dots \widetilde{\mathbf{H}}_K) - \mathrm{h}(\mathbf{x}_j | \mathbf{y}_j, \widetilde{\mathbf{H}}_1 \dots \widetilde{\mathbf{H}}_K) \\ &\geq \log |\mathbf{Q}_j| - \log |\mathbf{R}_{\mathbf{x}_j - \hat{\mathbf{x}}_j}| \end{aligned} \tag{B.1}$$

which assumes that $\mathbf{x}_j$ given $\widetilde{\mathbf{H}}_j$ is Gaussian with covariance $\mathbf{Q}_j$, the effective channel is $\widetilde{\mathbf{H}}_j = \hat{\mathbf{H}}_j + \mathbf{E}_{\mu,j}$, $\hat{\mathbf{x}}_j$ is the MMSE estimate of $\mathbf{x}_j$, $\mathrm{h}\{\cdot\}$ is the entropy function, and $\mathbf{R}_{\mathbf{uv}} = \mathrm{E}[\mathbf{u}\mathbf{v}^H]$ is the correlation matrix of the random vectors $\mathbf{u}$ and $\mathbf{v}$. The correlation matrix for the error vector can be found by

$$\begin{aligned} \mathbf{R}_{\mathbf{x}_j - \hat{\mathbf{x}}_j} &= \mathrm{E}\left[(\mathbf{x}_j - \hat{\mathbf{x}}_j)\mathbf{x}_j^H\right] \\ &= \mathbf{Q}_j - \mathbf{R}_{\mathbf{x}_j \mathbf{y}_j} \mathbf{R}_{\mathbf{y}_j \mathbf{y}_j}^{-1} \mathbf{R}_{\mathbf{y}_j \mathbf{x}_j} \\ &= \mathbf{Q}_j - \mathbf{Q}_j \widetilde{\mathbf{H}}_j^H \mathbf{R}_{\mathbf{y}_j \mathbf{y}_j}^{-1} \widetilde{\mathbf{H}}_j \mathbf{Q}_j^H. \end{aligned} \tag{B.2}$$

Using (B.2) with the received vector defined by (3.12) results is an upper-bound on the entropy expression

$$\mathrm{h}(\mathbf{x}_j|\mathbf{y}_j, \widetilde{\mathbf{H}}_1 \dots \widetilde{\mathbf{H}}_K) \leq \log \left| \mathbf{Q}_j - \mathbf{Q}_j \widetilde{\mathbf{H}}_j^H \left(\mathbf{I} + \widetilde{\mathbf{H}}_j \mathbf{Q}_j \widetilde{\mathbf{H}}_j^H + \mathbf{Z}_j \right)^{-1} \widetilde{\mathbf{H}} \mathbf{Q}_j \right| \tag{B.3}$$

where $\mathbf{Z}_j$ was defined for (3.13) and the notation $\mathbf{E}_{\mathrm{r},j} = \mathbf{E}_j(\Delta_\mathrm{r})$ and $\mathbf{E}_{\mathrm{t},j} = \mathbf{E}_j(\Delta_\mathrm{t})$ is used for simplicity. The matrix inversion lemma on (B.3) combined with (B.1) results in the lower bound on mutual information

$$\begin{aligned} I^{\mathrm{DPC}}(\mathbf{x}_j; \mathbf{y}_j | \widetilde{\mathbf{H}}_1 \dots \widetilde{\mathbf{H}}_K) &= \log \left| \mathbf{I} + \widetilde{\mathbf{H}}_j^H \left(\mathbf{I} + \mathbf{Z}_j \right)^{-1} \widetilde{\mathbf{H}}_j \mathbf{Q}_j \right| \\ \mathbf{Z}_j &= \mathbf{\Psi}_{\mathbf{E}_{\mathrm{r},j}}^{\sum_{i=j}^{K} \mathbf{Q}_i} + \mathbf{\Psi}_{\mathbf{E}_{\mathrm{t},j}}^{\sum_{i=1}^{j-1} \mathbf{Q}_i} + \mathbf{\Psi}_{\widetilde{\mathbf{H}}_j}^{\sum_{i>j} \mathbf{Q}_i}. \end{aligned} \tag{B.4}$$

For $K = j = 1$, Eq. (B.4) is equivalent to the single-user bound in [25] with an effective channel $\widetilde{\mathbf{H}}$ and the given correlated error matrix.

Following the same method used for the broadcast channel, the multiple-access channel with outdated/erroneous CSI and received signal (3.15) results in the mutual information bound

$$\begin{aligned} I^{\mathrm{MAC}}(\mathbf{x}_j; \mathbf{y}_j | \widetilde{\mathbf{H}}_1 \dots \widetilde{\mathbf{H}}_K) &\geq \log \left| \mathbf{I} + \widetilde{\mathbf{H}}_j^H \left(\mathbf{I} + \mathbf{Z}_j \right)^{-1} \widetilde{\mathbf{H}}_j \mathbf{Q}_j \right| \\ \mathbf{Z}_j &= \sum_{i=1}^{K} \mathbf{\Psi}_{\mathbf{E}_{\mathrm{r},i}}^{\mathbf{Q}_i} + \sum_{i=j+1}^{K} \mathbf{\Psi}_{\widetilde{\mathbf{H}}_i}^{\mathbf{Q}_i} \end{aligned} \tag{B.5}$$

where the interference term $\mathbf{Z}_j$ is unique to the channel under consideration.

Appendix C

Expected Sample Average Rate (ESAR) Bounds

Consider parameterizing the single-user, MISO, beamforming channel ergodic capacity into a function of scalar quantities as

$$C = \mathrm{E}\left[\log\left(1 + \frac{\sigma_s^2 s}{\sigma_n^2 n}\right)\right] \tag{C.1}$$

where s and n are random variables representing the signal and interference, respectively, and specific realizations are assumed known at the receiver. The quantities σ_s^2 and σ_n^2 are normalizing factors corresponding to the signal and interference powers. Equation (C.1) is the composition of a concave ($\log\{\cdot\}$) and quasiconvex (SINR) function leading to the constrained bounds

$$C^{\text{upper}} = \log\left(1 + \mathrm{E}\left[\frac{\sigma_s^2 s}{\sigma_n^2 n}\right]\right) \tag{C.2}$$

$$C^{\text{lower}} = \log\left(1 + \frac{\sigma_s^2 \mathrm{E}[s]}{\sigma_n^2 \mathrm{E}[n]}\right). \tag{C.3}$$

Equation (C.2) is always a true upper bound from Jensen's inequality and the concavity of the logarithm. The lower bound is conditionally true since the composed ergodic capacity is a quasiconvex function [78]. A straightforward example of when the lower bound holds is when s is held constant (i.e. signal power equalization over all time channel realizations). Although the lower bound fails when the interference is held constant, we later show numerically that, since the distribution on

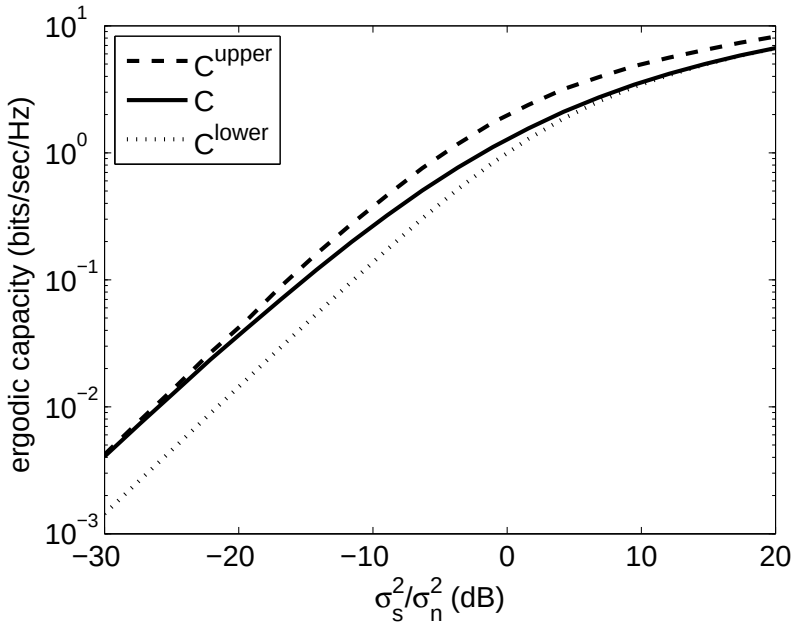

Figure C.1: Ergodic capacity with upper and lower bounds in an interference limited, single-user system with $m = 3$ degrees of freedom.

the SINR is a function of both channel realizations and beamforming weights, the lower bound will hold for the channels of interest in this work. Therefore, Eq. (C.3) is a constrained lower bound.

Since the MMSE-CDIT beamforming algorithm maximizes a bound rather than the exact ergodic capacity, we are interested in the tightness of each bound. For small SINR $\sigma_s^2/\sigma_n^2 \ll 1$ the ergodic capacity can be approximated using a first-order Taylor series expansion on the natural logarithm

$$\begin{aligned} C &= \mathrm{E}\left[\log\left(1+\frac{\sigma_s^2 s}{\sigma_n^2 n}\right)\right] \\ &= \sum_{i=1}^{i=\infty} \frac{(-1)^i}{(2i)!}\mathrm{E}\left[\left(\frac{\sigma_s^2 s}{\sigma_n^2 n}\right)^i\right], \ \frac{\sigma_s^2 s}{\sigma_n^2 n} < 1 \\ &\approx \mathrm{E}\left[\frac{\sigma_s^2 s}{\sigma_n^2 n}\right] \\ &\approx C^{\mathrm{upper}} \end{aligned} \tag{C.4}$$

where the final approximation comes from applying the same expansion to (C.2).

For larger SINR $\sigma_s^2/\sigma_n^2 \gg 1$, the ergodic capacity can be approximated by

$$\begin{aligned} C &\approx \mathrm{E}\left[\log\left(\frac{\sigma_s^2 s}{\sigma_n^2 n}\right)\right] \\ &= \mathrm{E}\left[\log\left(\sigma_s^2 s\right)\right] - \mathrm{E}\left[\log\left(\sigma_n^2 n\right)\right] \\ &= \log\left(\sigma_s^2\right) - \log\left(\sigma_n^2\right) + \mathrm{E}\left[\log\left(s\right)\right] - \mathrm{E}\left[\log\left(n\right)\right] \\ &= \log\left(\frac{\sigma_s^2 \mathrm{E}\left[s\right]}{\sigma_n^2 \mathrm{E}\left[n\right]}\right) \\ &\approx C^{\mathrm{lower}} \end{aligned} \tag{C.5}$$

where $\mathrm{E}[\log(s)] - \mathrm{E}[\log(n)] = 0$ if we assume that s and n are i.i.d. random variables. Figure C.1 plots ergodic capacity with upper and lower bounds as a function of SINR when s and n are chi-squared random variables each with three degrees of freedom and a base-2 logarithm. Fig. C.2 results are for measured data with various initial positions for $N_{\mathrm{t}} = 4$, $N_{\mathrm{r}} = 1$, $K = 6$, and $P = 10$. The optimal beamforming weights were found using the RCI algorithm and then fixed as the channel changes over time. Similar results were demonstrated for a variety of different datasets over all possible starting displacements and various beamforming algorithms.

The results show that C^{upper} is tight for small SINR while C^{lower} is a better approximation for large SINR. Since this work focuses on the high-capacity, multi-user channel, the high SINR region in Fig. C.1 is of interest, suggesting that the lower bound provides a tighter approximation to the actual ergodic (or sample) capacity and should be used for the MMSE-CDIT beamforming algorithm. It should be noted that 1) with beamforming the signal gains will not necessarily follow the same distribution as the interference plus noise and 2) the bound results from Fig. C.1 suggest performance in an ideal case. Even with these limitations, however, the results in Fig. C.2 on bound tightness still hold.

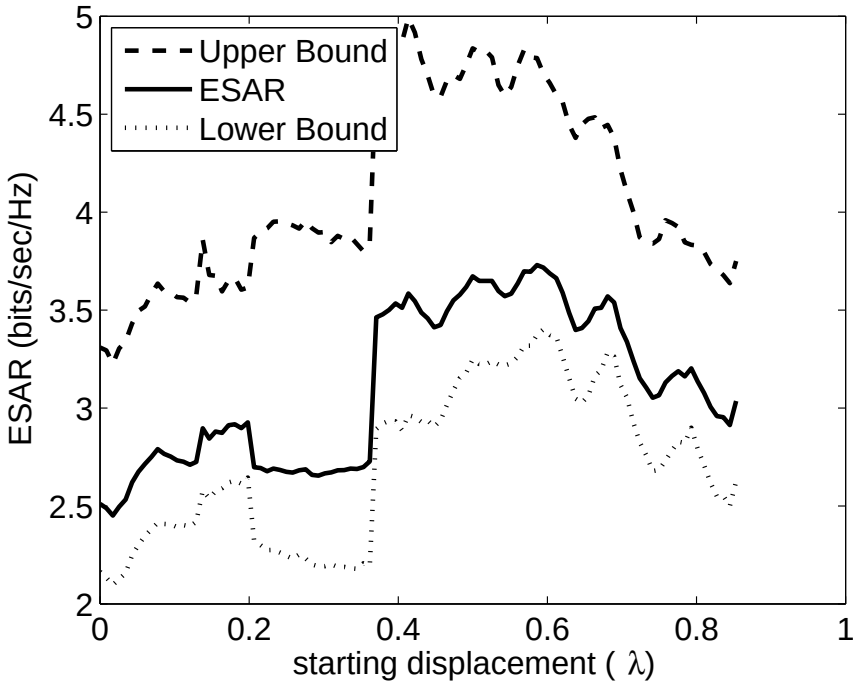

Figure C.2: The Expected Sample Average Rate (ESAR) with upper and lower bounds for various initial displacements. The measured channel was used for a system with $N_{\mathrm{t}} = 4$, $N_{\mathrm{r}} = 1$, $K = 6$, and $P = 10$.

Appendix D

Regularized Channel Distribution Inversion (RCDI)

The RCI algorithm from [42] was derived to maximize the sum-rate of a MISO broadcast channel with perfect CSI at the transmitter and receivers. This section details the steps taken to maximize an approximation of the average sum-rate of a MIMO broadcast channel with perfect CDI. During the maximization process for the sum-rate bound used in the current work, the following notation is defined

$$\begin{aligned}
\mathbf{S}_{t,j} &= \mathrm{E}[\mathbf{H}_j^T \otimes \mathbf{H}_j^H] \\
\mathbf{S}_{r,j} &= \mathrm{E}[\mathbf{H}_j^* \otimes \mathbf{H}_j] \\
\bar{\mathbf{H}}_j &= \mathrm{mat}\left(\mathbf{S}_{t,j}\mathrm{vec}(\mathbf{w}_j\mathbf{w}_j^H)\right) \\
\mathbf{\Lambda} &= \left[\frac{(\bar{\mathbf{H}}_1\mathbf{B})_{:,1}}{\bar{d}_1}, \ldots, \frac{(\bar{\mathbf{H}}_K\mathbf{B})_{:,K}}{\bar{d}_K}\right] \\
\mathbf{D} &= \mathrm{diag}\left(\frac{\bar{n}_1}{\bar{d}_1(\bar{d}_1+\bar{n}_1)}, \ldots, \frac{\bar{n}_K}{\bar{d}_K(\bar{d}_K+\bar{n}_K)}\right)
\end{aligned} \tag{D.1}$$

where $\mathrm{diag}(\cdot)$ returns a diagonal matrix of the input argument. In order to incorporate multiple antennas at the receivers, an effective MISO channel can be created using the beamforming vectors at each receiver. Including these values

with the bound in (4.17) produces an effective average rate that can be written as

$$\begin{aligned}\bar{C} &= \sum_{j=1}^{K} \log\left(1 + \frac{\mathrm{E}[|\mathbf{w}_j^H \mathbf{H}_j \mathbf{b}_j|^2]}{\mathrm{E}\left[\frac{\mathrm{tr}(\mathbf{B}\mathbf{B}^H)}{P} + \sum_{i\neq j} |\mathbf{w}_j^H \mathbf{H}_j \mathbf{b}_i|^2\right]}\right) \\ &= \sum_{j=1}^{K} \log\left(1 + \frac{\mathbf{B}_{:,j}^H \bar{\mathbf{H}}_j \mathbf{B}_{:,j}}{\frac{\mathrm{tr}(\mathbf{B}\mathbf{B}^H)}{P} + \sum_{i\neq j} \mathbf{B}_{:,i}^H \bar{\mathbf{H}}_j \mathbf{B}_{:,i}}\right) \end{aligned} \tag{D.2}$$

where $\bar{\mathbf{H}}_j = \mathrm{mat}\left(\mathbf{S}_{t,j}\mathrm{vec}(\mathbf{w}_j\mathbf{w}_j^H)\right)$ as defined in (D.1). Deriving the form of the RCDI beamformer follows the same formulation found in [42] for the capacity-optimal, CSI-based, RCI beamformer where, instead, the derivative of $\bar{C}$ is taken with respect to each of the transmit beamforming vector elements.

The average rate bound from (D.2) can be simplified and expanded as

$$\bar{C} = \sum_{j=1}^{K} \log(\bar{n}_j + \bar{d}_j) - \log(\bar{d}_j) \tag{D.3}$$

where the notation found in (4.17) and (D.1) will be used for convenience. In order to find the maximum value of $\bar{C}$ the partial derivative must be taken against each element of $\mathbf{B} = [\mathbf{b}_1, \ldots, \mathbf{b}_K]$. For simplicity, we show the first partial derivative of the first element; all other derivatives follow in a similar manner

$$\begin{aligned}\frac{\partial \bar{C}}{\partial \mathbf{B}_{1,1}} &= \frac{\bar{d}_1' + \bar{n}_1'}{\bar{d}_1 + \bar{n}_1} - \frac{\bar{d}_1'}{\bar{d}_1} + \left\{\frac{\bar{n}_1'}{\bar{d}_1} - \frac{\bar{n}_1'}{\bar{d}_1}\right\} + \sum_{i=2}^{K} \frac{\bar{d}_i' + \bar{n}_i'}{\bar{d}_i + \bar{n}_i} - \frac{\bar{d}_i'}{\bar{d}_i} \\ &= \frac{\bar{n}_1'}{\bar{d}_1} + \frac{-\bar{d}_1'\bar{n}_1 - \bar{n}_1'\bar{n}_1}{\bar{d}_1(\bar{d}_1 + \bar{n}_1)} - \sum_{i=2}^{K} \frac{\bar{d}_i'\bar{n}_i}{\bar{d}_i(\bar{d}_i + \bar{n}_i)} \\ &= \frac{\bar{n}_1'}{\bar{d}_1} - \sum_{i=1}^{K} \frac{[\mathbf{b}_1^H \bar{\mathbf{H}}_i \mathbf{b}_1]'\bar{n}_i}{\bar{d}_i(\bar{d}_i + \bar{n}_i)} - \sum_{i=1}^{K} \frac{\sigma_n^2 \mathbf{B}_{1,1}^* \bar{n}_i}{\bar{d}_i(\bar{d}_i + \bar{n}_i)} \\ &= \frac{\left(\bar{\mathbf{H}}_1 \mathbf{B}^*\right)_{1,1}}{\bar{d}_1} - \sum_{i=1}^{K} \frac{\left(\bar{\mathbf{H}}_i \mathbf{B}^*\right)_{1,1} \bar{n}_i}{\bar{d}_i(\bar{d}_i + \bar{n}_i)} - \sum_{i=1}^{K} \frac{\sigma_n^2 \mathbf{B}_{1,1}^* \bar{n}_i}{\bar{d}_i(\bar{d}_i + \bar{n}_i)} \end{aligned} \tag{D.4}$$

where $\bar{n}_i' = 0$ and $\bar{d}_i' = \sigma^2 \mathbf{B}_{1,1}^* + [\mathbf{b}_1^H \bar{\mathbf{H}}_i \mathbf{b}_1]'$ for $i \neq 1$. Finding the partial derivatives for all beamforming weights, setting each equation to zero, and then stacking each solution into matrix form leads to

$$\mathbf{\Lambda} - \sum_{i=1}^{K} \mathbf{D}_{i,i} \bar{\mathbf{H}}_i \mathbf{B} - \frac{\mathrm{tr}(\mathbf{D})}{P} \mathbf{B} = 0 \tag{D.5}$$

with the final solution becoming

$$\mathbf{B} = \left(\frac{\mathrm{tr}(\mathbf{D})}{P} \mathbf{I} + \sum_{i=1}^{i=K} \mathbf{D}_{i,i} \bar{\mathbf{H}}_i \right)^{-1} \mathbf{\Lambda}. \tag{D.6}$$

It should be noted that, though the form of the RCI and RCDI beamformers are similar, one cannot simply take the expectation of the beamformer from [42] directly in order to find the final solution here; special care needs to be taken with the expectation operator and the random quantities found in the rate bound.

Abbreviations and Definitions

AoA	angle of arrival
AoD	angle of departure
ASAINR	average-signal-to-average-interference-plus-noise ratio
ASINR	average-signal-to-interference-plus-noise ratio
AWGN	additive white Gaussian noise
BC	broadcast channel
BYU	Brigham Young University
CCI	channel covariance information
CDI	channel distribution information
CDIR	channel distribution information at the receiver
CDIT	channel distribution information at the transmitter
CMI	channel mean information
CSI	channel state information
CSIR	channel state information at the receiver
CSIT	channel state information at the transmitter
dB	decibels, $10\log_{10}(\cdot)$
DPC	dirty-paper coding
HC	hybrid channel
Hz	Hertz (1 cycle/s)
IC	interference channel
Indoor	measurements taken in the BYU engineering building
LP	linear processing
LOS	line-of-sight
MAC	multiple-access channel
MANET	mobile adhoc network
ML	maximum-likelihood
MMSE	minimum mean-square error
MMSE-CDIT	iterative MMSE beamforming with CDIT
MMSE-CSIT	iterative MMSE beamforming with CSIT
MPR	multi-packet reception
MIMO	multiple-input multiple-output
MISO	multiple-input single-output

Model	channel realizations created via random matrix models
MSE	mean-square error
Outdoor	measurements taken at DT field on BYU campus
P2P	peer-to-peer
QoS	quality of service
RCDI	regularized channel distribution inversion
RCDI-BC	broadcast channel regularized channel distribution inversion
RCDI-HC	hybrid channel regularized channel distribution inversion
RCDI-MAC	MAC regularized channel distribution inversion
RCI	regularized channel inversion
RCI-BC	regularized channel inversion for the broadcast channel
RCI-HC	regularized channel inversion for the hybrid channel
RCI-MAC	regularized channel inversion for the multiple-access channel
Rx	receiver
SIC	successive-interference cancellation
SIMO	single-input multiple-output
SINR	signal-to-interference plus noise ratio
SISO	single-input single-output
SNR	signal-to-noise ratio
SUC	broadcast channel
SVD	singular value decomposition
TDD	time division duplex
Transception	what transceivers do
Tx	transmitter
UCSD	Univeristy of California, San Diego
ULA	uniform linear array
Urban	measurements taken at the BYU coalyard
WSS	wide-sense stationary
ZF-DPC	zero-forcing dirty-paper coding

Operators and Miscellaneous Symbols

$\text{vec}(\cdot)$	the matrix column stacking operator
$\text{mat}(\cdot)$	inverse of vec (e.g. $\text{mat}(\text{vec}(\mathbf{A})) = \mathbf{A}$)
$\text{diag}(\cdot)$	either vector of diagonal elements or diagonal matrix
$E\{\cdot\}$	expected value
max	maximum
$\log(\cdot)$	log base 2
$n!$	factorial
$(\cdot)^*$	complex conjugate
$(\cdot)^T$	matrix transpose
$(\cdot)^H$	matrix conjugate transpose
$\lvert\cdot\rvert$	matrix determinant
$\text{tr}(\cdot)$	matrix trace
$\lvert\lvert\cdot\rvert\rvert$	vector or matrix norm
$=$	equal
$\approx$	approximately equal
$\leq$	less than or equal to
$\geq$	greater than or equal to
$<$	strictly less than
$>$	strictly greater than
$\ll$	much less than
$\gg$	much greater than
$\in$	in the set
$\forall$	for all
$\odot$	matrix Schur product
$\otimes$	matrix Kronecker product
$\binom{n}{k}$	"n choose k"
$\sqrt{\mathbf{A}}$	is the matrix square root operator $\sqrt{\mathbf{A}}\sqrt{\mathbf{A}} = \mathbf{A}$
$\mathbf{I}$	identity matrix

Bibliography

[1] M. A. Jensen and J. W. Wallace, "A review of antennas and propagation for MIMO wireless communications," *IEEE Trans. Antennas Propag.*, vol. 52, pp. 2810–2824, Nov. 2004.

[2] A. Goldsmith, S. A. Jafar, N. Jindal, and S. Vishwanath, "Capacity limits of MIMO channels," *IEEE J. Selected Areas Commun.*, vol. 21, pp. 684–702, June 2003.

[3] D. Gesbert, M. Shafi, D. Shiu, Peter J. Smith, and A. Naguib, "From theory to practice: An overview of MIMO spacetime coded wireless systems," *IEEE J. Selected Areas Commun.*, vol. 21, pp. 281–302, Apr. 2003.

[4] B. Ottersten K. Yu, "Models for MIMO propagation channels: A review," *Wireless Communications and Mobile Computing*, vol. 2, no. 7, pp. 653–666, 2002.

[5] B. T. Maharaj, J. W. Wallace, and M. A. Jensen, "A low-cost open-hardware wideband multiple-input multiple-output (MIMO) wireless channel sounder," Submitted to the *IEEE Trans. on Instrum. Meas.*

[6] J. W. Wallace, M. A. Jensen, A. L. Swindlehurst, and B. D. Jeffs, "Experimental characterization of the MIMO wireless channel: Data acquisition and analysis," *IEEE Trans. Wireless Commun.*, vol. 2, pp. 335–343, Mar. 2003.

[7] J. W. Wallace, M. A. Jensen, A. Gummalla, and H. Lee, "Experimental characterization of the outdoor MIMO wireless channel temporal variation," *IEEE Trans. Veh. Technol.*, vol. 56, pp. 1041–1049, May 2007.

[8] V. Anreddy and M. A. Ingram, "Capacity of measured Ricean and Rayleigh indoor MIMO channels at 2.4GHz with polarization and spatial diversity," in *Proc. IEEE Wireless Communications & Networking Conference (WCNC)*, April 2006.

[9] M. Herdin, N. Czink, H. Özcelik, and E. Bonek, "Correlation matrix distance, a meaningful measure for evaluation of non-stationary MIMO channels," in *Proc. 2005 IEEE 62nd Veh. Technol. Conf.*, 2005.

[10] M. A. Jensen and J. W. Wallace, "Recent advances in antennas and propagation for MIMO systems: Multi-user networks and channel temporal variation," in *Proc. of the 2005 International Conference on Electromagnetics in Advanced Applications.*, Sept. 2005.

[11] J.W. Wallace and M.A. Jensen, "Measurement and characterization of the time variation of indoor and outdoor MIMO channels," in *Proc. 2005 IEEE 62nd Veh. Technol. Conf.*, Sept. 2005, pp. 1289–1293.

[12] J. W. Wallace and M. A. Jensen, "Time varying MIMO channels: Measurement, analysis, and modeling," *IEEE Trans. Antennas Propag.*, vol. 54, pp. 3265–3273, Nov. 2006.

[13] J. W. Wallace and M. A. Jensen, "Modeling antenna coupling and correlation in rapidly fading MIMO channels," in *Proceedings of 2006 European Conference on Antennas and Propagation*, Nov. 2007.

[14] A. A. M Saleh and R. A. Valenzuela, "A statistical model for indoor multipath propagation," *IEEE J. Selected Areas Commun.*, vol. SAC-5, pp. 128–137, Feb. 1987.

[15] J. W. Wallace and M. A. Jensen, "Modeling the indoor MIMO wireless channel," *IEEE Trans. Antennas Propag.*, vol. 50, pp. 591–599, May 2002.

[16] S. Shiu, G. J. Foschini, M. J. Gans, and J. M. Khan, "Fading correlation and its effect on the capacity of multielement antenna systems," *IEEE Trans. Commun.*, vol. 48, pp. 502–513, Mar. 2000.

[17] K. Yu, M. Bengtsson, B. Ottersten, D. McNamara, P. Karlsson, and M. Beach, "Second order statistics of NLOS indoor MIMO channels based on 5.2GHz measurements," in *Proc. 2001 IEEE Global Telecomm. Conf.*, Nov. 2001, pp. 156–160.

[18] H. Ozcelik, M. Herdin, J. Wallace, and E. Bonek, "Deficiencies of 'Kronecker' MIMO radio channel model," *Electronics Letters*, vol. 39, pp. 1209–1210, Aug. 2003.

[19] W. Weichselberger, M. Herdin, H. Özcelik, and E. Bonek, "A stochastic MIMO channel model with joint correlation of both link ends," *IEEE Transactions on Wireless Communications*, vol. 5, no. 1, pp. 90–99, 2006.

[20] W. Jakes, *Microwave Mobile Communications*, Wiley, New York, 1974.

[21] A. L. Anderson, J. R. Zeidler, and M. A. Jensen, "Stable transmission in the time-varying MIMO broadcast channel," *EURASIP Journal on Advances in Signal Processing*, vol. 2008, Article ID 617020, 14 pages, 2008. doi:10.1155/2008/617020.

[22] A. L. Anderson, J. R. Zeidler, and M. A. Jensen, "Reduced-feedback linear precoding with stable performance for the time-varying MIMO broadcast channel," *IEEE J. Selected Areas Commun.*, Oct. 2008.

[23] M. Ghogho and A. Swami, "Channel estimation for MIMO systems using data-dependent superimposed training," in *Proc. of the 43rd Allerton Conf. on Comm., Control, and Comp.*, 2004.

[24] S. Theodoridis D. Katselis, E. Kofidis, "Training-based estimation of correlated MIMO fading channels in the presence of colored interference," *ScienceDirect Signal Processing*, vol. 87, pp. 2177–2187, Sept. 2007.

[25] T. Yoo and A. Goldsmith, "Capacity and power allocation for fading MIMO channels with channel estimation error," *IEEE Trans. Inf. Theory*, vol. 52, pp. 2203–2214, May 2006.

[26] S. Yang and J. Belfiore, "The impact of channel estimation error on the DPC region of the two-user Gaussian broadcast channel," in *Proc. of the 43rd Allerton Conf. on Comm., Control, and Comp.*, Sept. 2005.

[27] M. H. M. Costa, "Writing on dirty paper," *IEEE Trans. Inf. Theory*, vol. 29, pp. 439–441, May 1983.

[28] Q. H. Spencer, J. W. Wallace, C. B. Peel, T. Svantesson, A. L. Swindlehurst, and A. Gummalla, "Performance of multi-user spatial multiplexing with measured channel data," in *MIMO System Technology and Wireless Communications*. CRC, 2006.

[29] J. Jootar, J. R. Zeidler, , and J. G. Proakis, "On the performance of concatenated convolutional code and alamouti space-time code with noisy channel estimates and finite depth interleaving," To appear in the *IEEE Trans. on Comm.*

[30] J. Jootar, J. R. Zeidler, , and J. G. Proakis, "On the performance of closed-loop transmit diversity with noisy channel estimates," To appear in the *IEEE Trans. on Comm.*

[31] E. Visotsky and U. Madhow, "Space-time transmit precoding with imperfect feedback," *IEEE Trans. Inf. Theory*, vol. 47, pp. 2632–2639, Sept. 2001.

[32] S. Jafar, S. Vishwanath, and A. Goldsmith, "Channel capacity and beamforming for multiple transmit and receive antennas with covariance feedback," in *Proc. 2001 IEEE Intl. Conf. Commun.*, June 2001, pp. 2266–2270.

[33] M. Sánchez-Fernández and A. Lozano, "Doppler sensitivity of link reciprocity in TDD MIMO systems," in *Proc. 2005 IEEE Global Telecomm. Conf.*, 2005, pp. 3073–3076.

[34] A. Vakili, M. Sharif, and B. Hassibi, "The effect of channel estimation error on the throughput of broadcast channels," in *Proc. 2006 IEEE Intl. Conf. Acoustics, Speech, and Signal Processing*, May 2006, pp. 29–32.

[35] A. Dana, M. Sharif, and B. Hassibi, "On the capacity region of multi-antenna Gaussian broadcast channels with estimation error," in *Proc. 2006 IEEE Intl. Symp. on Info. Theory*, July 2006, pp. 1851–1855.

[36] P. Viswanath and D. Tse, "Sum capacity of the vector Gaussian broadcast channel and uplink-downlink duality," *IEEE Trans. Inf. Theory*, vol. 49, pp. 1912–1921, Aug. 2003.

[37] P. Ding, D. Love, and M. Zoltowski, "On the sum rate of multi-antenna broadcast channel with channel estimation error," in *39th Asilomar Conf. Signals, Systems and Computers*, Oct. 2005, pp. 1524–1528.

[38] R. Doostnejad, T. J. Lim, and E. Sousa, "Precoding for the MIMO broadcast channels with multiple antennas at each receiver," in *Conference on Info. Sciences and Systems*, Mar. 2005.

[39] M. Schubert and H. Boche, "Iterative multiuser uplink and downlink beamforming under SINR constraints," *IEEE Trans. Signal Processing*, vol. 53, pp. 2324–2334, July 2005.

[40] M. Stojnic, H. Vikalo, and B. Hassibi, "Rate maximization in multi-antenna broadcast channels with linear preprocessing," in *Proc. 2004 IEEE Global Telecomm. Conf.*, Dec. 2004, pp. 3957–3961.

[41] T. Fugen, C. Kuhnert, and W. Wiesbeck, "Capacity of the MIMO broadcast channel under realistic propagation conditions," in *Proc. of the 2005 IEEE 16th Intl. Symp. on Personal, Indoor and Mobile Radio Comm.*, Sept. 2005, pp. 2660–2664.

[42] M. Stojnic, H. Vikalo, and B. Hassibi, "Rate maximization in multi-antenna broadcast channels with linear preprocessing," *IEEE Trans. Commun.*, vol. 5, pp. 2338–2342, Sept. 2006.

[43] J. Chung, C.-S. Hwang, K. Kim, and Y. Kim, "A random beamforming technique in MIMO systems exploiting multiuser diversity," *IEEE J. Selected Areas Commun.*, vol. 21, pp. 848–855, Jun. 2003.

[44] R. Zhang, J. Cioffi, and Y. Liang, "Throughput comparison of wireless downlink transmission schemes with multiple antennas," in *Proc. 2005 IEEE Intl. Conf. Commun.*, May 2005.

[45] A. Soysal and S. Ulukus, "Optimum power allocation for single-user MIMO and multi-user MIMO-MAC with partial CSI," *IEEE J. Selected Areas Commun.*, vol. 25, pp. 1402–1412, Sept. 2007.

[46] V. Raghavan, A. Sayeed, and V. Veeravalli, "Limited feedback precoder design for spatially correlated MIMO channels," *Information Sciences and Systems, 2007. CISS '07. 41st Annual Conference on*, pp. 113–118, March 2007.

[47] M. Kountouris, D. Gesbert, and L. Pittman, "Transmit correlation-aided opportunistic beamforming and scheduling," in *Proc. Europ. Signal Processing Conf.*, Sept. 2006.

[48] D. Hammarwall, M. Bengtsson, and B. Ottersten, "Acquiring partial CSI for spatially selective transmission by instantaneous channel norm feedback," *IEEE Trans. Signal Processing*, vol. 56, no. 3, pp. 1188–1204, Mar. 2008.

[49] D. Gesbert, M. Kountouris, R. W. Heath, C.-B. Chae, and T. Sälzer, "Shifting the MIMO paradigm," *IEEE Sig. Proc. Mag.*, pp. 36–46, Sept. 2007.

[50] P. Viswanath, D. Tse, and R. Laroia, "Opportunistic beamforming using dumb antennas," *IEEE Trans. Inf. Theory*, vol. 48, no. 6, pp. 1277–1294, June 2002.

[51] H. Kim, J.S. Kim, L. Jianjun, and M. Kountouris, "On the performance of limited feedback multiuser MIMO transmission in 3GPP HSDPA," *Proc. 2005 IEEE 62nd Veh. Technol. Conf.*, vol. 1, pp. 473–476, Sept. 2005.

[52] M. Kountouris, T. Sälzer, and D. Gesbert, "Scheduling for multiuser MIMO downlink channels with ranking-based feedback," *EURASIP Journal on Advances in Signal Processing*, vol. 2008, Article ID 854120, 14 pages, 2008. doi:10.1155/2008/854120.

[53] D. Love, R. Heath, and T. Strohmer, "Grassmannian beamforming for multiple-input multiple-output wireless systems," *IEEE Trans. Inf. Theory*, vol. 49, pp. 2735–2747, Oct. 2003.

[54] C.-B. Chae, T. Inoue, R. Heath, and D. Mazzarese, "Non-iterative multiuser MIMO coordinated beamforming with limited feedforward," *Proc. 2008 IEEE Intl. Conf. Acoustics, Speech, and Signal Processing*, pp. 2393–2396, April 2008.

[55] H. Zheng, Y. Wu, Y. Li, S. Zhou, and J. Wang, "Limited feedback precoding scheme for downlink multiuser MIMO systems," *IEICE Trans. Commun.*, vol. E90-B, no. 3, pp. 689–692, Mar. 2007.

[56] P. Ding, D. J. Love, and M. D. Zoltowski, "Multiple antenna broadcast channels with shape feedback and limited feedback," *IEEE Trans. Signal Processing*, vol. 55, pp. 3417–3428, July 2007.

[57] N. Jindal, "MIMO broadcast channels with finite-rate feedback," *IEEE Trans. Inf. Theory*, vol. 52, no. 11, pp. 5045–5060, Nov. 2006.

[58] G. Caire, N. Jindal, M. Kobayashi, and N. Ravindran, "Quantized vs. analog feedback for the MIMO broadcast channel: A comparison between zero-forcing based achievable rates," in *Proc. 2007 IEEE Intl. Symp. on Info. Theory*, June 2007.

[59] W. Cheng and R. Murch, "MU-MISO transmission with limited feedback," *IEEE Trans. Wireless Commun.*, vol. 6, no. 11, pp. 3907–3913, Nov. 2007.

[60] T. Yoo, N. Jindal, and A. Goldsmith, "Multi-antenna downlink channels with limited feedback and user selection," *IEEE J. Selected Areas Commun.*, vol. 25, pp. 1478–1491, Sept. 2007.

[61] M. Cho, Y. Kim, Yo. Kim, and D. Hong, "An efficient CQI feedback scheme for multiuser MIMO systems," *Proc. 2007 IEEE 66nd Veh. Technol. Conf.*, pp. 625–629, Oct 2007.

[62] C. F. Van Loan and N. Pitsianis, "Approximations with Kronecker products," in *Linear Algebra for Large Scale and Real Time Applications*, M. S. Moonen and G. H. Golub, Eds. Kluwer Academic Publishers, 1993.

[63] M.-O. Pun, W. Ge, D. Zheng, J. Zhang, and V. Poor, "Distributed opportunistic scheduling for MIMO ad-hoc networks," *Proc. 2008 IEEE Intl. Conf. Commun.*, pp. 3689–3693, May 2008.

[64] T. ElBatt, "Towards scheduling MIMO links in interference-limited wireless ad hoc networks," in *Proc. 2007 Military Comm. Conf. (MILCOM)*, Oct. 2007.

[65] K. Sundaresan, R. Sivakumar, and M. A. Ingram, "Medium access control in ad hoc networks with MIMO links: Optimization considerations and algorithms," *IEEE Trans. Mobile Computing*, vol. 3, pp. 350–365, Oct.-Dec. 2004.

[66] S. Vishwanath, N. Jindal, and A. Goldsmith, "On the capacity of multiple input multiple output broadcast channels," *Proc. 2002 IEEE Intl. Conf. Commun.*, vol. 3, pp. 1444–1450, 2002.

[67] S. Gupta and P. R. Kumar, "The capacity of wireless networks," *IEEE Trans. Info. Theory*, vol. 46, pp. 388–404, Mar. 2000.

[68] B. Chen and M. J. Gans, "MIMO communications in ad hoc networks," *IEEE Trans. Signal Processing*, vol. 54, pp. 2773–2783, July 2006.

[69] Z. Wang, H. R. Sadjadpour, and J. J. Garcia-Luna-Aceves, "Closing the capacity gap in wireless ad hoc networks using multi-packet reception," *Information Theory and Applications Workshop*, pp. 287–292, Feb. 2008.

[70] Z. Wang, H. R. Sadjadpour, and J. J. Garcia-Luna-Aceves, "A unifying perspective on the capacity of wireless ad hoc networks," *27th Conference on Computer Communications (INFOCOM)*, pp. 211–215, April 2008.

[71] C. B. Peel, A. L. Swindlehurst, and W. Utschick, "Transport capacity regions for wireless networks with multi-user links," in *Proc. 2006 European Signal Proc. Conf. (EUSIPCO)*, Sept. 2006.

[72] S. Toumpis and A. J. Goldsmith, "Capacity regions for wireless ad hoc networks," *IEEE Trans. Wireless Commun.*, vol. 2, pp. 736–748, July 2003.

[73] R. A. Iltis, S.-J. Kim, and D. A. Hoang, "Noncooperative iterative MMSE beamforming algorithms for ad hoc networks," *IEEE Trans. Commun.*, vol. 54, no. 4, pp. 748–759, Apr. 2006.

[74] S. Ye and R. S. Blum, "Optimized signaling for MIMO interference systems with feedback," *IEEE Trans. Signal Processing*, vol. 51, pp. 2839–2848, Nov. 2003.

[75] A. L. Anderson, J. R. Zeidler, and M. A. Jensen, "Instantaneous and average rate maximization in MIMO multiple-access channels (MAC) with linear processing," in *42nd Asilomar Conf. Signals, Systems and Computers*, Pacific Grove, CA, Oct. 2008.

[76] J.Y. Yu and P.H.J. Chong, "A survey of clustering schemes for mobile ad hoc networks," *Communications Surveys & Tutorials, IEEE*, vol. 7, no. 1, pp. 32–48, 2005.

[77] M.A. Maddah-Ali, A.S. Motahari, and A.K. Khandani, "Communication over MIMO X Channels: Interference alignment, decomposition, and performance analysis," *IEEE Trans. Inf. Theory*, vol. 54, no. 8, pp. 3457–3470, Aug. 2008.

[78] S. Boyd and L. Vandenberghe, *Convex Optimization*, Cambridge University Press, 2004.

[79] A. Anderson, J. R. Zeidler, and M. Jensen, "Regularized channel distribution inversion and parameterization in the MIMO broadcast channel," in *Proc. 2008 IEEE 68nd Veh. Technol. Conf.*, Calgary, Canada, Sept. 2008.

[80] A. Anderson, J. R. Zeidler, and M. Jensen, "Parameterized channel feedback using correlation-based channel models for multi-user MIMO systems," in *Proceedings of the 2008 USNC/URSI National Radio Science Meeting*, Boulder, CO, Jan. 2008, paper # BS11-4, 1 page, Invited.

[81] A. L. Anderson, J. R. Zeidler, and M. A. Jensen, "Performance of transmit precoding in time-varying point-to-point and multi-user MIMO channels," in *Conference Record of the IEEE Asilomar Conference on Circuits, Systems and Computers*, Nov. 2006.